

**Groundwater Recharge and Flow Processes in Rivirivi
Catchment Underlain by Fractured and Faulted
Lithology, Malawi**

January 2018

KAMBUKU Dwight Davison

**Groundwater Recharge and Flow Processes in Rivirivi
Catchment Underlain by Fractured and Faulted
Lithology, Malawi**

A Dissertation Submitted to
the Graduate School of Life and Environmental Sciences,
the University of Tsukuba
in Partial Fulfillment of the Requirements
for the Degree of Doctor of Philosophy in Environmental Sciences
(Doctoral Program in Sustainable Environmental Studies)

KAMBUKU Dwight Davison

Abstract

With increased demand for water resources as a result of settlement patterns, communities, particularly in drier climatic regions, are now looking to fractured rock aquifers as primary sources of potable water for domestic, agricultural and industrial use. To enable sustainable management of this resource, knowledge of dominant hydrogeological processes is vital. In this study, the author investigated how overburden soil, fractured hornblende-biotite-gneiss and geological fault affect recharge and groundwater flow processes using stable isotopes ($\delta^{18}\text{O}$ and δD), geochemistry and hydraulic tests. A total of 99 samples were collected for stable isotopic and geochemical analyses in both dry and rainy seasons. Pumping tests were conducted on four wells juxtaposed across Ntcheu Fault.

Stable isotopic and geochemical data suggested that a leaky interface between thin overburden soils of up to 30 mm and fractured Hornblende-biotite-gneiss rock formation enabled rapid preferential recharge processes into the Mg-Ca- HCO_3 dominated aquifers. All water samples in the study area registered total dissolved solids (TDS) of not more than 500 mg/L implying that they have a short residence time with little time for intense hydrochemical processes. The seasonal decrease in TDS concentrations in shallow waters in rainy season is as a result of contact or mixing with rainwater suggesting that shallow waters could be directly recharged from rainfall. Additionally, groundwater samples also showed a significant concentration of NO_3^- ions (10 to 100 mg/L) which is indicative that groundwater in this catchment is very young in age.

The $\delta^{18}\text{O}$ and δD showed that groundwater and surface water plot close to both Local Meteoric Water Line (LMWL) and Global Meteoric Water Line (GMWL) indicating a relatively constant isotopic composition and a well mixed system. It also mirrors the average isotope composition of rainwater (-6.1‰). This further reveals that water in this study area is of meteoric origin and that modern rainfall is the dominant component of these waters. In addition, this suggested a rapid infiltration process that seemed to preserve precipitation isotopic signatures in these fractured hornblende-biotite-gneiss rock formations.

Shallow groundwater and a few deep groundwater samples in both dry and rainy seasons fell below both LMWL and GMWL, indicating that they could have been subjected to evaporation before or during infiltration process. The $\delta^{18}\text{O}$ and deuterium excess values showed an inverse relationship further suggesting that evaporation could be the main cause of isotopic enrichment in the study area. In addition, the slope of the regression lines of $\delta^{18}\text{O}$ and δD values for these shallow groundwater samples was lower (6.3) than that of LMWL (7.6) further indicating that isotopic fractionation during rainwater evaporation could be the main cause of the enrichment.

Spring water, some deeper groundwater (DGW) in the valley section and shallow groundwater away from the ridge, show more depleted stable isotopic values in dry season and plots slightly away from LMWL and GMWL. This is indicative that these waters were recharged under climatic conditions different from the rest of the samples. Their depleted values suggest that their recharge might have happened under lower air temperatures or probably from big rainfall events recharged at a higher altitude. Deuterium excess values for these samples are also different from sampled rainfall. These depleted samples that plot away from LMWL and GMWL are very similar to precipitation samples collected in February, 1974 about 650 km away at Harare Global Network of Isotopes in Precipitation (GNIP) in Zimbabwe. Ndola GNIP data which was used to construct LMWL has missing data in this period. Since Malawi, Zambia and Zimbabwe share similar rainfall systems, there is a high chance that these isotopically depleted waters were recharged from this period.

An isotopic gradient of -0.36‰ per 100 m increase in elevation was deduced from proxies for precipitation in the study area. Three recharge zones corresponding to three water groups identified according to their average total dissolved solids concentrations were revealed against recharge water line. Deep groundwater in the valley section seems to be recharged from a regional recharge zone that lies between 1317 and 1513 meters above sea level (masl). River water seems to be recharged from intermediate recharge zone lying between 1094 and 1317 masl. Deep groundwater along Ntcheu geological fault seems to be recharged from local recharge zone lying between 954 and 1094 masl. All these recharge

zones are characterized by fractured Hornblende-biotite-gneiss formations with very thin overburden soils (up to 30 mm).

Hydraulic gradients and derivatives of drawdown data in wells juxtaposed across Ntcheu Fault coupled with similarities in stable isotopic and geochemical compositions strongly suggest permeability across the geological fault. Lithological data from a borehole drilled in the fault itself at Wanyemba Village (BP4) also shows permeable geological formation across the fault.

From the foregoing, isotopic, geochemical and hydraulic test data have strongly suggested that the interface between thin overburden soils and fractures aid rapid localized groundwater recharge and flow systems in Upper Rivirivi Catchment. Meanwhile, Ntcheu Fault acts as a conduit for lateral groundwater flow in the NW-SE and SSW-NNE directions. This approach and subsequent interpretations may be replicated in similar geological settings elsewhere. Since the nature and type of the geological formation enables rapid recharge and flow processes, it leaves the catchment susceptible to inter-annual climatic variabilities and anthropogenic contamination. Informed catchment management decisions are thus critical for sustainable management of this resource.

Keywords: Overburden soil, fractured Hornblende-biotite-gneiss, geological fault, groundwater recharge, groundwater flow, stable isotopes, geochemistry, pumping tests, drawdown derivatives, Rivirivi Catchment, Malawi

Table of Contents

Abstract.....	i
List of Tables	vi
List of Figures.....	vii
Chapter 1: Introduction.....	1
1.1 General setting	1
1.2 Literature Review	3
1.3 Objectives	11
Chapter 2: Study Area	14
2.1 Site description	14
2.2 Sampling points	29
2.3 Groundwater Level Contours	35
Chapter 3: Methodology.....	39
3.1 Geochemistry and stable isotopes.....	39
3.2 Pumping Test.....	40
Chapter 4: Results.....	49
4.1 Spatial and temporal variations of physical and geochemical data	49
4.2 Spatial and temporal variations of stable isotopic data	63
4.3 Pumping Test data	68
Chapter 5: Discussion.....	74
5.1 Dominant geochemical processes associated with fractured Hornblende- biotite-gneiss rock formation.....	74
5.2 Groundwater recharge sources and its mechanisms	83
5.3 Recharge and flow boundaries as revealed by hydraulic tests	97
5.4 Fracture locations and flow types	102
5.5 Linking hydraulic tests and stable isotopes	110
5.6 Local flow process and effect of Ntcheu Fault.....	119
Chapter 6: Conclusions.....	125
Acknowledgement	129

References	130
APPENDIX	142

List of Tables

Table 1: Representative boreholes' screen location.....	26
Table 2: Characteristics of aquifer systems in Malawi.....	28
Table 3: In situ parameters, isotopic and geochemical data.....	60
Table 4: Pump discharge rates and storativity values.....	69
Table 5: Correlation coefficient of major parameters in groundwater.....	77
Table 6: Correlation coefficient of major parameters in pumped wells.....	122

Appendix

Table A1-A4: Pumping Test Data.....	142
Table A5: Chloro-alkaline indices (CAI) for water samples.....	146
Table A6: Ionic balance for water samples.....	147

List of Figures

Figure 1a: Different flow phases in fractures.....	8
Figure 1b: Double porosity fractured rock.....	8
Figure 2a: Watershed Drainage System in the study area.....	15
Figure 2b: Mean Annual Rainfall at Nkhande Rain-station in Upper Rivirivi Catchment.....	17
Figure 2c: Rainfall and Altitude Relationship in Southern Malawi.....	17
Figure 2d: Geological map of the study area.....	19
Figure 2e: Hydrogeological cross-section of Upper Rivirivi Catchment.....	23
Figure 3: Daily Rainfall and River Discharge at IR19 River Gauging Station.....	24
Figure 4: Outcrop fractures and fault structure at BP4.....	27
Figure 5: Sampling points.....	30
Figure 6: Groundwater level contours.....	36
Figure 7: Sensitivity Analysis - observed drawdown versus modeled drawdown.....	47
Figure 8a: Local water temperature variations with depth in dry season.....	50
Figure 8b: Local water temperature variations with depth in rainy season.....	50
Figure 8c: Monthly rainfall in the 2015/16 Rainy Season.....	51
Figure 9: pH variations in groundwater with changes in Elevation and seasons.....	52
Figure 10: Variation of NO_3^- concentration in groundwater with changes in Elevation.....	54
Figure 11: Variations in Silica concentration with Elevation.....	56
Figure 12: Trilinear diagrams for samples taken in (a) Dry Season (b) Rainy Season.....	58
Figure 13: Spatial and temporal variation of geochemical data.....	59
Figure 14: Local Meteoric Water Line (LMWL) Plots.....	64
Figure 15: δ - diagram for samples collected in Dry and Rainy Seasons.....	67
Figure 16: Screen locations, lithology and neighbor features for pumped wells.....	71

List of Figures

Figure 17: Variation of water levels with increase in pumping time.....	73
Figure 18: (a) $\text{Ca}^{2+} + \text{Mg}^{2+}$ vs $\text{HCO}_3^- + \text{SO}_4^{2-}$ (b) Na^+ vs Cl^- (c) d-excess vs $\delta^{18}\text{O}$	76
Figure 19: Chloro-Alkaline Indices (CAI) for Groundwater.....	79
Figure 20: Gibbs Plot of Groundwater samples.....	81
Figure 21: Similarity between stable isotopes of spring water from study area and Precipitation sampled in February, 1974 at Harare GNIP Station.....	85
Figure 22: Spatial distribution of $\delta^{18}\text{O}$ in local waters (a) Dry Season (b) Rainy Season...	87
Figure 23: Relationship between $\delta^{18}\text{O}$ and Cl^- concentrations.....	89
Figure 24: Variation of $\delta^{18}\text{O}$ in local waters with altitude.....	92
Figure 25: Vertical distribution of $\delta^{18}\text{O}$ and recharge water line for Upper Rivirivi Catchment.....	95
Figure 26: Relationship between drawdown data and pumping time.....	99
Figure 27: Comparing water level changes during pumping and recovery after pump Stoppage.....	103
Figure 28: Relationship between derivatives of drawdown data and pumping time.....	106
Figure 29: $\delta^{18}\text{O}$ and δD for pumped wells during pumping.....	112
Figure 30: Variations in water level and $\delta^{18}\text{O}$ values with pumping time.....	112
Figure 31: Stable isotopic and geochemical variations at pumped wells.....	114
Figure 32: Relationship between water level, deuterium and pumping time.....	115
Figure 33: Silica and Chloride values in pumped wells across Ntcheu Fault.....	121
Figure 34: Geochemical, hydraulic head and isotopic variations with well depth.....	123
Figure 35: Conceptual model of localized recharge and flow processes in Rivirivi Catchment.....	127

Chapter 1: Introduction

1.1 General setting

Lack of access to safe and sustainable water resources for domestic, agricultural and industrial use is central to a daily crisis faced by millions of the world's most vulnerable societies in developing countries. This situation is restraining human progress, pushing large segments of humanity to lives of poverty, vulnerability and insecurity (UNDP, 2006).

Globally, it is predicted that by the year 2050, a water crisis will arise due to a lacking access to safe drinking water. Demand for water is expected to increase by 55% (UN Water, 2015). Drought, increased population and economic activities, among other factors, are continuously pushing communities to live in areas where groundwater from fractured rock aquifers is the only reliable source of potable water (Berkowitz, 2002; Holland & Witthuser, 2011). For example, Shapiro, (2002) reports that with increased demand for water in the US, communities are now looking to fractured rock aquifers as a source of safe water for domestic, agricultural and industrial use. This phenomenon is not only unique to the US. In South Africa, for example, 15% of the total land area cover is characterized by fractured aquifers (Holland & Witthuser, 2011) while 40% of Australia's groundwater is stored in fractured rock aquifers (Hamza et al., 2016). In Malawi, about 35% of the total land area cover is characterized by fractured basement aquifers (MoAIWD, 2015; Mapoma et al., 2014; Chilton & Foster, 1995). However, due to perceived lower yields of these aquifers, less attention is given to the understanding of their hydrogeological processes for sustainable resource management.

Elsewhere in semi-arid regions, particularly sub-Saharan Africa, communities are largely dependent on rain-fed agriculture and groundwater is the only significant and reliable source of drinking water for rural masses and yet this region is characterized by erratic rainfall, and high evapotranspiration rates (Stadler et al., 2010; Macdonald et al., 2009; Beekman et al., 1999).

With a growing population, additional pressure will be exerted on the water resources due to contamination and over-exploitation resulting in the need for sound groundwater management measures that feed into Sustainable Development Goals (SDGs). This in turn requires a better understanding of hydrogeological processes that impact groundwater sustainability in these environments.

To understand these hydrogeological processes, there is also need to understand major factors that control groundwater at various scales of time and space. At a catchment scale, groundwater resource is controlled by precipitation input, recharge pathways which are largely controlled by geological settings and finally the time (residence time) it takes before groundwater could be discharged or withdrawn at a spring, rivers or at a well (Nimmo et al., 2005).

The broader focus of this study is to understand the role pathways play on recharge mechanisms as a function of geological settings. This information is important because generally pathways determine recharge and flow mechanisms in a catchment. These pathways are in turn defined by nature and type of the geological formations. So, various natures and types of geological formations are expected to differently affect recharge processes and subsequent dominant geochemical mechanisms in groundwater (de Vries and Simmers, 2002; Scanlon et al., 2002).

1.2 Literature Review

General concepts of groundwater recharge

Globally, groundwater is the primary source of potable water to more than 1.5 billion people and its quality is relatively better than surface water sources. In rural areas where centralized water supply systems are underdeveloped, groundwater is typically the only reliable source of water (Worldwatch, 2017; Kambuku, 2009). The case is no different from Upper Rivirivi Catchment where more than 85% of the population relies on groundwater as main source of potable water (Knoema, 2015). Due to drought cases, growing worldwide economy and increasing population, use of groundwater resources continues to rise. This scenario puts pressure on the resource itself and that is why it is important to understand the processes that enable replenishment of the resource (Wang et al., 2015). Groundwater recharge is the important process of the hydrological cycle that replenishes groundwater. Understanding the dominant groundwater recharge mechanisms therefore help water resource managers understand if groundwater is being renewed annually or not. It also helps the identification of potential vulnerability of the resource to climatic variations and further understanding if groundwater is also vulnerable to anthropogenic contamination.

Definition and sources of recharge

Groundwater recharge is generally defined as water that moves from land surface or unsaturated zone into the saturated zone, forming an addition to the groundwater reservoir (de Vries and Simmers, 2002; Scanlon et al., 2002; Nimmo et al., 2005). Sources of recharge include natural phenomenon like precipitation, lakes, ponds and rivers and human induced phenomenon like artificial recharge, irrigation, leaking water mains, septic tanks, sewers, gardens and other public facilities. Surface water bodies, for example, rivers and lakes do not always act as recharge sources. Instead, they can act as aquifer discharge points as well.

Types of recharge

Groundwater recharge is generally categorized as direct, preferential, indirect or mountain front recharge. Direct or diffuse recharge is the water added to the groundwater reservoir in excess of soil-moisture deficits and evapotranspiration, happening below the point of impact of precipitation by direct vertical percolation through the unsaturated zone. It is spatially distributed with percolation through the entire vadose zone. This type of recharge is common to humid climates. Contrary to percolating through the entire vadose zone, preferential recharge occurs in macropores or rock fractures which essentially have diameters larger than 3 mm. Preferential recharge is dominated by viscous forces and gravity (de Vries and Simmers, 2002).

Indirect recharge results from percolation to the water table following runoff and localization in joints or through the beds of surface water courses. It is further distinguished as to whether it is associated with surface water courses or it is in localized form resulting from horizontal surface concentration of water in the absence of well defined channels. In semi-arid regions, indirect and localized recharge are often the most important sources of natural recharge although factors like geology and overburden soils can alter such phenomenon (Gleeson et al., 2009).

Mountain front recharge is one type that involves complex processes of unsaturated and saturated flow in fractured rocks as well as infiltration along channels flowing across alluvial fans. On a large scale, mountain front recharge through fractured bedrock is primarily diffuse recharge process whereas infiltration from mountain streams is considered a localized recharge process (Sophocleous, 2004).

Main factors affecting recharge

Climate, topography, soil, geology and vegetation may influence spatial variation of groundwater recharge. A decrease in slope or presence of fractures may lead to greater infiltration and thus greater recharge. Vegetation influences recharge mainly through its water-distributing activity. Where water is a limiting factor of vegetation growth, roots usually extract most of the water that

infiltrates. The result is that evapotranspiration may nearly equal infiltration thus leaving recharge as a small fraction of infiltration (Nimmo et al, 2005; Lerner et al., 1990). However, in the study area, deforestation has altered this mode of effect of vegetation on groundwater recharge. The degree of this alteration was not investigated further in this research but provides a good thematic area for further research.

Since groundwater recharge represents replenishment of aquifers necessary for maintaining water supplies and ecosystems, it still remains as a vital component for evaluating sustainability in the same way stream-flow is to surface water.

Types of groundwater flow in fractured rock media

A prominent characteristic of fractured aquifers is that most of the water flows along the fractures. During pumping tests, the flow towards a fully penetrating borehole may be two dimensional (radial) throughout the fractured rock aquifer with well connected fracture system. During initial stages of pumping, water comes from fractures where it is temporarily stored after which, it flows from the matrix or minor fractures towards main fractures of the system (Karay, 2013; van Tonder et al., 2002).

Groundwater flow in fractured rock media is generally classified as either linear flow, bilinear, radial flow or spherical flow (Fig. 1a). Linear flow occurs when the fractures are infinite conductive features with negligible storage capacity. This phenomenon is common in sub-vertical fractures, geological faults or dykes (Kruseman et al., 1991). Bilinear flow happens when during pumping flow comes from formation towards fractures, typical in permeable matrix and conductive and storative fractures (Fig. 1b). It is common when there is a continuous fracture network that is embedded in porous matrix, a condition also called double porosity (Barenblatt et al., 1960). This condition was observed in the study area.

Radial flow also known as pseudo-radial flow is generally observed in a fully penetrating well drilled in any fractured reservoir that can be considered as a continuum. It happens when the cone of depression during pumping appears almost circular. Spherical flow occurs when spherical cone

of depression develops during pumping. However, this is short-lived as it further develops into radial flow because the spherical cone of depression reaches the bottom of the aquifer. Due to anisotropy effects in the aquifer, the spherical mode sometimes becomes an ellipsoid (van Tonder, 2002). These flow phenomena have an important implication on the renewal of groundwater resources and also movement of the contaminants or other dissolved substances.

Effects of geological conditions on groundwater recharge mechanisms

Geology is one key environmental factor that controls groundwater recharge in a catchment. Variations in geological conditions may thus affect groundwater recharge in different ways. Understanding the nature of the geological conditions, including nature of overburden soil and bedrock formation, is therefore critical when it comes to the effect it may have on groundwater recharge mechanisms.

Various researchers have investigated the effect of geological condition on recharge mechanisms. For example, Stadler et al., (2010) established that thick overburden sands of the Kalahari beds in Botswana influence lateral recharge mechanisms in the area. Liu et al., (2016) revealed that piedmont sediments of Hohhot Basin in China also enable lateral groundwater recharge. Kamchueng et al., (2015) also discovered that fractured rock Lake Nyos catchment in Cameroon aided lateral recharge process. Villeneuve et al., (2015) established that the riverbed sands of the perched aquifer system of Ti Tree Basin of central Australia enabled riverbed leakage type of recharge mechanism.

In unconsolidated deposits of lower reaches of Shire River Basin in Malawi, Monjerezi et al., (2011) revealed that diffuse recharge was the dominant mechanism in this geological condition. Li et al., (2017) also established that the loess overburden soils of Heihe Watershed in semi-arid China enabled diffuse type of recharge. Preferential recharge mechanisms were established in cenozoic sandstones of Mongolia (Tsujimura et al., 2007), thin glacial overburden of Tay River Watershed in Canada (Praamsma et al., 2009) and weathered crystalline rocks of Maheshwaram watershed in India by Alazard et al., (2016). In these studies, the nature of the

overburden soil and the condition of the primary geology determined the dominant recharge mechanism in each catchment.

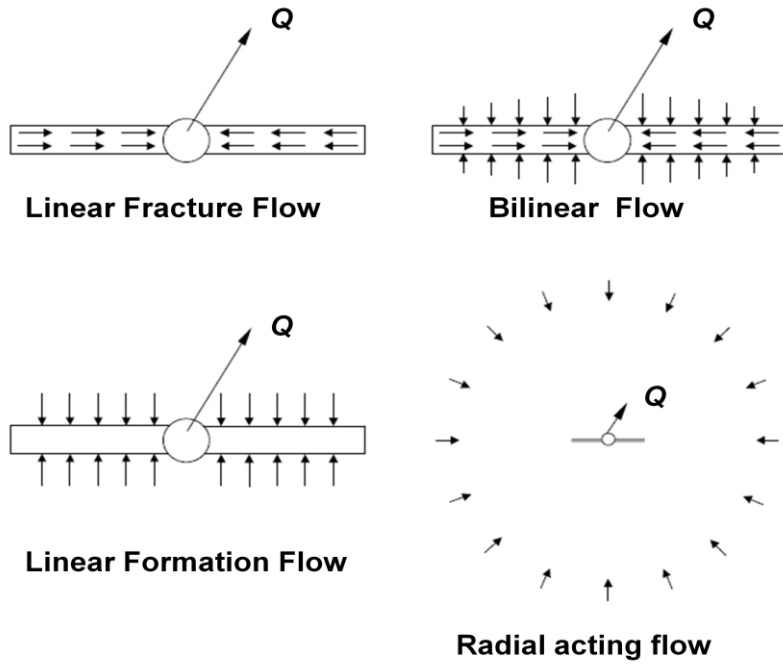


Fig. 1a: Different flow phases in fractures and/or matrix (adapted from Horne, 1997)

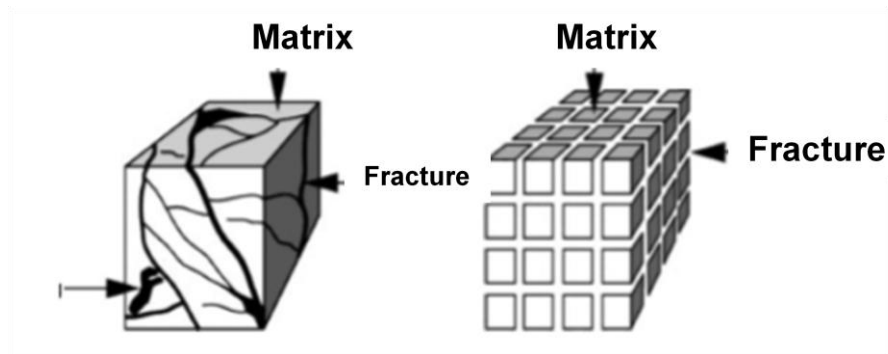


Fig. 1b: Double porosity fractured rock (Bilinear flow)

Effect of geological fault material on hydrological processes

Geological faults are fractures along which significant movements have occurred. The broken or sheared material in the fault zone may create a fault-zone-breccia. Depending on the original rock material and the nature or condition of the fault zone, geological faults may affect hydrological processes in different ways including acting as a conduit for flow, barrier to flow or a complex conduit/barrier phenomenon (Folch et al., 2011; Folch and Mas-Pla, 2008). This understanding provided the motivations for various researchers to try to understand how different geologies and fault materials influence hydrological processes.

In poorly lithified cenozoic sandstones of Paraiba Basin in Brazil, Balsamo et al., (2013) established that this kind of material enabled the geological fault to act as preferential conduit for flow. Williams et al., (2013) found out that Rio Grande Rift fill in most faults in the rift system of central New Mexico acted as preferential conduit to groundwater flow. Yuan et al., (2011) in Beiyishui River Watershed, North China Plain, established that sandy clay materials in the buried main normal geological fault enabled it to act as preferential conduit to groundwater flow in the Basin.

In Awash River Basin in Ethiopia, the clayey basalts were found to be enabling the fault to act as transverse conduit to groundwater flow (Ayenew et al., 2008). However, Delinom, (2009) established that consolidated brecciated rock material within the Lembang Fault enabled it to act as a barrier to groundwater flow. Similar observations were made in a fault with clay smearing in Roer Valley Rift System in Netherlands by Bense et al., (2003).

Apaydin, (2010) revealed that geological fault with siliciclastic deposits in Beypazari region in Turkey acted as both a conduit and a barrier from section to section. This phenomenon was also established in a geological fault with clay and sandy materials in Baton Rouge Fault in Louisiana (Bense and Person, 2006). All these studies showed how differently varied fault materials may affect hydrological processes in a catchment.

General remarks on literature review

In the described studies, it was specifically shown that overburden soils and fractured rock formations from selected geologies play critical role in groundwater recharge mechanisms and flow processes. However, the combined role of thin overburden soils, geological faults and fractured rock formations in semi-arid regions was not exhaustively clarified, providing room for further research.

Upper Rivirivi Catchment has a unique geology of fractured Hornblende-biotite-gneiss that is overlain by thin overburden soils in most parts and cut by geological faults. Understanding dominant recharge mechanisms in such rock formation and the effect of a geological fault cutting through it on groundwater flow is an interesting scientific task. Understanding how the thin overburden soils and underlying fractured Hornblende-biotite-gneiss affect the geochemical and stable isotopic fingerprints of the water molecules could provide insights into the sources of groundwater recharge and its flow processes.

1.3 Objectives

Gleeson et al., (2009) stated that climate, morphology and geology are some of the main factors that control groundwater recharge and flow processes in a catchment. In drier environments like semi-arid and arid regions, groundwater in fissured or fractured aquifers provides a reliable source of drinking water to millions of citizens. Generally, such groundwater is of better quality than surface water. However, fractured rock aquifers are susceptible to inter-annual climate variabilities due to their shallow depths (Guiheneuf et al., 2014).

In Malawi, about 35% of the total land area cover is characterized by fractured basement aquifers (MoAIWD, 2015; Mapoma and Xu, 2014). However, due to perceived low yields of these aquifers, less attention is given to the understanding of their hydrogeological processes for sustainable resource management. In Rivirivi Catchment, the majority of the boreholes fall in the fractured basement complex, servicing about 85% of the population (Knoema, 2015). In this regard, understanding how overburden soils, geological fault and fractured rock formations affect hydrological processes is an important water resource management tool. In this study, fractures (or joints) mean planes along which stress has caused partial loss of cohesion in the rock.

Various studies have addressed recharge and groundwater flow processes in different climatic regions and geological media (Oxtobee and Novakowski, 2003; Monjerezi et al., 2011, 2012; Senthilkumar et al., 2015; Villeneuve et al., 2015; Verbovsek et al., 2016). Local-scale rapid recharge to fractured rock aquifers overlain by glacial deposits has been investigated using hydraulic, isotopic and thermal data (Praamsma et al., 2009; Gleeson et al., 2009). The effect of geological faults in thick overburden siliciclastic formations has been highlighted, for example, where the fault acted as both a conduit and barrier from section to section (Apaydin, 2010). Generally, heterogeneities within the fractured rock formations make basic assumptions regarding recharge and groundwater flow processes that are applicable to porous media largely irrelevant in fractured rock formations. The role of overburden soils, geological fault and fractured Hornblende-biotite-gneiss on isotopic and geochemical fingerprinting and ultimately

deduction of subsequent groundwater recharge and flow processes provides an interesting research thematic area for sustainable resource management.

The combined use of isotopic and geochemical fingerprints of the water molecule rather than relying solely on hydraulic information, has been proved to be useful in providing insights into characteristics of recharge and groundwater flow processes in various rock media (Tsujimura et al., 2007; Steinbruch and Weise, 2014; Doveri et al., 2014). The objectives of this study were to use a combination of stable isotopes, geochemistry and hydraulics test to;

- (1) Investigate spatial and temporal isotopic and geochemical evolution of an uncharacterized fracture network;
- (2) Identify dominant recharge and groundwater flow processes in a leaky fractured formation with unknown parameters and;
- (3) Clarify effect of a geological fault cutting through a fractured network of unknown size and geometry on flow processes.

The author's hypothesis was that such unique geological setting could have a unique effect on hydrological processes, divergent from other geologies. Understanding these factors is necessary for sustainable management of the resource particularly in data scarce catchments like Upper Rivirivi Catchment, which is an exorheic catchment within Shire River Basin.

Dissertation outline

There are five (5) main parts to this dissertation followed by conclusion chapter. General setting on the condition of water resources in semi-arid regions is presented in the first part. It specifically highlights the role fractured rock aquifers play in supporting rural livelihoods in developing countries. It is followed by literature review which stipulates the various studies on recharge and groundwater flow processes that have been carried out in different climatic and geological conditions and why it is important to understand the role specific geological conditions play on recharge and groundwater flow processes. The research objectives are

presented and the methods used to achieve these objectives are also discussed in this part. Part two (2) discusses the general description of Upper Rivirivi Catchment and the status of groundwater resource in the study area. It also dwells on communities' access to potable water and provides first attempt to estimate average annual recharge rate for the catchment.

Part three (3) presents the methods used in this study. This specifically includes geochemistry, stable isotopes and pumping tests. Part four (4) presents the results as established from the methods discussed in part (3). Part five (5) discusses the dominant geochemical processes associated with fractured Hornblende-biotite-gneiss. It also highlights the groundwater recharge sources and mechanisms associated with this geological formation. Understanding of recharge and flow processes active in such medium is also attempted. Effect of Ntcheu Fault as regards groundwater flow is also established and explained under this section. The way how overburden soils, geological fault and fractured Hornblende-biotite-gneiss rock formation affect recharge and groundwater flow processes is then presented for the reader to appreciate such processes. The final part provides the conclusions of the final findings from this study and how the results may inform sustainable water resource management measures or strategies in similar geological settings.

Chapter 2: Study Area

2.1 Site description

Location

Upper Rivirivi Catchment lies within middle Shire River Basin between longitudes 34° 34' 0"E and 34° 49' 0" E and latitudes 14° 44' 0"S and 15° 00' 0"S and on the border between administrative regions of central and southern Malawi (Fig. 2d). It covers an area of about 744 km² and has an estimated population of over 72,000, 85% of which rely on groundwater sources (Knoema 2015; MoAIWD, 2015). The elevation generally decreases from northwest towards southeast, ranging from 1,700 to 800 meters above sea level (Fig. 2a). It falls within the western branch of the East African Rift Valley system.

The Great East African Rift is an active continental rift zone in East Africa. It began developing around the emergence of the Miocene, about 25 million years ago. It is believed that the rift is in the process of splitting into the Somali Plate and the Nubian Plate at a rate of 6 mm per year (Chorowicz, 2005) raising fears that it will break off in about 10 million years time. The rift runs through Ethiopia, Kenya, Uganda, Rwanda, Burundi, Zambia, Tanzania, Malawi and Mozambique.

The Malawi Rift is 650 km long and 60 km wide and is mostly covered by Lake Malawi which in itself is 500 km long and water surface at 472 m. Its shoulders are at more than 2000 m in the central part and 1500 m in the southern. The maximum recorded depth is 700 m (Chorowicz, 2005). The study area falls under the rift fault line that connects Lake Malawi to the Zambezi rift.

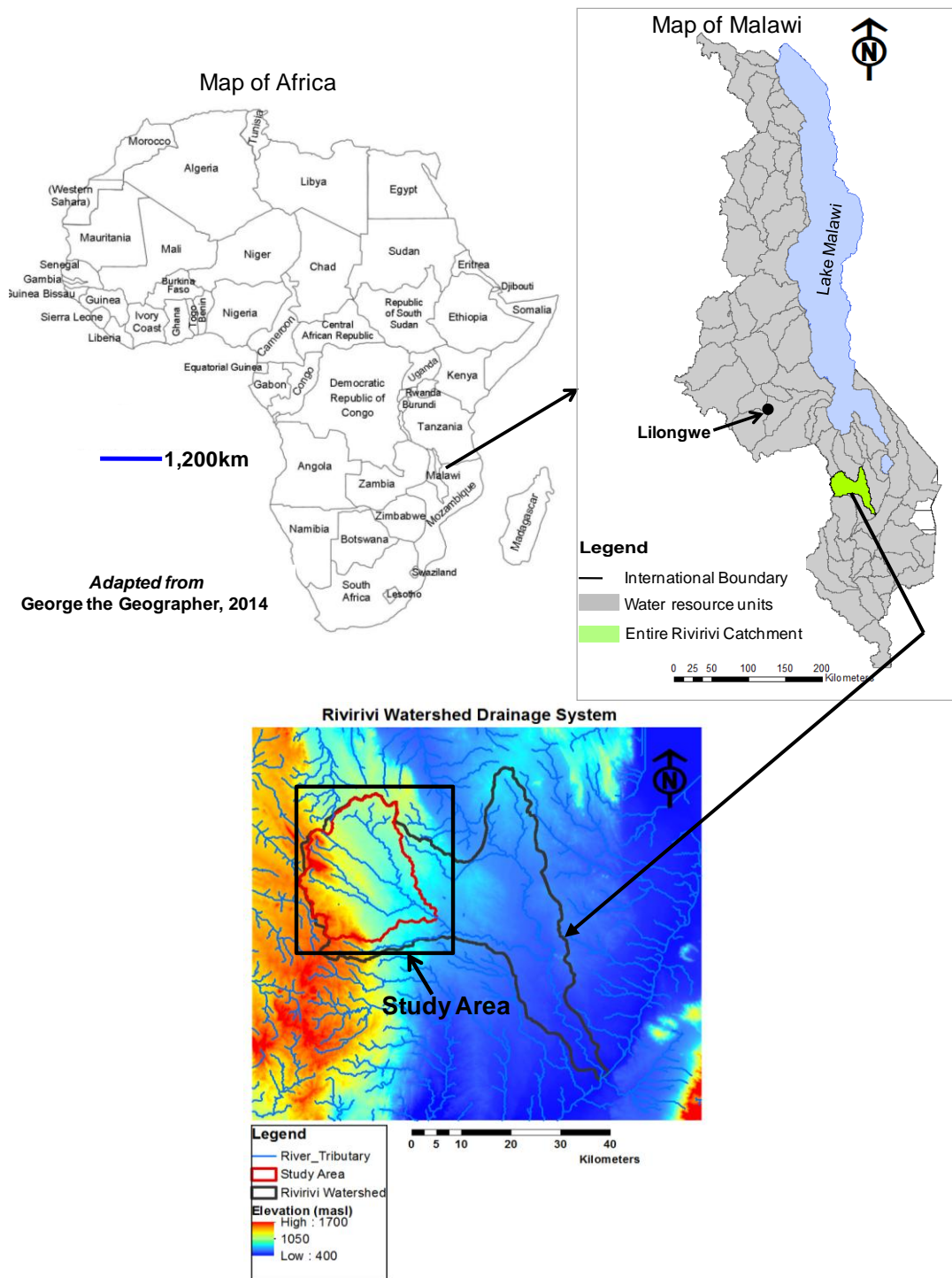


Fig. 2a: Watershed Drainage System in the study area (Kambuku, 2018)

Climate

The study area has a dry sub-humid to semi-arid climate, with the higher areas receiving more rainfall than the low-lying locations. It has two main seasons - rainy season running from November to April and dry season from May to October every year. It receives a mean annual rainfall of 1060mm. Average Potential Evapotranspiration (PET) is estimated to be 933mm per year. Mean Annual Temperature varies from 14°C in June to around 24°C in October. The rain events are affected by three major synoptic systems - the Inter Tropical Convergence Zone (ITCZ), the Zaire Air Boundary (ZAB), and tropical cyclones. Like any location in Malawi, Rivirivi catchment is equally vulnerable to the less predictable El Nino and Southern Oscillation (ENSO) phenomena (Meteorological Services 2016; Chavula, 2012).

The United Nations Environment Program (UNEP, 1997) has adopted an index of aridity, defined as:

$$AI = P/PET \quad (1)$$

where *PET* is the potential evapotranspiration and *P* is the average annual precipitation. Hyper-arid: <0.05, arid: 0.05-0.20, semi-arid: 0.20-0.50, dry sub-humid: 0.5-0.65 and sub-humid to humid: >0.65. The study area has a Mean Annual Precipitation of 1060 mm/year and estimated Potential Evapotranspiration (PET) of 933 mm/year, giving Aridity Index (IA) value of 1.1 and thus classified as sub-humid to humid region. Most of this precipitation falls from November to April (6 months) with the rest of the months of the year with no or near zero precipitation values. Fig. 2b shows mean annual rainfall values for the study area from 1998 to 2009. As can be seen from Fig. 2b, Upper Rivirivi Catchment experienced highest mean annual precipitation of around 1600 mm in 2003 followed by drier year in 2004. No average monthly temperature data was available for the study area within the same time frame as precipitation.

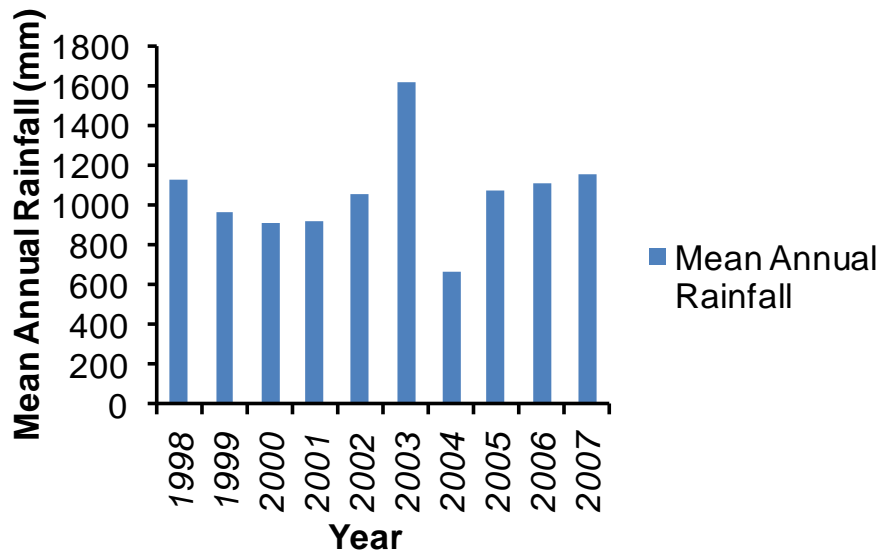


Fig. 2b: Mean Annual Rainfall at Nkhande Rain-station in Upper Rivirivi Catchment

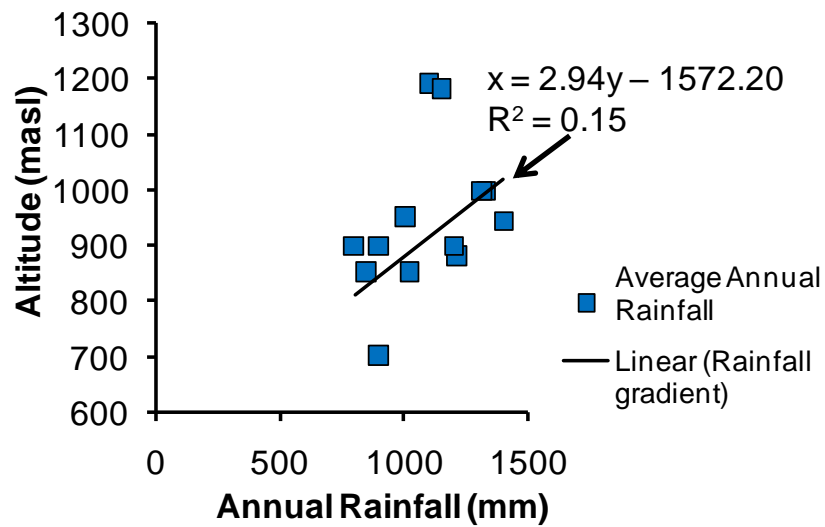


Fig. 2c: Rainfall and Altitude Relationship in Southern Malawi
 (adapted from Ministry of Agriculture, Irrigation and Water Development, 2015)

Fig. 2c shows the relationship between altitude and rainfall. It illustrates a positive correlation in altitudes of over 700 m above sea level. In as much as it presents a generally weaker positive correlation, this relationship can help us estimate preliminary precipitation values in areas where there are no rain-stations if we know their average altitude information. The annual rainfall and altitude data used in this figure were from rain-stations in southern region of Malawi. This helped understand the variations of precipitation with altitude in the study area since Upper Rivirivi Catchment had only one operational rain-station at Nkhande Residential Training Centre of Ministry of Agriculture at the time of this research (Fig. 5).

Geology

Physiographically, the study area has the Kirk Plateau which lies between the Malawi-Mozambique international border and the Kirk range scarp and merges into the Angoniland Plateau to the north. It also has The Nsipe-Livelezi Shelf which extends from the foot of the Kirk Range scarp to the lower scarp overlooking the Bwanje Valley and which has been faulted in the south to form an additional step called Kanzati step. The steps and the plateau were regarded as fault-splintered sections of the mid-Tertiary peneplain with easterly or westerly tilts, separated from the early Cretaceous Shire Valley floor by early Cretaceous and Late Tertiary faults. The residuals were thought to be remnants of the late Jurassic peneplain (Bloomfield & Garson, 1965).

Basement Complex rocks, mainly paragneisses, cover over 80% of the area. These comprise hornblende-biotite-gneisses, often garnetiferous and locally containing a high proportion of epidote; biotite-nepheline-gneisses; quartzofeldspathic granulites; diopside bearing gneisses; psammitic and pelitic gneisses; charnockitic gneisses; marbles and thin bands of metadolerite. Ntcheu Fault and many other smaller local faults cut through upper Rivirivi Catchment (Fig. 2d). Most of the upper layer gneisses (about 50 m) is fractured and may be assigned to the almandine-amphibolite metamorphic facies except the small areas of higher grade charnockitic granulite (Bloomfield & Garson, 1965).

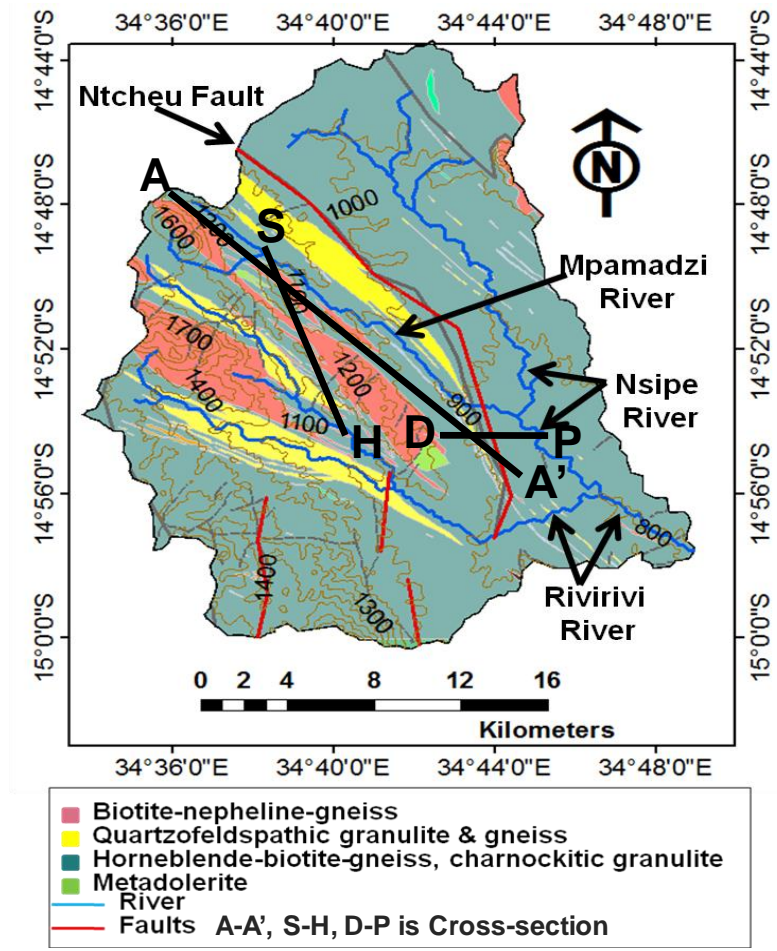


Fig. 2d: Geological map of the study area (Kambuku, 2018)

Hydrogeology

The basement complex covers about 70% of Malawi's land surface area and supplies water to approximately 60% of the population (Mapoma et al., 2014). This includes the fractured basement aquifers to which this study area falls into.

Unlike most plateau areas that are largely drained by grass-covered swampy valleys, Upper Rivirivi Catchment has incised valleys that cut through the fractured basement formations (Photo 3). The other unique characteristic that distinguishes it from other plateau areas is the presence of thin overburden soils. Groundwater in this type of rock formation is believed to be confined to narrow fault-zones, bands of pervious granulite or gneiss and local or regional pockets of superficial weathered rock (Warshaw, 1965).

Fig. 2e shows hydrogeological cross-section constructed from borehole lithological data collected from Department of Water Resources and Department of Geological Surveys. It also shows stratigraphic outlay of weathered lateritic overburden from 30 mm up to 3 m thickness, weathered biotite gneiss to about 20 m thick, basal breccia (aquitard) 0.5 m thick, fractured hornblende-biotite-gneiss of about 35 m thickness and impermeable bedrock. Borehole yields data collected from Ntcheu District Water office and the hydraulic tests we conducted show that Upper Rivirivi Catchment has borehole yields ranging from 0.3 L/s to 2 L/s.

In situ measurements done during field surveys in September, 2015 showed that static water levels for shallow groundwater (SGW) at ridge section were at a shallower depth ranging from 9.5 meters below ground level (mbgl) to 11 mbgl than deeper groundwater (DGW) at valley section that ranged from 15 mbgl to 38 mbgl. Piezometric data indicates groundwater regime that flows following decrease in topography and presence of geological features such as faults and ridges. As a result, screens were located at shallower depths for ridge section boreholes (around 20 mbgl) than those at valley section (around 35 mbgl). Borehole depths ranged from 28 m to 30 m for SGW and 36 m to 48 m for DGW (Table 1). In this study, description of shallow groundwater and deeper groundwater followed borehole architecture. Wells with screens located

not deeper than 23 m were classified as shallow groundwater and were largely located along the ridge section while those with screens located deeper than 23 m were classified as deeper groundwater and were largely located in the valley section and close to Ntcheu fault.

The Ministry of Agriculture, Irrigation and Water Development published characteristics of major aquifer systems in Malawi in 2006 (Ministry of Irrigation and Water Development, 2006) that focused on Weathered Basement Complex and Alluvial aquifers only. In this study, we have attempted to provide aquifer characteristics of the fractured rock formation from hydraulic tests and numerical models. Table 2 shows comparison of these characteristics with those previously published by the Ministry. It is worth noting that despite fractured rock aquifers being regarded as generally low yielding, the study area shows geological sections that are higher yielding than Weathered Basements with yields reaching as high as 2L/s and sustaining a constant pumping test of the same yield for 12 hours. In this regard, understanding hydraulic conductivity of the fracture itself and of the medium in the direction parallel to the fractures and the variations of the Transmissivity is important. Equations 2 and 3 show how the discussed hydraulic conductivities are calculated with 2 for single fracture and 3 for medium;

$$K_f = (2b)^2 \frac{\rho g}{12\mu} \quad (2)$$

$$K = \frac{(2b)^3}{2B} \frac{\rho g}{12\mu} \quad (3)$$

where b is the fracture aperture, ρ is density of water, g is acceleration due to gravity, $2B$ is fracture spacing and μ is viscosity of water.

The calculated hydraulic conductivity of the fractured rock formation in the study area ranged from 0.3 to 4.5 m/day. In any other direction, the hydraulic conductivity is zero. This is called the CUBIC LAW because of the nature of the dependence of hydraulic conductivity on fracture aperture. Cook et al., (2003) stated that a doubling of the fracture aperture results in a factor-of-eight (8) increase in conductivity. Fig. 4 shows the fracture aperture of up to 1 cm resulting in a hydraulic conductivity of about 3.5 m/day if the fracture spacing of $2B = 1$ m.

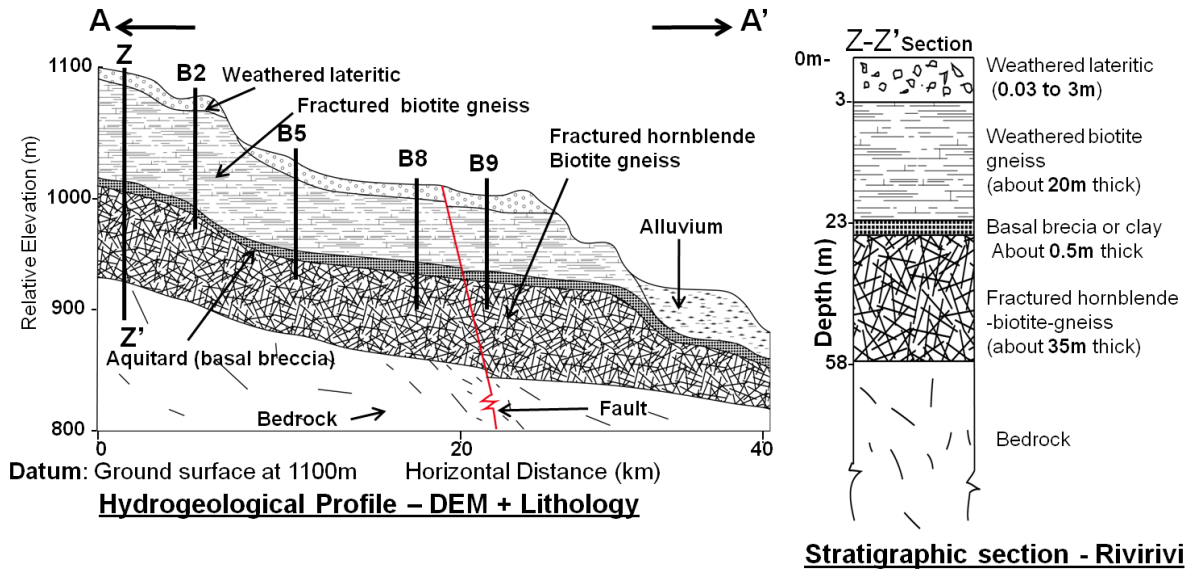


Fig. 2e: Hydrogeological cross-section of Upper Rivirivi Catchment. Location of A-A' is as shown in Figure 2d (Kambuku, 2018)

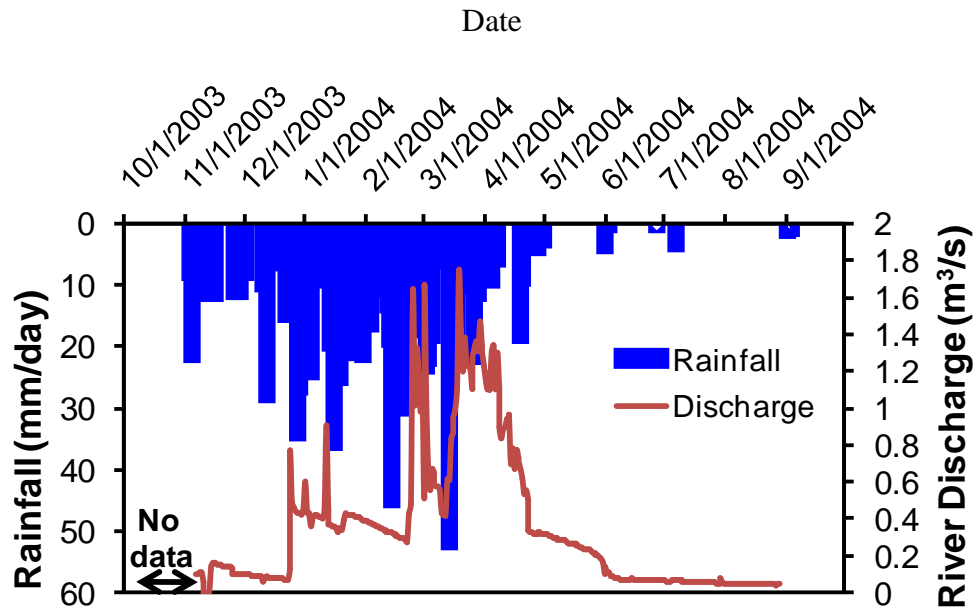


Fig. 3: Daily Rainfall and River Discharge at IR19 River Gauging Station as shown in Figure 5

Rivirivi River is one of the perennial rivers that cut through the fractured hornblende-biotite-gneiss in the study area. Fig. 3 shows daily rainfall in millimeters (mm) and river discharges in cubic meters per second (m^3/s) as recorded at 1R19 River Gauging Station (Fig. 5) in 2003/2004. Baseflow data shows an immediate response to the amount of precipitation in the study area. This baseflow data phenomenon provides first cue to the role fractures play in river water and groundwater interaction in this area.

Table 1: Representative boreholes location data, water level and screen location.

ID	y	X	Location		Water Level (mbgl)	Water Level (masl)	BH Depth (mbgl)	Screen location (mbgl)	Screen length (mm)
			Distance (km) from upstream	Elevation (masl)					
Deep groundwater (DGW) at Valley section									
B4	-14.861	34.6493	9.0	1178	29.00	1149.0	43.0	30	2900
B6	-14.901	34.6768	13.1	1068	19.00	1049.0	40.0	30	2900
B10	-14.876	34.7136	16.6	949	10.20	938.8	38.1	28	2900
B11	-14.900	34.7350	19.4	872	11.00	861.0	36.0	33	1000
B8	-14.905	34.7286	19.1	872	38.00	834.0	48.0	36	2900
B14	-14.931	34.7432	22.0	869	18.00	851.0	47.0	24	1000
B9	-14.908	34.7353	20.0	862	17.00	845.0	45.0	36	1450
B19	-14.910	34.7478	23.0	862	17.10	845.0	41.0	35	1450
B13	-14.936	34.7509	22.5	854	15.00	839.0	38.0	28	1000
B12	-14.925	34.7503	21.2	838	16.00	822.0	36.0	27	2900
Shallow groundwater (SGW) at Ridge section									
B3	-14.853	34.6436	7.9	1187	9.5	1177.5	30	22	1450
B2	-14.837	34.6354	6.7	1158	10.0	1148.0	31	20	1450
B1	-14.822	34.6400	5.4	1140	10.1	1129.9	29	20	1450
B5	-14.866	34.6661	11.0	1126	11.0	1115.0	28	21	1450

Where mbgl is *meters below ground level* and masl is *meters above sea level*

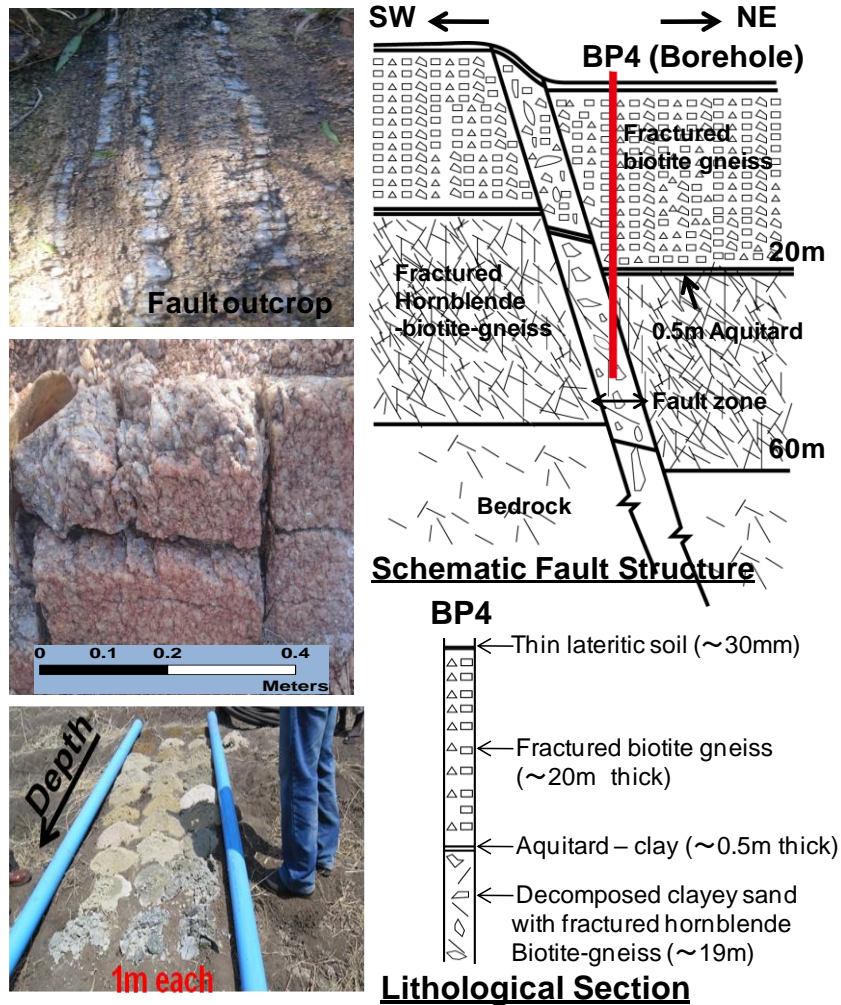


Fig. 4: Outcrop fractures and fault structure at BP4. See the location in Figure 5

Table 2: Characteristics of aquifer systems in Malawi (revised from Ministry of Irrigation and Water Development, 2006)

Parameters	Weathered Basement Complex	Alluvial Aquifer	Fractured Basement Aquifer (this study)
Borehole Yield (L/s)	1.0-2.0	15	0.3-2.0
Hydraulic conductivity (m/day)	0.5-1.5	1-10	0.3-4.5
Depth of boreholes (m)	45-50	60	28-48
Depth of water table (m)	15-25	5-10	10-20
Transmissivity (m ² /day)	5-35	50-300	10-136
Storage coefficient	5×10^{-3} - 1×10^{-2}	1×10^{-2} - 5×10^{-2}	1.35×10^{-6} - 2.2×10^{-3}

2.2 Sampling points

A detailed geochemical and isotopic sampling was conducted in dry season (September, 2015) and the other in rainy season (March, 2016) where a total of 64 groundwater samples, 10 river samples, 2 dam samples, 6 spring samples and accumulated rain sample at Nkhande Weather Station were collected (Fig. 5). During rainy season, the samples were collected a week after a major rainfall event. pH values (HORIBA Ltd., Twin PH Meter B121), Total Dissolved Solids (TDS; Hanna 50-HI9033), Temperature (Nikkyo Technos Co. Ltd., Petten Kocher), and groundwater levels (dry season) were measured *in situ*. Portable Global Positioning System meter (GPS meter; GARMIN Ltd., GPSMAP 76S) was used to establish locations of the sampling points.

Two pairs of borehole sites juxtaposed across Ntcheu fault (Fig. 5) were selected for pumping tests in rainy season (March, 2016) to infer fracture location, connectivity and the role of the fault on groundwater flow. Step tests with varying discharge rates were conducted at all sites for one hour after which a constant rate for each site was determined, that is 1 Liter per second (L/s) for Borehole Pumping Test Point No. 1 (BP1), 2 L/s for Borehole Pumping Test Point No. 2 (BP2) and 0.5 L/s for Borehole Pumping Test No. 3 (BP3) and Borehole Pumping Test No. 4 (BP4) (Table 4). van Tonder et al. (2002; 2001) specifies that if the purpose of the pumping test in fractured rock aquifers is to identify fracture location, connectivity and understand flow responses to pumping, a minimum of 8-hour constant pumping test is required. However, for this study, a 12-hour constant pumping test was selected. We used a negative displacement pump (2.2kw Franklin Submersible pump Model; Franklin Electric South Africa PTY Ltd) to carry out these hydraulic tests. Drawdown water levels were measured in graduating sequences of 1's, 2's, 5's, 10's, 15's, 30's, and 60 minutes until a total of 720 minutes (12 hours) using Electronic Module IP65 dipper-T water level meter (Heron Instruments Groundwater Monitoring Inc., Canada). All water level observations were done within the pumped wells (single well tests) as no observation wells were present.

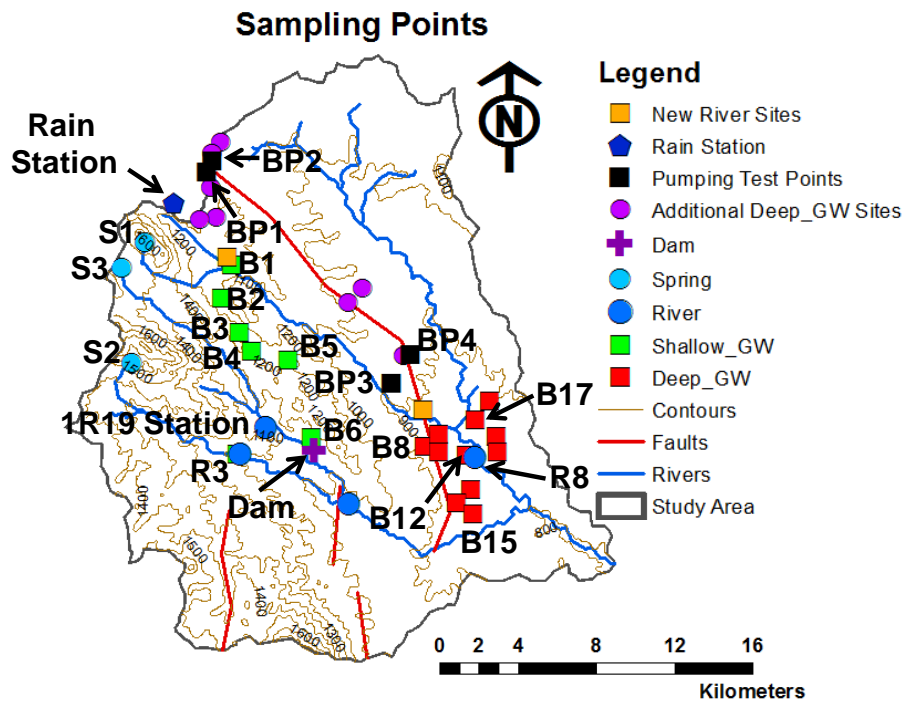


Fig. 5: Sampling Points (Kambuku, 2018)

The shallow groundwater sites (borehole screens located not deeper than 23 m and with thin overburden soils of up to 30 mm) are mainly located along the ridge while deeper groundwater sites (borehole screens located deeper than 23m and with thicker overburden soils of up to 3 m) are located along the valley and close to Ntcheu Fault. Springs are located in the higher altitude areas and are the sources of the perennial rivers (including Rivirivi River) in the catchment (Fig. 2d; Fig. 5). Photos 1-5 show agricultural activities that are supported by spring water close to S2, Dam sampling point at D1, incised gaining river at Kaiyatsa (R3), a visual of a well drilled into the fractured formation at Ntcheu Boma and pumping test exercise in progress at BP3.



Photo 1: Agricultural activities using spring water next to S2



Photo 2: Mpira Dam sampling point (D1). For location see Figure 5



Photo 3: River sampling point at Kaiyatsa (R3)



Photo 4: Borehole drilled in fractured formation at Ntcheu Boma



Photo 5: Pumping Test exercise at BP3. For location see Figure 5

2.3 Groundwater Level Contours

Groundwater level monitoring is a useful tool to establish resource variations with time (Lachaal et al., 2016). Fig. 6 shows groundwater levels as measured in dry season (September, 2015) at high altitude areas (Springs), ridge section with thin overburden soils of about 30 mm (shallow groundwater) and valley section with thicker overlying soils of about 3 m (deeper groundwater). Groundwater level contours show that springs in high altitude areas have groundwater levels close to the land surface and distributed in a similar pattern as surface water. Groundwater level contours also show reverse local groundwater flow pattern at ridge section (B4).

At valley section, groundwater level contours show deeper orientation as opposed to higher altitude areas. This is the area that has thicker overburden soils. The contours also show convergence of two flow patterns originating in the NW and NE direction and converging at B13. Generally, however, groundwater level contours show regional groundwater flow that follows the topography in the NW-SE direction, signifying that the catchment could have lateral fracture connectivity. Since all wells are production wells, the communities did not permit water level measurements in rainy season (March, 2016) for us to establish temporal variations.

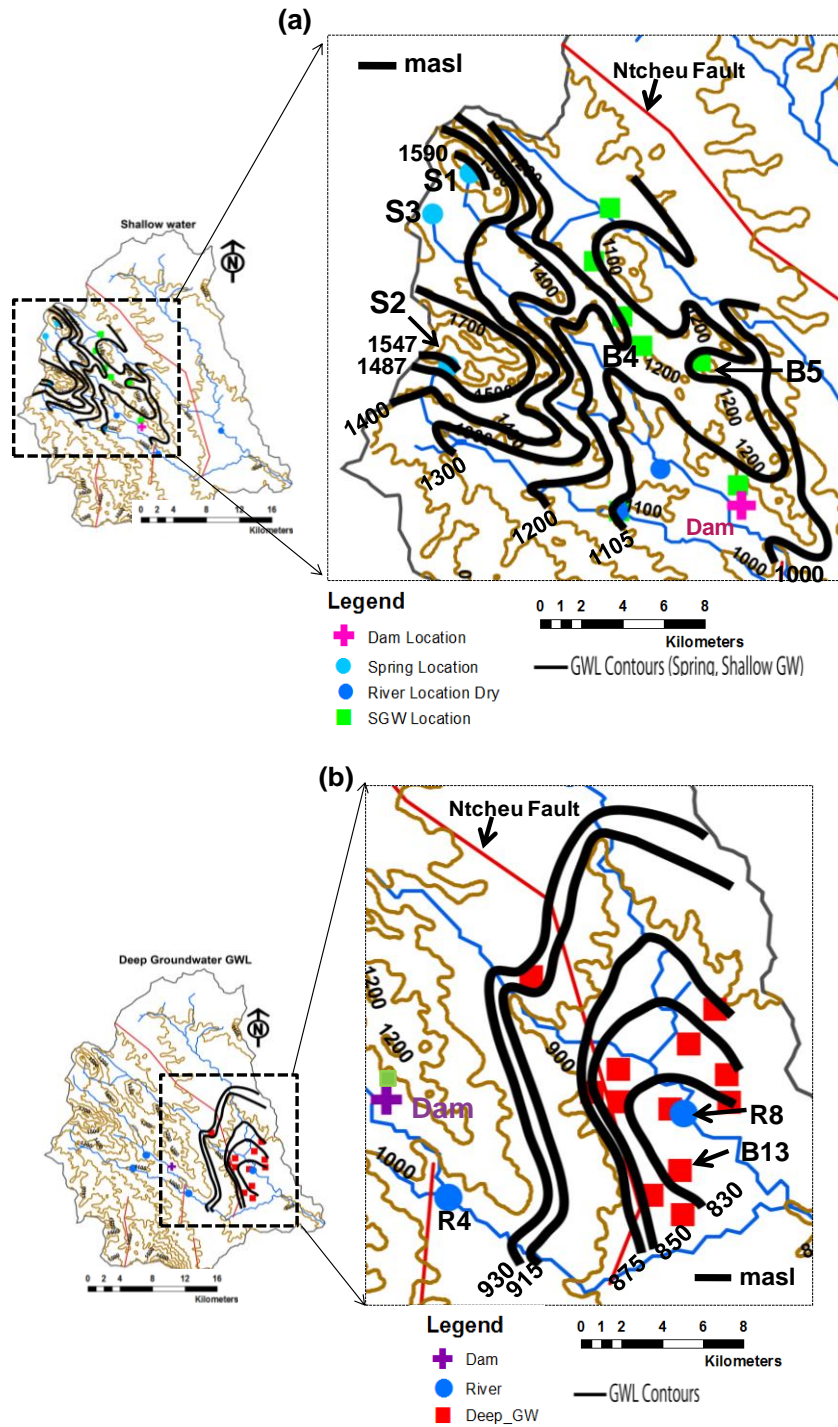


Fig. 6: Groundwater level contours at (a) Shallow groundwater ridge section (b) Deeper groundwater valley section. Water levels collected in dry season (September, 2015)

Average Annual recharge rate (AARR) estimates

Groundwater recharge is an important component of the hydrological cycle and in the study area the most dominant source of groundwater recharge is precipitation. Hill and Kidd (1980) stated that the Run-off/Rainfall mean ratio for Malawi is 27%. Despite that a lot of geomorphologic features have changed since 1980, 27% was used as a conservative figure in the calculation of Average Annual Recharge Rate (AARR).

According to Marechal et al., (2009) and some insights from Dassi (2010), AAAR can be calculated using Chloride Mass Balance equation as below;

$$\text{AARR} \left(\text{mm/year} \right) = \frac{\{(P[\text{Cl}^-]_{\text{rain}}) - (\text{run-off}[\text{Cl}^-]_{\text{river}})\}}{[\text{Cl}^-]_{\text{groundwater}}} \quad (4)$$

where P is annual rainfall in mm/year, $[\text{Cl}^-]$ is mean annual chloride concentration in mg/L, $[\text{Cl}^-]_{\text{rain}}$ is mean annual chloride in rain and $[\text{Cl}^-]_{\text{groundwater}}$ is mean annual chloride concentration in groundwater.

The conditions under which this formula is valid include the establishment that there is no geogenic source of chloride in the study area, negligible residual chloride in soil originating from evaporation of atmospheric water or capillary rise water and that chloride input from anthropogenic sources is also negligible.

Upper Rivirivi Catchment receives an annual rainfall of 1060 mm. Considering 27% of this as run-off gives run-off value of 286.2 mm/year. Chloride values were established from inorganic ion analysis using Ion Chromatograph (Shimizu Co., Ltd., HIC-SP/VP Super).

Therefore, with;

Rainfall (P) = 1060 mm/year; Run-off = 286.2 mm/year; $Cl_{rain} = 2.5$ mg/L;
 $Cl_{river} = 2.55$ mg/L; $Cl_{groundwater} = 16.3$ mg/L and substituting in Equation (4),

Average Annual Recharge Rate (AARR) = 117.8 mm/year

This recharge component is supposed to be added to aquifers through the fracture pathways of the fractured rock formation. This hypothesis was tested and proved by using stable isotopic, geochemical and hydraulic test data sets as can be seen in the Chapters 4-5.

Chapter 3: Methodology

3.1 Geochemistry and stable isotopes

Selection of type of methods to be used in any research is a critical step to realize the intended goals. In this study, geochemistry, stable isotopes and hydraulic tests were selected to help achieve the study objectives. To achieve this, a detailed geochemical and isotopic sampling was conducted in dry season (September, 2015) and the other in rainy season (March, 2016) where a total of 64 groundwater samples, 10 river samples, 2 dam samples, 6 spring samples and accumulated rain sample at Nkhanda Weather Station were collected (Fig. 5). During rainy season, the samples were collected a week after a major rainfall event. The pH values (HORIBA Ltd., Twin PH Meter B121), Total Dissolved Solids (TDS; Hanna 50-HI9033), Temperature (Nikkyo Technos Co. Ltd., Petten Kocher), and groundwater levels (dry season) were measured *in situ*. Portable Global Positioning System meter (GPS meter; GARMIN Ltd., GPSMAP 76S) was used to establish locations of the sampling points.

Major anions (Cl^- , NO_3^- and SO_4^{2-}) were measured using Ion Chromatograph (Shimadzu Co., Ltd., HIC-SP/VP Super) while major cations (Na^+ , Ca^{2+} , Mg^{2+} , K^+) were measured using Optima 7300 V ICP-OES Spectrometer (PerkinElmer Inc.). Bicarbonate (HCO_3^-) concentration was measured using a titration method with sulphuric acid (H_2SO_4). To validate the geochemical data, ionic balance of the major ions was conducted on all samples. All samples showed ionic balance of less than 10% indicating that the geochemical data was reliable for further interpretation (Table 6A).

All groundwater samples were collected from production wells an hour before the communities started using each well. To avoid air intrusions, the samples were loaded while fully immersed under water into a 100 mL polyethylene bottle each and transported to Japan (University of Tsukuba) for isotopic and major ions analyses. All the samples were analyzed for stable isotopes of water ($\delta^{18}\text{O}$ (‰) and δD (‰)) using PICARRO L2120i Cavity Ringdown Spectrometer and values are herein reported as per mil (‰) deviations from Vienna Standard

Mean Ocean Water (V-SMOW). In this analysis, the analytical reproducibility for $\delta^{18}\text{O}$ and δD was better than 0.5‰ and 1‰ respectively.

3.2 Pumping Test

Two pairs of borehole sites juxtaposed across Ntcheu fault (Fig. 5) were selected for pumping tests in rainy season (March, 2016) to infer fracture location, fracture connectivity and the role of the fault on groundwater flow. Step tests with varying discharge rates were conducted at all sites for one hour after which a constant rate for each site was determined, that is 1 Liter per second (L/s) for Borehole Pumping Test Point No. 1 (BP1), 2 L/s for Borehole Pumping Test Point No. 2 (BP2) and 0.5 L/s for Borehole Pumping Test No. 3 (BP3) and Borehole Pumping Test No. 4 (BP4) (Table 4). van Tonder et al. (2002) specifies that if the purpose of the pumping test in fractured rock aquifers is to identify fracture location, connectivity and understand flow responses to pumping, a minimum of 8-hour constant pumping test is required. However, for this study, a 12-hour constant pumping test was selected. We used a negative displacement pump (2.2kw Franklin Submersible pump Model; Franklin Electric South Africa PTY Ltd) to carry out these hydraulic tests. For BP1, the pump was set at a depth of 29 m, BP2 at 45 m, BP3 at 37 m while BP4 was set at 37 m as well. Drawdown water levels were measured in graduating sequences of 1's, 2's, 5's, 10's, 15's, 30's, and 60 minutes until a total of 720 minutes (12 hours) using Electronic Module IP65 dipper-T water level meter (Heron Instruments Groundwater Monitoring Inc., Canada). All water level observations were done within the pumped wells (single well tests) as no observation wells were present.

To validate observed pumping test data and calculate additional parameters like transmissivity, storativity and understand the dominant hydraulic phenomena of the fractured Hornblende-biotite-gneiss rock formation, numerical models were used.

Governing equations

Fractured rock aquifer is usually a heterogeneous medium with storativity potential but low permeable rock matrix and highly permeable fractures of low volume. Groundwater flow takes place between fractures and blocks. The fractures provide the main flow path while the rock matrix act as a source or sink to fractures. These conditions make the behavior of naturally fractured rock aquifers different from those composed entirely of inter-granular porosity and permeability (Altinors and Onder, 2008). In this regard, groundwater flow in fractures is usually governed by laminar flow which in turn can be expressed by a special case of Darcian Law called Cubic Law (5) as;

$$Q = \frac{b^3 \rho g h}{3\mu} \left(\frac{\Delta h}{\Delta l} \right) \quad (5)$$

Q is flow through the area A (L^3T^{-1}), Δh is potential or head difference over the length of interest l (L), Δl is length of interest (L), b is aperture or width of the fracture (L), h is the height of the fracture (L), μ is dynamic viscosity ($ML^{-1}T^{-1}$), g is acceleration due to gravity (LT^{-2}), and ρ is density of the fluid (ML^{-3}).

Considering (5) above, the cone of depression produced by a pumped well at location $P(r, z)$ in a fracture system is described by diffusivity equation in cylindrical coordinates as developed by Moench, (1984) as below;

$$K \frac{1}{r} \frac{\partial}{\partial r} \left[r \frac{\partial h(r,t)}{\partial r} \right] + K_z \frac{\partial^2 h(r,t)}{\partial z^2} = S_s \frac{\partial h(r,t)}{\partial t} + q_b \quad (6)$$

h is hydraulic head (L), r is distance P to the borehole (L), with $r \geq r_w$, r_w is drilled radius (L), z is vertical location of P (L), K is conductivity of the continuum fracture network (LT^{-1}), K_z is vertical conductivity of the fracture network (LT^{-1}), S_s is specific storage coefficient of the aquifer (LT^{-1}) and q_b is additional source function.

Equation (6) is valid only when gravity acceleration and fluid properties remain constant. In a fully penetrating well, the second term on the left-hand side in equation (6) becomes zero. This is because hydraulic head, h does not change with depth, z .

Solving equation (6) under different boundaries is usually possible with the use of Laplace transformation as shown in equation (7) below. The boundary conditions considered under this are radial symmetric boundary conditions.

$$L\{h(t)\} = \bar{h}(p) = \int_0^{\infty} e^{-pt} h(t) dt \quad (7)$$

Using Stehfest, (1970) algorithm, Laplace transform (equation (7)) can be easily inverted to be used in derivation of solutions for drawdown in wells. Stehfest, (1970) algorithm is as follows;

$$h(t) \approx \left(\frac{\ln 2}{t}\right) \sum_{i=1}^N V_i \bar{h}(p) \left[\frac{i \ln 2}{t}\right] \quad (8)$$

V_i in this case represents weighing factors calculated as

$$V_i = -1 \binom{N}{2} + 1 \sum_{k=\frac{i+1}{2}}^{\min(i, \frac{N}{2})} \frac{k^{\frac{N}{2}+1} (2k)!}{\left(\frac{N}{2}-k\right)! k! (k-1)! (i-k)! (2i-k)!} \quad (9)$$

With N as even number and i, k as integer values.

Warren and Root, (1964), Kazemi et al., (1969), and Bourdet and Gringarten (1980) as pioneers in this field showed how to calculate Transmissivity (T_f) and Storage coefficient (S_f) of the fracture system and that of the rock matrix (S_m) and how to determine drawdown in a fractured aquifer of the double porosity nature in a pumped well as below;

$$T_f = \frac{0.183Q}{d} \quad (10)$$

$$S_f = \frac{2.25t_{01}T_f}{r_w^2} \quad (11)$$

$$S_m = \left[\frac{2.25t_{02}T_f}{r_w^2} - S_f \right] \beta \quad (12)$$

For early pumping times, the water is entirely coming from the fracture system where ($\beta = 0$) and drawdown, d_p is calculated as below;

$$d_p = \frac{2.25Q}{4\pi T_f} \log_{10} \left[\frac{2.25T_f t}{S_f r_w^2} \right] \quad (13)$$

For late pumping times, water is assumed to come from both the fracture and the low permeable rock matrix and drawdown d_p is calculated as below;

$$d_p = \frac{2.25Q}{4\pi T_f} \log_{10} \left[\frac{2.25T_f t}{(S_f + \beta S_m) r_w^2} \right] \quad (14)$$

where d_p is drawdown response to pumping [L], t is pumping time, r_w is effective well radius [L], T_f is transmissivity of fractured system [L^2T^{-1}], S_f is storage coefficient of the fracture system [-], S_m is storage coefficient of the rock matrix [-], β represents shape factor: 1/3 for spherical blocks for late pumping times in this study area [-], t_{01} is time the first straight line intercepts the time

axis (T), t_{02} is time the second straight line intercepts the time axis (T) and d is drawdown of the straight lines over one log cycle [-] and is calculated as

$$= \frac{(3((d_p-1)\text{Log}_{10}(t-1)+(d_p)\text{Log}_{10}(t)+(d_p+1)\text{Log}_{10}(t+1))-((d_p-1)+(d_p)+(d_p+1))(\text{Log}_{10}(t-1)+\text{Log}_{10}(t)+\text{Log}_{10}(t+1)))}{(3((\text{Log}_{10}(t-1))^2+(\text{Log}_{10}(t))^2+(\text{Log}_{10}(t+1))^2)-(\text{Log}_{10}(t-1)+\text{Log}_{10}(t)+\text{Log}_{10}(t+1))^2)} \quad (15)$$

The conditions under which these equations are valid include the fact that the wells are drilled in a double porosity media which has a lower permeable and higher storativity rock matrix than fracture system and that the wells fully penetrate the aquifer. The well-bore storage and well-bore skin must be negligible for the equations to be realistic. All these conditions were satisfied in Rivirivi Catchment.

To detect very small variations in the pumping test data and help locate the dominant fractures in the pumped wells, log-log drawdown derivatives were calculated. Equation (16) provides drawdown derivatives for the early pumping times while equation (17) is for late pumping times.

$$\frac{\partial \log_{10} d_p}{\partial \log_{10} t} = \frac{1}{\ln \left\{ \frac{2.25 T_f t}{r_w^2 S_f} \right\}} \quad (16)$$

$$\frac{\partial \log_{10} d_p}{\partial \log_{10} t} = \frac{1}{\ln \left\{ \frac{2.25 T_f t}{r_w^2 (S_f + \beta S_m)} \right\}} \quad (17)$$

Assumptions

Verweij and Barker, (1999) stated that hydraulic data analyses in fractured rock aquifers usually rely on models that assume characteristics representative of the actual aquifers. In this study, we assumed that aquifer was heterogeneous and had double porosity condition where permeability and conductivity of the fractures were of three magnitudes higher than rock matrix, making fissure flow system the dominant hydraulic system. Because of the perceived low hydraulic conductivity of hornblende-biotite-gneiss rock matrix, the problem of flow to a production well is solved by assuming that water enters the borehole only through the fractures and not through the rock matrix. We also assumed possibility of recharge and barrier boundaries in the study area. Lithological data on the pumped wells collected from Department of Water Resources (MoAIWD, 2015) was useful in making an informed assumption that all the wells were fully penetrating wells. However, it could not be assumed beforehand as to whether Ntcheu Fault acted as a conduit or a barrier to lateral groundwater flow and thus we could not use Single Fracture Model to estimate aquifer parameters as suggested by Kruseman et al., (1994). Instead, we compared the time-drawdown plots with the theoretical plots to identify the fitting model to be used. As a result of the informed assumptions and the results of the plot comparisons, we selected Double Porosity Model as first introduced by Barenblatt et al., (1960) and according to application by Bourdet-Gringarten, (1980) as the appropriate model for aquifer parameter estimation and to allow type-curve matching on a log-log graph.

Double Porosity Model requires some conditions to be satisfied and subsequent to this, some assumptions to be made. In the early usage of Double Porosity Model, Barenblatt et al., (1960) and Warren and Root (1963) assumed that the flow from fractures to blocks takes place under quasi-steady-state conditions. Kazemi et al., (1969) assumed that the flow occurs under fully transient conditions. Altinors and Onder (2008), however, mentioned that the quasi-steady-state fracture to block flow has the advantage over transient flow assumptions as it provides greater mathematical simplicity.

Double Porosity Model can therefore be successfully applied if the aquifer is infinite, confined and if Darcian flow prevails in the fracture and matrix network. It is also applicable if the fracture and matrix networks are considered continuum in the whole abstraction period and that the well penetrates the aquifer fully with negligible well bore storage and well bore skin. However, the situation in Upper Rivirivi Catchment is not as exactly as this. The aquifers may have a limited extent due to no-flow or recharge boundaries and often the fractures may be connected through smaller fractures to the surface (particularly as the study area has thin overburden soils of up to 30 mm only) implying semi-confined conditions in most parts. In fractures and under high abstraction rates, non-linear or turbulent flow will occur, subduing Darcian flow (Neuman, 2005). In addition, during pumping test, the volume of the fracture network which takes part in the test keeps changing with time.

Sensitivity analysis

As a confirmation to the choice of the applied model, the estimated parameters from Double Porosity Model equations were used to plot the time-drawdown response which essentially simulates the hydraulic behavior of the actual fractured rock aquifer. The calculated type curve (response curve) gave a good match with the observed time-drawdown data (Fig. 7) suggesting that the model and the interpretation procedure are correct for this type of aquifer. If the calculated time-drawdown plot does not match the observed time-drawdown plot, it is advisable to select a different model as indicated by Verweij and Barker (1999).

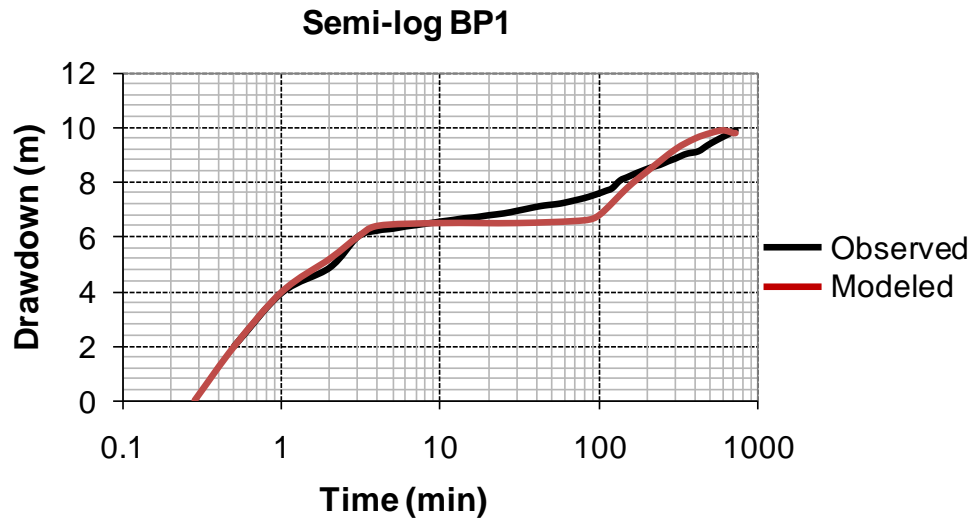


Fig. 7: Sensitivity Analysis - observed drawdown versus modeled drawdown

Diagnostic plots

Derivative analysis of the drawdown data from 12-hour constant rate pumping tests was employed. Time derivative of the pressure (p) has been used for years in the oil industry to analyze the data from the pumping tests (e.g. Horne, 1997). To identify specific aquifer conditions, the observed drawdown behavior was compared with the theoretical drawdown responses in double porosity model. This is because the time-drawdown data observed during a test may start and end at any point within the theoretical drawdown curve. As a result, one or more theoretical flow periods may not be shown in the observed data or the pumping test may not be long enough to record the effects of aquifer boundaries among others (Kruseman and Ridder, 1994).

Diagnostic plots allowed the dominating flow periods to be easily identified in this study area and the most important diagnostic plot used was plot of logarithm of derivative of drawdown data versus logarithm of pumping time. Derivative plots are important because they can show even small variations in the rate of drawdown that occurs during pumping test. They also work well in instances where data observation is done in pumped wells themselves, as was the case in this study. Diagnostic plots have since been used in groundwater resources by Sarma et al., 2014; Xiao and Xu, (2014), Dewandel et al., 2014, van Tonder et al., (2001) and Verweij and Barker, (1999) among other researchers.

Chapter 4: Results

4.1 Spatial and temporal variations of physical and geochemical data

In situ measurements of temperature show a range of 23-24°C in dry season and 24-25°C in rainy season for shallow groundwater along the ridge, 24-28°C in dry season and 25-27°C in rainy season for deeper groundwater along the valley (Table 3). River water values varied according to location, with those in the lower reaches having slightly higher temperatures of about 26°C and similar with deeper groundwater in dry season. Two wells (B8 and B9) located within 500 m from Ntcheu Fault showed highest temperature values of about 28°C in dry season while the average air temperature was 21°C (Fig. 8a). Upwelling of groundwater through the geological fault was suspected at these wells. However, no further investigation on this was carried out under this study.

The high altitude springs registered lowest temperatures in both seasons, ranging from 17-19°C in dry season and 20-21°C in rainy season. The average air temperature in rainy season (March, 2016) was 23°C (Fig. 8b; Table 3b). In rainy season, local water samples showed similar temperature with average air temperature measured in January, 2016. Monthly rainfall data (Fig. 8c) also showed that the study area received highest rainfall amount in this month. It is plausible that the fractured rock aquifers received recharge from this precipitation.

Power of Hydrogen, (pH) measurements show seasonal variations with a general increase from 6 in dry season to about 8 in rainy season in all samples. This indicates an alkaline nature of the geological setting and also suggesting possible contact with rain water (Fig. 9). In dry season, pH values in groundwater show an increase with decrease in elevation. pH values from pumped wells (Table 3c) show a decrease with an increase in depth. In dry season, pH values for deep groundwater (7) and river water (7.5) showed a uniquely similar trend.

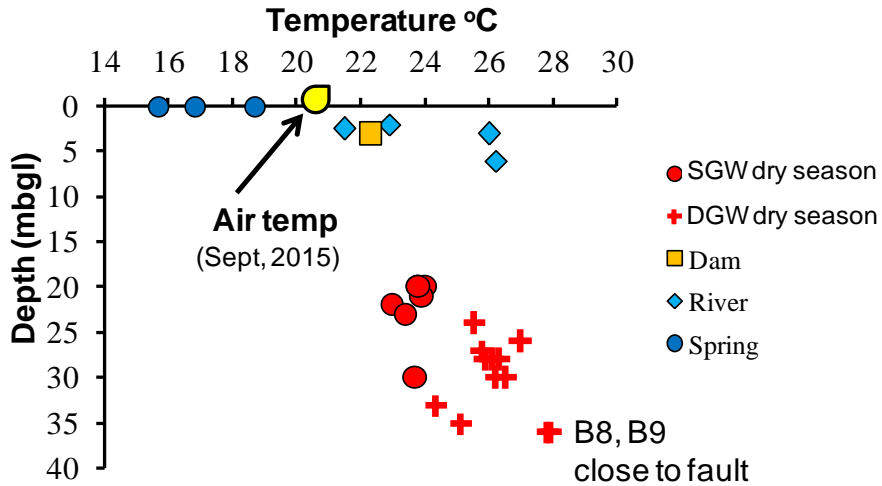


Fig. 8a: Local water temperature variations with depth in dry season.

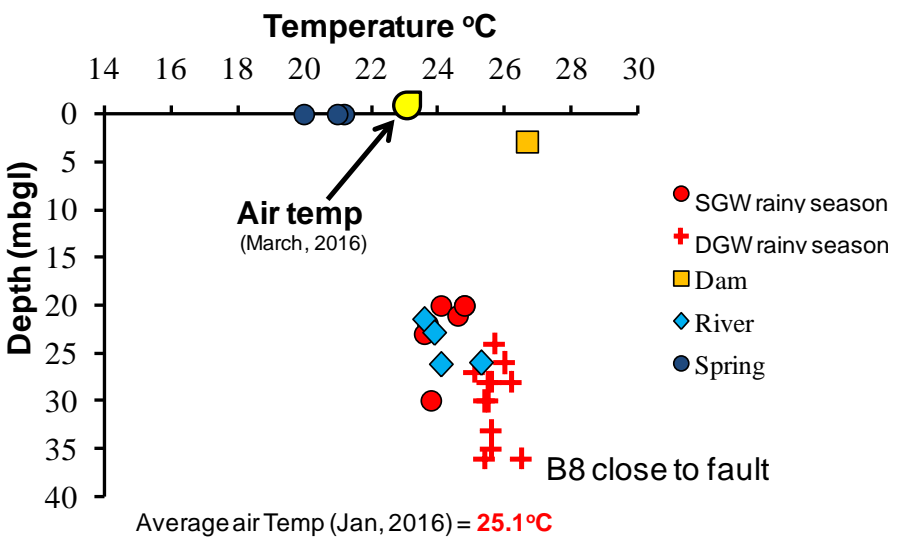


Fig. 8b: Local water temperature variations with depth in rainy season.

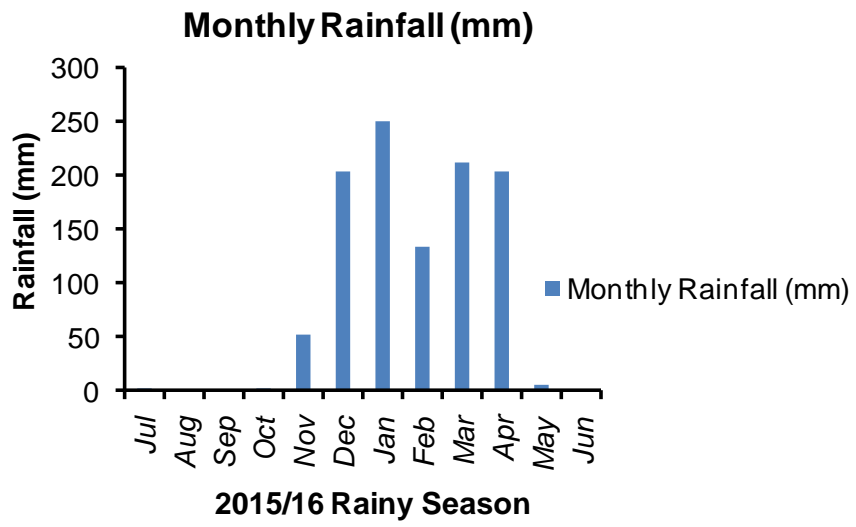


Fig. 8c: Monthly rainfall in the 2015/16 Rainy Season.

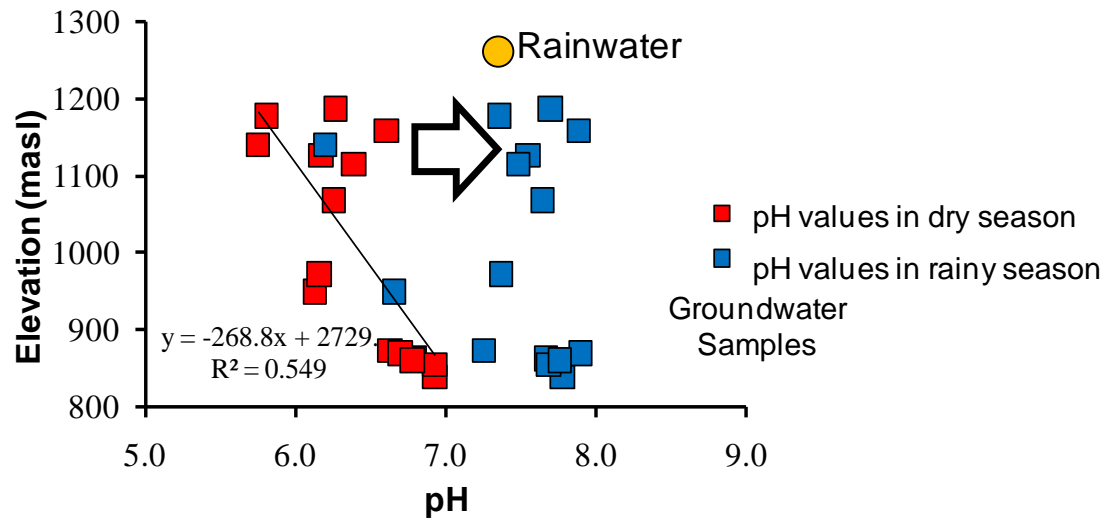


Fig. 9: pH variations in groundwater with changes in Elevation and seasons.

Nitrate concentrations in groundwater samples were highly variable in both space and time (Fig. 10; Table 3). However, shallow groundwater (B1) and deeper groundwater (B13, B15, and B17) showed pronounced concentrations of nitrate. Presence of higher nitrate concentrations even at depth in these wells indicates that groundwater is of young age and that it is vulnerable to anthropogenic contamination, for example chemical fertilizers. Interestingly, during sampling exercise, all these wells were established to be located in agricultural dominated areas.

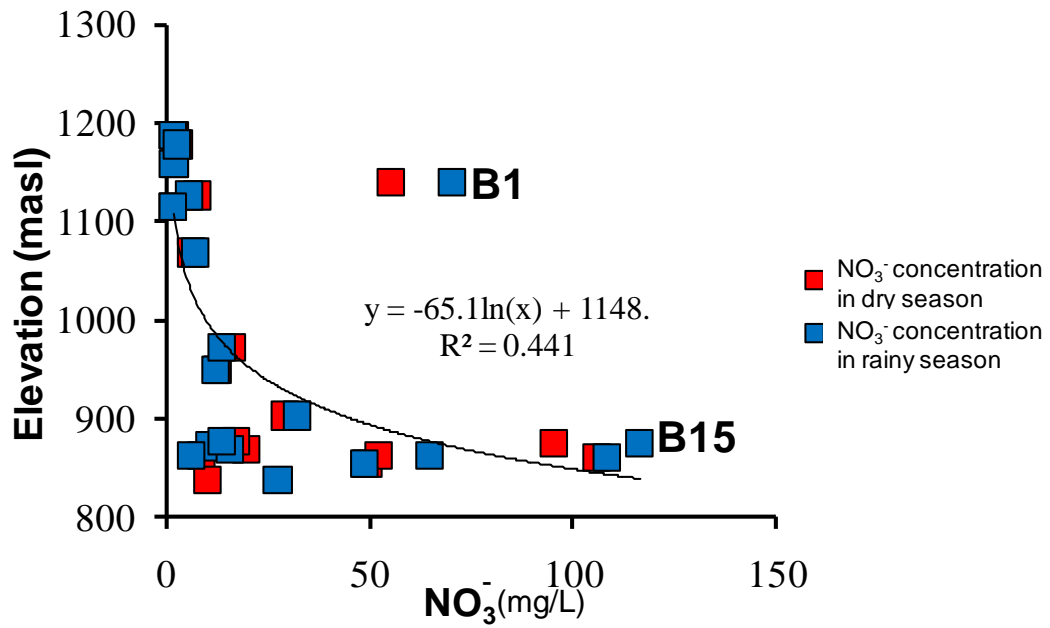


Fig. 10: Variation of NO₃⁻ concentration in groundwater with changes in Elevation.

Generally, silica concentration increases in groundwater with increasing contact time with silica rich geological materials. Rain water dissolves silica from silicate minerals by chemical weathering process. This is the reason why higher silica concentrations in groundwater regime usually indicate increased groundwater residence times (Mandal et al., 2011). When silica concentration increases with decrease in altitude, it may as well indicate that groundwater in lower reaches may have longer residence time than those in upstream.

In Upper Rivirivi Catchment, Silica (SiO_2) show similar values in spring water in upstream, some shallow groundwater along the ridge (B3), and some deep groundwater (B8, B9 and B10) in the valley section (about 20 mg/L in dry season and 30 mg/L in rainy season) (Fig. 11). The visible fractures could be influencing preferential recharge mechanism at these points, enabling groundwater mixing and thus altering apparent residence time of groundwater. In dry season, silica concentration seems to be increasing from springs in the upstream towards shallow groundwater at B6 and B7 (Fig. 11a).

In rainy season, however, silica concentration shows an increase with decrease in elevation from spring water towards groundwater sites at the valley section through shallow groundwater at B6 and B7. However, mixing tendency is suspected at other deeper groundwater locations in the valley section as shown in their distribution (Fig. 11b). Hexa-diagrams equally show temporal and spatial variations in geochemical data for the other sampled points, indicating possibility of mixing of groundwater from different recharge sources (Fig. 13).

Total dissolved solids (TDS) in the parallel transects of Rivirivi River and groundwater (Fig. 2d; Fig. 5; Table 3) ranged from 149 mg/L to 252 mg/L in dry season and 56 mg/L to 88 mg/L in rainy season for river water and 103 to 392 mg/L in dry season and 107 to 318 mg/L in rainy season for shallow groundwater respectively. Wells located close to Ntcheu geological fault registered TDS values of 175 mg/L to 428 mg/L in dry season and 194 to 444 mg/L in rainy season. TDS values for pumped wells (BP1, BP2, BP3 and BP4) showed a general increase from those located upstream of the fault to those located downstream. For example, BP1 has an average value of 97 mg/L while its neighbour feature across the fault (BP2) has 162 mg/L. BP3 had an average value of 222 mg/L while BP4 downstream across the fault had an average value of 262 mg/L. In all cases, these values increased with depth (Table 3c). All samples, however, registered TDS values of less than 500 mg/L.

Spatial and temporal geochemical distributions in Upper Rivirivi Catchment showed that it is dominated by Mg-Ca-HCO₃ water types. Shallow groundwater along the ridge section showed Mg-HCO₃ facies with Mg²⁺>Ca²⁺>Na⁺>K⁺ and HCO₃⁻>Cl⁻>SO₄²⁻>NO₃⁻ while deeper groundwater in the valley area showed Ca-HCO₃ type in both dry and rainy seasons with Ca²⁺>Mg²⁺>Na⁺>K⁺ and HCO₃⁻>Cl⁻>NO₃⁻>SO₄²⁻. River water was consistently Ca-HCO₃ dominated while spring water changed from Mg-HCO₃ in dry season to Ca-Na-HCO₃ in rainy season (Fig. 12).

B17 which is located near Nsipe River has a very distinct Ca-Na-HCO₃-NO₃ water type with pronounced average Na⁺ ion concentration of 36 mg/L (Table 3a and 3b). Geomorphologically, B17 and its neighbor wells seem to be receiving water from North-Eastern direction where Nsipe River flows from (Fig. 12; Fig. 13). During dry season, river water had similar geochemical concentrations as deeper groundwater while shallow groundwater had similar concentrations as spring water. In both seasons, however, concentrations of major ions in deeper groundwater remained higher than shallow groundwater and largely increased in concentration with decrease in elevation in the NW-SE direction (Fig. 13).

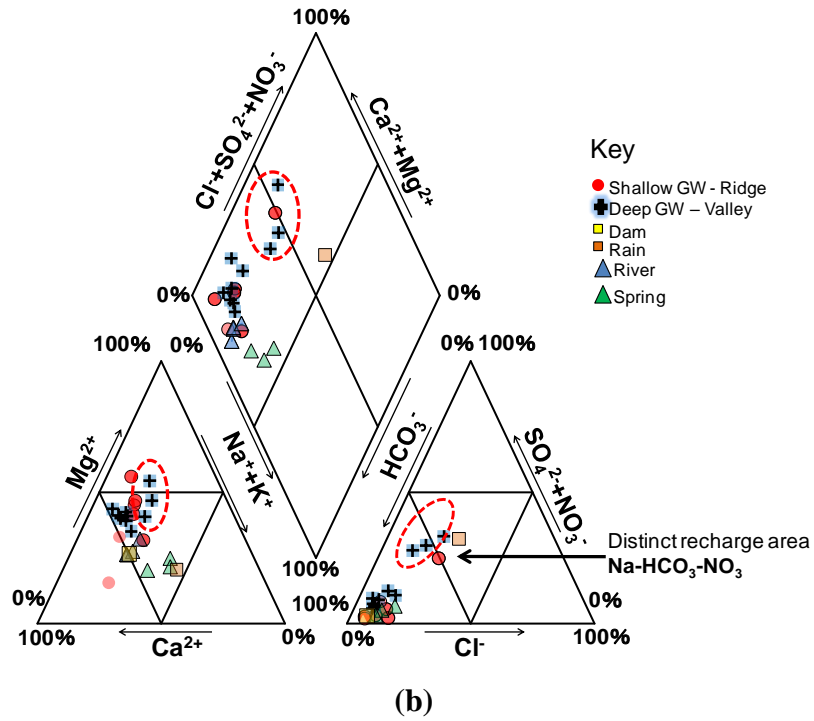
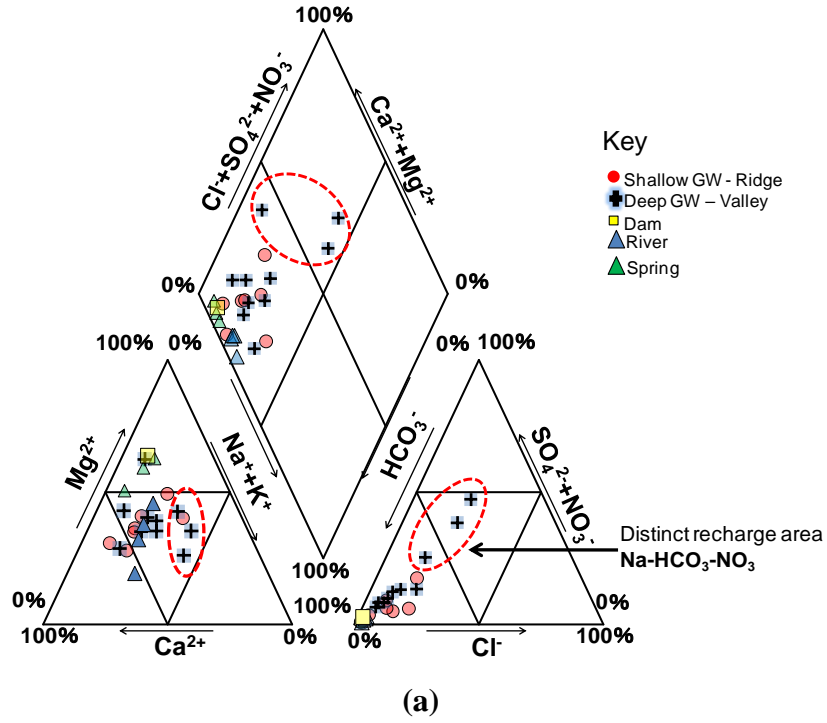


Fig. 12: Trilinear diagrams for samples taken in (a) Dry Season (b) Rainy Season.

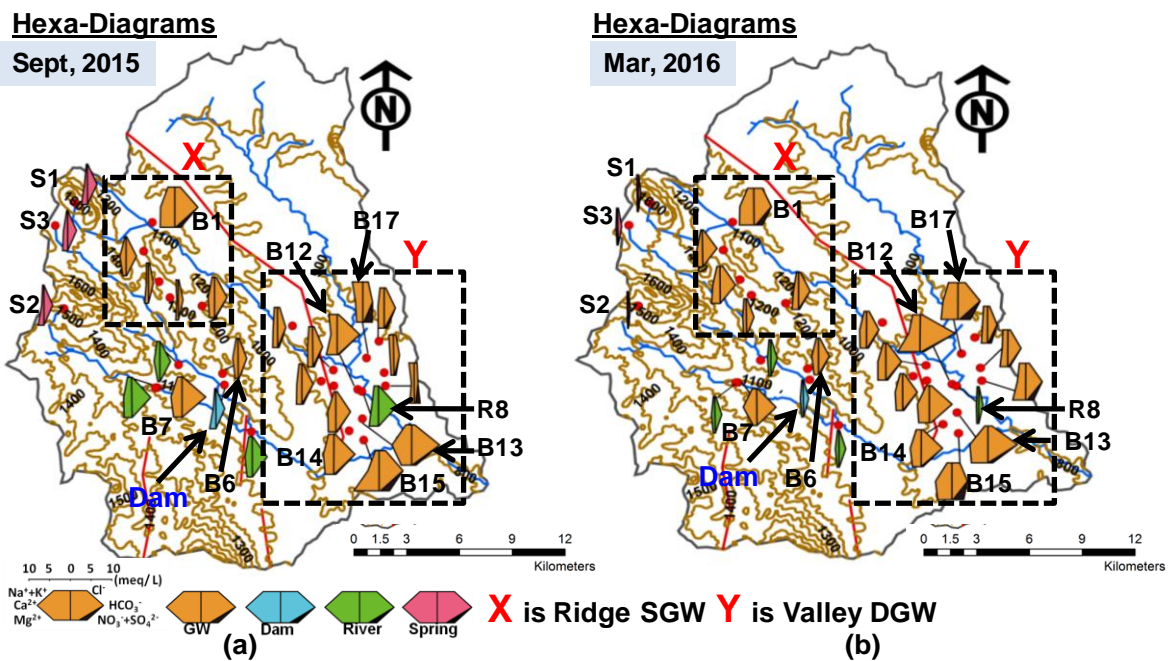


Fig. 13: Spatial and temporal variation of geochemical data for groundwater, dam water, river water and spring water in the study area in (a) Dry Season (b) Rainy Season as shown by hexa-diagrams.

Table 3a: In situ parameters, isotopic and geochemical data - Dry Season (September, 2015) Average Air Temperature = 20.8°C.

ID	Location (decimal degrees)		Altitude (m amsl)	$\delta^{18}\text{O}$ (‰)	δD (‰)	d- excess (‰)	T (°C)	p H	TDS (mg/L)	Na (mg/L)	Mg (mg/L)	K (mg/L)	Ca (mg/L)	Cl (mg/L)	HCO_3 (mg/L)	SO_4 (mg/L)	NO_3 (mg/L)	SiO_2 (mg/L)
	X	y																
B1	34.6400	-14.8216	1140	-5.4	-36.3	7.2	23.8	5.8	392	25.8	33.1	5.4	52.9	38.2	267.3	13.2	55.2	25.6
B2	34.6354	-14.8369	1158	-5.7	-39.4	6.2	24.0	6.6	232	4.3	8.7	2.9	26.8	3.3	130.4	2.4	2.2	32.1
B3	34.6436	-14.8528	1187	-5.2	-33.3	4.9	23.0	6.3	222	4.7	8.0	4.9	6.7	8.8	60.8	2.3	2.0	19.6
B4	34.6493	-14.8613	1178	-5.1	-36.8	4.3	23.7	5.8	103	8.8	5.5	0.9	5.3	5.2	56.5	0.3	3.2	43.6
B5	34.6661	-14.8657	1126	-5.3	-36.6	5.4	23.9	6.2	175	7.9	12.2	6.5	24.8	9.5	141.4	2.2	7.8	28.1
B6	34.6768	-14.9013	1068	-9.4	-49.4	26.0	23.8	6.3	144	7.4	6.7	2.5	20.6	5.7	99.4	3.7	6.3	25.4
B7	34.6426	-14.9088	1115	-9.1	-50.4	22.6	23.4	6.4	242	16.2	19.7	6.5	42.4	3.4	271.1	1.8	1.9	43.8
B8	34.7286	-14.9053	872	-8.7	-49.7	19.6	27.8	6.6	175	10.9	12.7	3.2	19.5	7.5	128.5	1.1	14.6	21.1
B9	34.7353	-14.9077	862	-8.3	-47.2	19.2	27.9	6.8	247	6.1	17.3	3.5	30.5	8.8	169.0	6.7	8.7	9.9
B10	34.7136	-14.8761	949	-7.5	-44.4	15.8	25.9	6.1	185	9.3	11.0	7.3	16.2	14.7	96.1	4.9	12.8	19.9
B11	34.7350	-14.8995	972	-8.1	-45.1	19.8	24.3	6.2	227	7.7	10.9	14.4	18.8	10.6	115.9	3.8	16.1	13.2
B12	34.7478	-14.9096	838	-7.4	-43.7	15.8	25.8	6.9	426	32.1	25.1	6.9	23.8	8.8	259.3	7.8	10.3	16.6
B13	34.7503	-14.9251	854	-6.7	-41.4	11.9	26.3	6.9	433	12.6	23.6	21.5	74.1	21.4	322.6	2.0	49.5	10.8
B14	34.7432	-14.9314	869	-5.9	-38.7	8.3	25.5	6.7	304	20.4	19.8	4.5	39.6	8.9	242.2	3.4	19.7	29.1
B15	34.7509	-14.9363	860	-7.5	-42.1	17.7	26.1	6.8	428	12.7	58.1	6.6	42.8	42.4	274.4	11.4	105.9	12.6
B16	34.7589	-14.8843	903	-6.2	-40.7	9.2	26.5	6.0	196	14.8	13.5	4.6	23.7	11.3	130.8	5.9	29.3	14.2
B17	34.7524	-14.8930	875	-7.1	-41.7	15.1	26.2	6.3	454	35.0	14.7	18.7	28.2	35.9	111.2	11.4	95.5	9.6
B18	34.7618	-14.9008	877	-5.5	-39.1	4.6	27.0	6.2	242	19.3	5.7	1.6	13.4	15.7	68.2	8.8	17.4	10.8
B19	34.7624	-14.9078	862	-6.3	-39.7	11.0	25.1	6.1	299	21.8	10.3	1.8	10.9	19.4	43.2	13.6	52.4	11.2
D1	34.6779	-14.9072	1048	-6.3	-33.5	16.8	22.3	7.4	98	2.1	13.9	3.4	9.4	1.3	103.8	1.9	0.8	33.3
R2	34.6537	-14.8966	1064	-6.6	-37.9	15.2	21.5	7.0	149	11.3	4.9	2.7	22.2	1.8	121.7	0.3	0.8	11.7
R3	34.6417	-14.9088	1108	-6.5	-36.5	15.1	26.0	7.7	222	11.3	17.4	12.3	30.7	3.5	219.3	2.2	1.5	14.7
R4	34.6920	-14.9319	955	-7.2	-36.9	20.3	26.2	7.9	232	13.4	11.8	3.3	27.5	3.5	171.6	3.3	1.5	15.0
S1	34.5999	-14.8115	1590	-9.3	-48.0	26.2	18.7	8.0	24	3.8	13.5	1.3	11.3	1.8	110.5	0.1	0.8	22.9
S2	34.5936	-14.8670	1443	-9.3	-48.2	26.5	15.7	7.1	39	2.8	13.2	4.3	8.2	1.3	102.1	0.3	0.8	21.5
S3	34.5891	-14.8233	1547	-8.2	-44.8	21.0	16.8	5.8	60	2.6	11.1	0.7	15.2	1.2	104.7	1.9	0.8	21.1
R8	34.7500	-14.9106	833	-6.7	-36.6	17.2	22.9	7.8	252	16.8	21.0	2.8	24.8	4.4	216.7	3.0	1.5	21.9

Table 3b: In situ parameters, isotopic and geochemical data - Rainy Season (March, 2016) Average Air Temp =22.5°C.

ID	Location (decimal degrees)		Altitude (m amsl)	$\delta^{18}\text{O}$ (‰)	δD (‰)	d- excess (‰)	T (°C)	p H	TDS (mg/L)	Na (mg/L)	Mg (mg/L)	K (mg/L)	Ca (mg/L)	Cl (mg/L)	HCO_3 (mg/L)	SO_4 (mg/L)	NO_3 (mg/L)	SiO_2 (mg/L)
	X	y																
B1	34.6400	-14.8216	1140	-5.3	-39.3	3.0	24.1	6.2	318	23.6	30.2	1.4	48.5	51.9	184.3	16.6	70.5	32.6
B2	34.6354	-14.8369	1158	-5.7	-42.4	3.4	24.8	7.9	178	5.8	18.7	0.8	19.0	5.5	154.0	2.1	2.1	33.7
B3	34.6436	-14.8528	1187	-4.8	-34.9	3.6	23.7	7.7	180	11.2	17.4	1.4	24.5	17.4	159.8	1.8	1.8	40.9
B4	34.6493	-14.8613	1178	-5.7	-40.0	5.6	23.8	7.4	107	9.0	6.0	1.1	12.9	5.5	82.4	0.3	2.7	124.2
B5	34.6661	-14.8657	1126	-5.2	-37.9	3.8	24.6	7.6	167	8.7	13.8	0.5	18.1	11.3	120.7	2.0	5.6	36.7
B6	34.6768	-14.9013	1068	-5.5	-39.2	4.9	24.8	7.7	154	7.8	9.2	1.5	23.0	7.4	114.7	3.5	7.2	87.7
B7	34.6426	-14.9088	1115	-5.1	-38.2	2.6	23.6	7.5	228	17.4	6.9	0.4	46.6	8.0	205.7	1.8	1.8	38.8
B8	34.7286	-14.9053	872	-5.4	-40.8	2.0	26.5	7.3	194	10.2	14.3	1.6	26.8	8.4	156.7	0.9	10.9	46.8
B9	34.7353	-14.9077	862	-5.1	-38.7	1.8	25.4	7.7	255	11.0	21.8	1.9	40.7	11.3	230.9	7.0	6.3	29.5
B10	34.7136	-14.8761	949	-5.2	-38.6	3.1	25.6	6.7	204	8.9	13.9	2.0	24.3	14.2	128.0	4.8	12.1	54.2
B11	34.7350	-14.8995	972	-5.2	-38.8	2.6	25.6	7.4	120	10.4	17.0	1.1	28.4	9.6	166.4	3.4	13.9	156.3
B12	34.7478	-14.9096	838	-5.1	-38.7	2.0	25.1	7.8	444	28.5	47.8	2.8	40.1	14.2	375.5	11.9	27.5	7.3
B13	34.7503	-14.9251	854	-6.5	-40.4	11.6	25.5	7.7	401	12.1	34.8	1.6	62.7	24.1	309.6	1.2	48.8	24.1
B14	34.7432	-14.9314	869	-6.0	-38.3	9.5	25.7	7.9	283	19.6	18.2	0.6	38.0	10.1	223.7	2.7	15.9	32.5
B15	34.7509	-14.9363	860	-6.3	-38.7	11.9	26.2	7.8	403	18.4	29.6	1.0	56.4	48.8	164.3	12.6	108.4	16.1
B16	34.7589	-14.8843	903	-6.8	-41.3	13.4	25.4	5.7	180	15.1	12.9	1.3	17.3	12.4	99.8	5.2	32.2	42.7
B17	34.7524	-14.8930	875	-6.7	-39.6	13.8	25.5	6.1	414	37.0	35.9	2.1	52.7	44.2	235.1	13.0	116.3	23.6
B18	34.7618	-14.9008	877	-6.5	-39.1	12.6	26.0	6.0	209	18.3	16.5	2.2	19.3	15.8	143.5	7.4	13.8	49.5
B19	34.7624	-14.9078	862	-6.4	-38.7	12.5	25.6	6.0	296	23.5	27.2	2.4	29.1	21.6	173.6	13.2	65.0	55.4
D1	34.6779	-14.9072	1048	-5.4	-32.2	10.8	26.7	7.8	67	4.8	3.3	1.4	10.2	2.4	56.5	0.2	1.5	1.7
R2	34.6537	-14.8966	1064	-6.2	-36.6	13.2	23.6	8.4	80	6.4	4.1	0.8	11.6	2.4	68.7	0.3	0.9	40.5
R3	34.6417	-14.9088	1108	-6.2	-36.9	12.3	25.3	8.1	85	6.1	4.1	1.4	13.2	3.0	71.3	1.6	1.0	27.9
R4	34.6920	-14.9319	955	-6.2	-36.9	12.6	24.1	8.2	88	6.0	4.1	1.2	13.1	3.1	70.1	1.6	1.0	28.1
S1	34.5999	-14.8115	1590	-7.0	-40.9	15.4	21.2	8.4	37	4.8	1.8	1.2	3.9	2.4	29.6	0.1	1.7	32.9
S2	34.5936	-14.8670	1443	-7.0	-42.2	13.8	20.0	7.5	29	4.1	1.3	1.1	3.5	2.8	23.0	0.2	1.7	33.2
S3	34.5891	-14.8233	1547	-7.1	-41.6	15.4	21.0	7.5	50	4.1	1.8	3.1	6.8	2.6	39.4	0.1	1.3	31.2
R8	34.7500	-14.9106	833	-7.4	-42.3	16.6	23.9	8.1	56	3.7	3.6	2.9	7.9	3.0	48.3	0.8	2.1	1.95
R9	34.6379	-14.8181	1112	-6.3	-36.8	13.5	25.4	8.1	98.8	6.9	6.0	0.8	12.7	3.3	80.5	1.1	0.9	41.3
R10	34.7282	-14.8887	873	-6.4	-36.9	14.6	25.2	7.8	82.9	6.4	5.1	3.0	10.7	4.4	68.8	1.2	1.8	11.9

Table 3c: In situ parameters, isotopic and geochemical data for Pumping Test Sites (March, 2016) Average Air Temp =22.5°C.

ID	Location (decimal degrees)		Altitude (m amsl)	Pumpin g Time (hr)	Water level (m bgl)	$\delta^{18}\text{O}$ (‰)	δD (‰)	d- exces s (‰)	T (°C)	p H	TDS (mg/L)	Na (mg/L)	Mg (mg/L)	K (mg/L)	Ca (mg/L)	Cl (mg/L)	HCO_3 (mg/L)	SiO_2 (mg/L)
	X	y																
BP1	34.6320	-14.7800	1134	0	12.1	-6.8	-39.8	14.3	25.0	6.1	96.8	6.1	6.9	1.2	13.4	2.3	86.6	108.9
					20.7	-7.1	-42.1	15.0	25.4	6.0	98.0	6.4	6.2	1.8	13.9	2.8	93.0	112.3
					21.2	-7.0	-41.1	14.9	25.9	5.9	97.9	6.5	6.7	2.1	13.7	2.5	93.4	113.9
					22.0	-6.5	-40.3	12.0	24.7	6.0	97.0	6.1	7.3	1.1	14.2	2.4	90.3	114.2
BP2	34.6300	-14.7720	1128	0	19.6	-6.9	-41.4	13.7	25.0	6.0	158.1	8.6	13.0	1.9	25.1	7.0	148.3	125.6
					35.9	-7.1	-42.3	14.1	25.0	5.6	163.0	8.5	12.7	1.8	28.2	7.4	154.3	128.2
					36.2	-7.1	-42.8	14.0	25.5	5.8	163.0	8.5	12.9	1.7	28.7	7.7	154.9	129.3
					36.3	-7.0	-43.0	13.0	25.8	5.7	165.0	8.7	12.0	1.7	29.8	7.9	156.2	131.2
BP3	34.7130	-14.8750	949	0	10.2	-5.2	-38.6	3.1	25.6	6.7	204.0	8.9	13.9	2.0	24.3	14.2	128.0	116.0
					17.3	-4.8	-34.5	4.2	26.0	6.0	220.0	8.7	14.3	2.0	25.1	16.3	128.1	117.2
					17.6	-5.0	-36.4	3.6	26.1	6.7	231.0	9.4	14.0	2.1	28.3	17.3	127.8	117.4
					17.9	-5.1	-37.1	3.4	26.6	6.2	233.0	8.9	14.2	1.9	27.9	17.5	128.3	121.6
BP4	34.7200	-14.8620	947	0	11.9	-6.7	-40.9	12.3	25.4	6.6	246.0	16.2	11.9	1.6	37.0	7.2	174.5	71.5
					19.2	-5.9	-38.2	9.3	25.8	6.3	261.0	17.3	11.8	2.9	38.2	9.3	175.2	83.2
					19.6	-6.5	-40.8	11.1	26.2	6.0	266.0	16.9	12.5	1.9	39.0	9.5	175.0	85.3
					20.0	-6.6	-40.0	12.4	26.2	6.0	273.0	17.2	13.2	1.7	42.3	10.2	174.8	91.2
Rain	34.6120	-14.7920	1252	-	-	-6.1	-33.8	15.1	24.4	7.0	14.9	1.4	0.6	1.9	1.6	2.5	5.5	0.0

4.2 Spatial and temporal variations of stable isotopic data

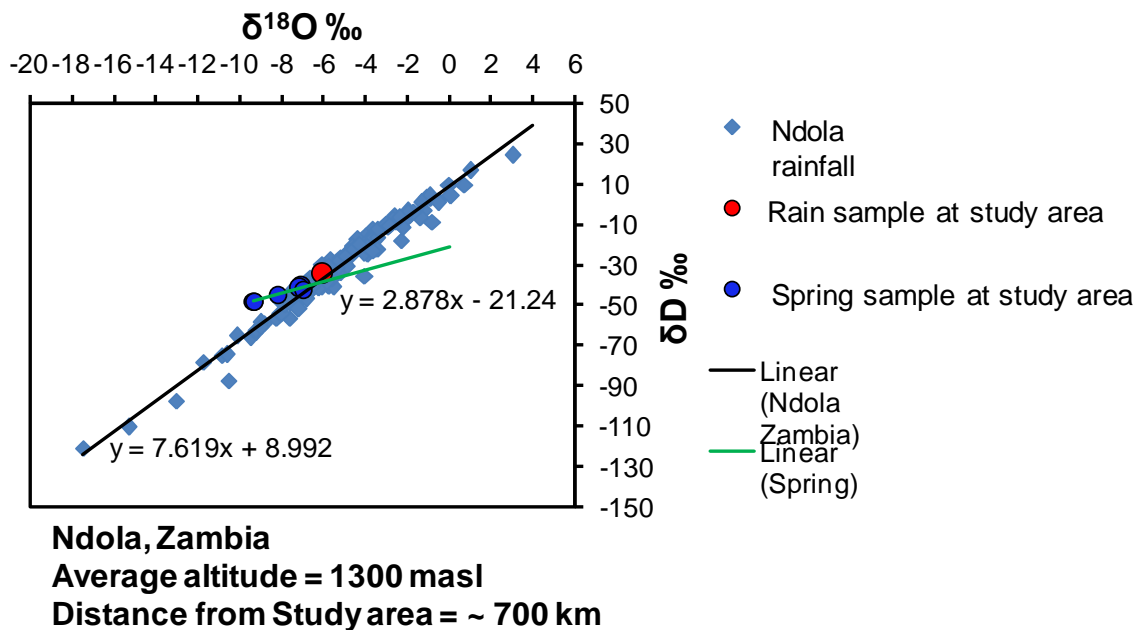
Malawi had no International Atomic and Energy Agency (IAEA) Global Network of Isotopes in Precipitation (GNIP) station at the time of this research. To construct Local Meteoric Water Line (LMWL), two GNIP stations within a radius of about 700 km from study area were selected for comparison. These were Ndola IAEA GNIP station in Zambia (WMO 6756100) and Harare IAEA GNIP station in Zimbabwe (WMO 6777400). These two stations have relatively similar climate with Upper Rivirivi Catchment in Malawi.

At a time of this research, Upper Rivirivi Catchment had one operational rain-station located at Nkhande Residential Training Center (Fig. 5) which has an average altitude of 1252 masl. Ndola and Harare GNIP stations are located at average altitudes of 1300 and 1500 masl respectively. Only springs located in the upstream of the study area had similar average altitude of 1527 masl with Harare GNIP station (1490 masl). This similarity in average altitude proved to be a significant factor in understanding why stable isotopic data for springs plotted away from LMWLs. Fig. 14 shows scatter plots of weighted monthly rainfall isotopic data for both GNIP sites and their respective LMWLs. Due to general similarities in average altitude with study area, November 1968 to March 2014 data from Ndola IAEA GNIP station in Zambia (VWO 6756100; IAEA, 2006) was selected for construction of LMWL for Upper Rivirivi Catchment. This data yielded the equation:

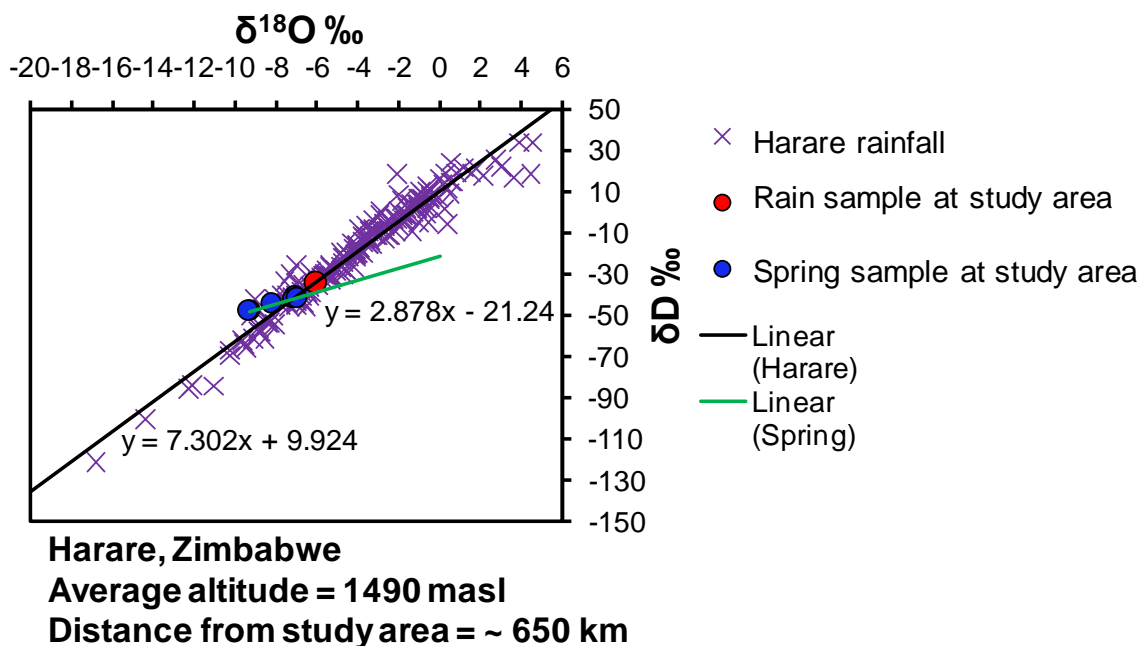
$$\text{LMWL: } \delta\text{D} (\text{‰}) = 7.62(\delta^{18}\text{O} (\text{‰})) + 8.99 \quad (18)$$

which is closer to the Global Meteoric Water Line (GMWL) by Craig, (1961):

$$\text{GMWL: } \delta\text{D} (\text{‰}) = 8(\delta^{18}\text{O} (\text{‰})) + 10 \quad (19)$$



(a) Ndola GNIP station



(b) Harare GNIP station

Fig. 14: Local Meteoric Water Line (LMWL) plots for monthly rainfall stable isotopes measured at (a) Ndola GNIP station (1968-2009) (b) Harare GNIP station (1960-2003).

Shallow groundwater (SGW) along the ridge showed enriched $\delta^{18}\text{O}$ values in both dry and rainy seasons (-5.7 ‰ to -4.8‰). However, two shallow groundwater points (B6 and B7) showed depleted $\delta^{18}\text{O}$ values (-9.4‰ and -9.1‰ respectively) in dry season and enriched $\delta^{18}\text{O}$ values (-5.5‰ and -5.1‰ respectively) in rainy season. Deeper groundwater (DGW) along the valleys showed both depleted values (up to -8.7‰) in dry season to enriched values (up to -5.1‰) in rainy season. $\delta^{18}\text{O}$ values for river water samples showed small variations ranging from -7.2‰ to -6.5‰ in dry season and -7.4‰ to -6.2‰ in rainy season. Spring sample values however, showed more depleted $\delta^{18}\text{O}$ values similar to SGW at B6 and B7 and DGW located in the valleys. These values ranged from -9.3‰ to -8.2‰ in dry season and -7.1‰ to -7.0‰ in rainy season (Fig. 15). Meanwhile, Pumping Test wells demonstrate generally well mixed systems where BP1, BP2 and BP4 show $\delta^{18}\text{O}$ average values of -7‰ as constant pumping increased from 0 hr to 12 hrs. At the same time, BP 3 showed enriched $\delta^{18}\text{O}$ average values of -5‰ (Table 3c).

δD values for the majority of SGW sites ranged from -39.4‰ to -33.3‰ in dry season and -42.4‰ to -34.9‰ in rainy season except for B6 and B7 which ranged from -49.4‰ and 50.4‰ in dry season to -39.2‰ and 38.2‰ in rainy season respectively. δD values for DGW ranged from -49.7‰ to -38.7‰ in dry season and -41.3‰ to -38.3‰ in rainy season. δD values for river samples ranged from -37.9‰ to -36.5‰ in dry season and -42.4‰ to -36.6‰ in rainy season. Spring values ranged from -48.2‰ to -44.8‰ in dry season and -42.2‰ to -40.9‰ in rainy season. δD values for Pumping Test sites ranged from -39.8‰ (0 hr) to -40.3‰ (12 hr) for BP1, -41.4‰ (0 hr) to -43‰ (12 hr) for BP2, -38.6‰ (0 hr) to -37.1‰ (12 hr) for BP3 and -40.9‰ (0 hr) to -40‰ (12 hr) for BP4.

The spatial and temporal variations of $\delta^{18}\text{O}$ and δD in DGW were larger than those in river and SGW. The slope of the regression line of the less varied SGW values was lower than that of LMWL, which is:

$$\text{SGW: } \delta\text{D (‰)} = 6.3(\delta^{18}\text{O (‰)}) - 5.22 \quad (20)$$

against

$$\text{LMWL: } \delta\text{D} (\text{‰}) = 7.62(\delta^{18}\text{O} (\text{‰})) + 8.99 \quad (18)$$

This suggests that isotopic fractionation during rainwater evaporation could be the main cause of the enrichment (e.g. Fontes et al., 1980).

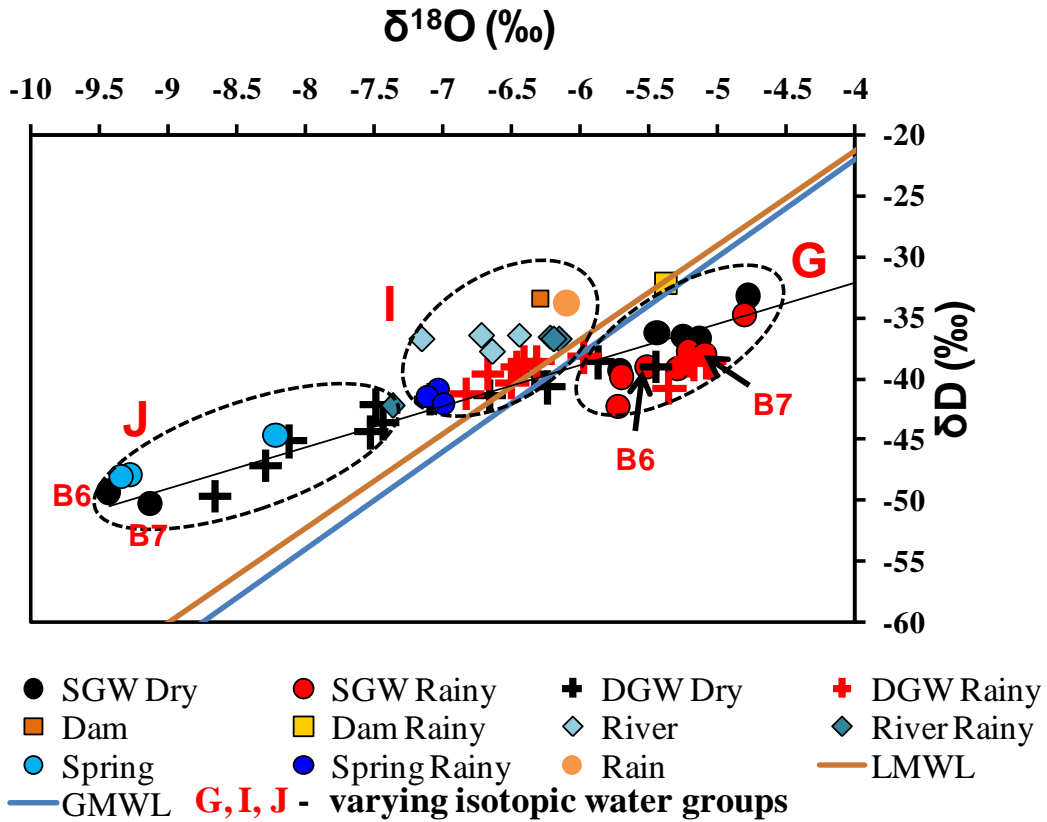


Fig. 15: δ - diagram for samples collected in Dry and Rainy Seasons. River water, dam water, spring water, rainwater and some deeper groundwater show a higher deuterium excess (see sections J and I) than selected Local Meteoric Water Line (LMWL) indicating dissimilarities between local precipitation patterns in the study area and the selected GNIP station.

4.3 Pumping Test data

Step tests with varying pump discharge rates were conducted at each well for an hour to determine the yield that could sustain constant pumping test thereafter. After establishing the appropriate pump yield, constant pumping tests were conducted for a period of 12 hrs at each well on 25, 26, 27, 28, and 29 March, 2016. BP1 which was 32 m deep and with screens located from 3 to 30 mbgl, yielded 1 L/s as the discharge rate to be used for constant pumping test. At 47 m deep and with screens located from 5 to 45 mbgl, BP2 yielded 2 L/s as the appropriate discharge rate to be used for constant pumping test. BP3 was 38 m deep and had its screens located from 1 to 35 mbgl. It yielded 0.5 L/s as the pump discharge rate for constant pumping test. BP4, 40 m deep and its screens located from 1 to 35 mbgl, had yielded 0.5 L/s as the pump discharge rate to be used during constant pumping test.

Fig. 16 and Table 4 show elevation and location of the pumped wells in relation to Ntcheu Fault, location of the screens and total depth for each well, static water levels before pumping at each well, lithological outline of fractured rocks, pump discharge rates and geometric mean storativity values for each pumped vicinity. Static water level for BP1 which is about 150 m away from Ntcheu Fault and 250 m away from BP2 is higher (1123 meters above sea level) than that of BP1 (1109 masl), depicting possible direction of flow. Static water level for BP3 (939 masl) also shows potential of flow towards BP4 (936 masl) across the fault.

Table 4a: Site and screen locations for Pumping Test wells.

Location (Pumping test sites)	Elevation (meters above sea level)	Screen location (mbgl)	Constant Pumping Rate, Q (L/s) 12 hr
BP1 (32m deep)	1134	3-30	1.0
BP2 (47m deep)	1128	5-45	2.0
BP3 (38m deep)	949	1-35	0.5
BP4 (40m deep)	947	1-35	0.5

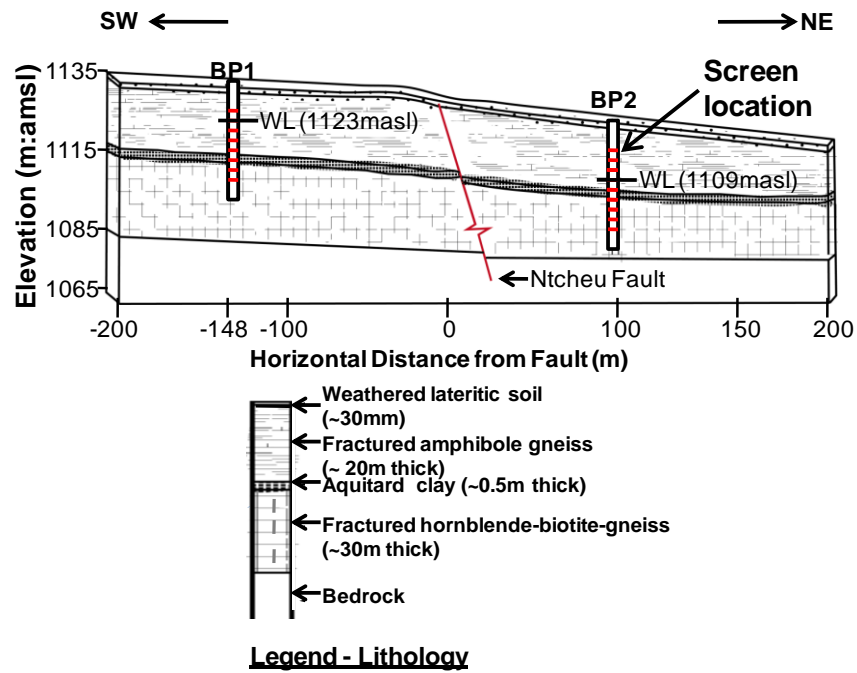
*mbgl is *meters below ground level*

Table 4b: Pump discharge rates and storativity values (geometric mean) for wells.

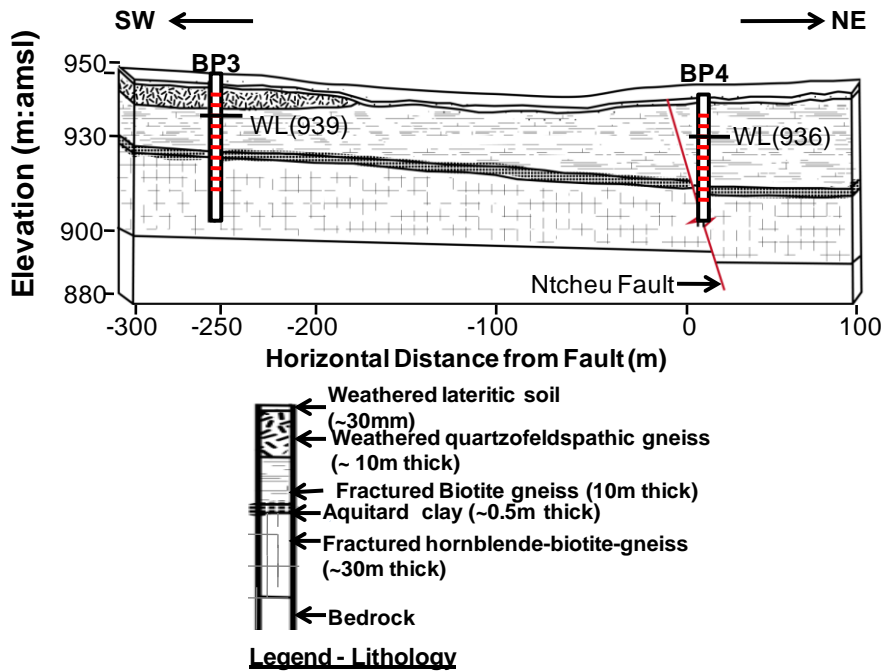
Location (Pumping test sites)	Elevation (meters above sea level)	Pump Discharge Rate (L/s)	Average Storativity Values
BP1 (32m deep)	1134	1.0	1.24×10^{-3}
BP2 (47m deep)	1128	2.0	1.35×10^{-6}
BP3 (38m deep)	949	0.5	2.12×10^{-3}
BP4 (40m deep)	947	0.5	1.65×10^{-3}

Water level and Transmissivity

Transmissivity values were calculated using equations 7-17. As a way of validation, these results were compared to those calculated from Logan (1964) Equation ($T=1.22Q/s$). Fig. 17b shows that the highest Transmissivity value for BP1, which is $21 \text{ m}^2/\text{day}$, occurs at a depth of 18.7 meters below ground level (mbgl). It also shows that the highest Transmissivity values for BP2 ($136.5 \text{ m}^2/\text{day}$) were recorded at a depth of 35 mbgl. Logarithmic Transmissivity values for BP2 suggest dominance nature of the highly permeable fractures in this hydrological system.



(a)



(b)

Fig. 16: Screen locations, lithology and neighbor features for pumped wells located across Ntcheu Fault.

Plot for BP3 shows two sections within the well profile which had pronounced Transmissivity values of $8.7 \text{ m}^2/\text{day}$ at 12.1 mbgl and $12.8 \text{ m}^2/\text{day}$ at 18.1 mbgl respectively. The highest Transmissivity value for BP4 is $10 \text{ m}^2/\text{day}$ and occurring at a depth of 17.5 mbgl. As stated by Bai et al., (1993), in a double porosity phenomenon, fractures are more permeable than the rock matrix hence all sections within the well profile of this study that show pronounced Transmissivity values are probable fracture locations as screens covered almost the whole sections of the well profile.

BP3 shows average Storativity values for fractures (S_f) in the early times as 7.1×10^{-4} while the system's combined Storativity for fractures and rock matrix ($S_f + S_m$) in later times is 2.2×10^{-3} . BP4's average Storativity for fractures (S_f) is 9.0×10^{-4} and 2.2×10^{-3} is for combined fracture and rock matrix ($S_f + S_m$) in later times respectively. The similarities in combined Storativity values between these juxtaposed wells suggest resemblance in hydrogeological formation.

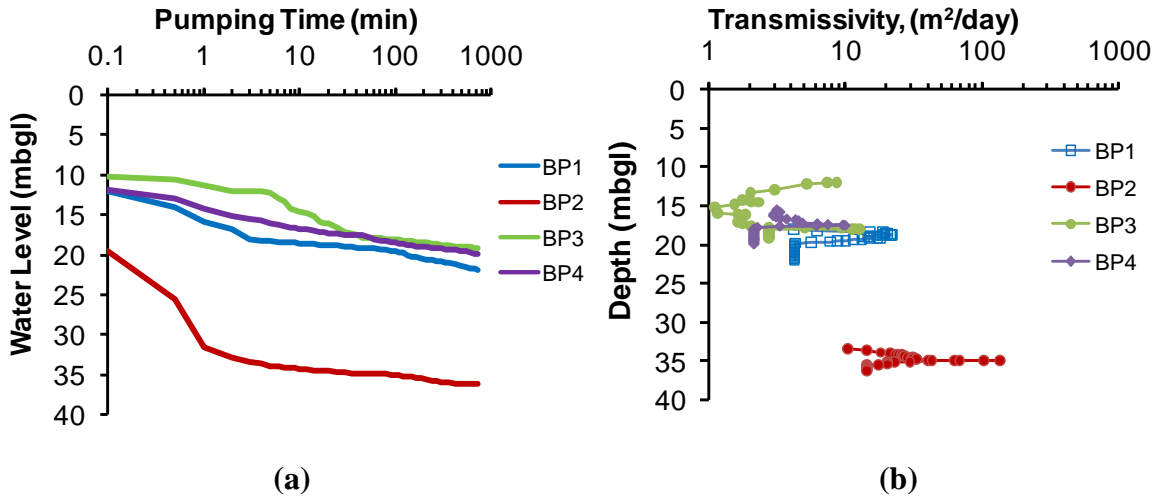


Fig. 17: Variation of water levels in pumped wells with increase in pumping time at (a) and variation of Transmissivity values in each pumped well with increase in borehole depth at (b).

Chapter 5: Discussion

5.1 Dominant geochemical processes associated with fractured Hornblende-biotite-gneiss rock formation

Geochemical fingerprints have been widely used to understand dominant processes, sources of groundwater and groundwater flow processes in various geological formations (Gastmans et al., 2016; Edoulati et al., 2013; Mulligan et al., 2011; Williams et al., 2013). Understanding the dominant hydrochemical processes in an aquifer is therefore important when interpreting stable isotopic and geochemical data.

Piper plots (Fig. 12) and Hexa-diagrams (Fig. 13) show that Upper Rivirivi Catchment is dominated by Mg-Ca-HCO₃ water types. Shallow groundwater along the ridge section showed Mg-HCO₃ facies while deeper groundwater in the valley area showed Ca-HCO₃ type in both dry and rainy seasons. River water was consistently Ca-HCO₃ dominated while spring water changed from Mg-HCO₃ in dry season to Ca-Na-HCO₃ in rainy season.

According to Ako et al., (2012), Kebede et al., (2005) and Edmunds and Smedley, (2000), Mg-Ca-HCO₃ and Ca-Na-HCO₃ water types usually represent groundwater that is at early stages of geochemical evolution (recent recharge) or rapidly circulating groundwater that has not undergone significant water-rock interactions. The presence of thin overburden soils and fractures in the study area seem to corroborate this argument.

Despite these water types suggested to being at early stages of geochemical evolution, they show water-rock interaction involving the dissimilar dissolution of silicate minerals. Upper Rivirivi Catchment is underlain by fractured Hornblende-biotite-gneiss, thus the weathering of hornblende is believed to partially contribute to concentrations of Mg²⁺, Ca²⁺, Na⁺ and HCO₃⁻. This is because such water types may also result from other processes like reverse-ion exchange and ion exchange.

Singh et al., (2017) stipulate that $\text{Ca}^{2+} + \text{Mg}^{2+}$ versus $\text{HCO}_3^- + \text{SO}_4^{2-}$ plots can help understand the ion-exchange process occurring in an aquifer. Reverse ion-exchange tends to shift the points left of the equiline due to excess $\text{Ca}^{2+} + \text{Mg}^{2+}$ while if ion-exchange is the main process, it will shift the points right of the equiline. Fig. 18a shows that both reverse-ion exchange and ion-exchange are active processes in the study area.

Fig. 18b shows a stable 1:1 ratio of Na^+/Cl^- in shallow groundwater (SGW) with some samples plotting below the equiline indicating that evaporation is the most active process happening in these locations (e.g. Zhang et al., 2014). 95% of the samples plotted in Fig. 18b have Na^+/Cl^- values around 1 indicating that evaporation is not only the most dominant process in shallow groundwater but also in the other locations as well. This process is also confirmed by inverse relationship between d-excess values with $\delta^{18}\text{O}$ as shown in Fig. 18c. However, deep groundwater (DGW) and river samples plotting slightly above 1:1 equiline in Fig. 18b indicate that silicate weathering (weathering of hornblende-biotite-gneiss) is another active hydrochemical process occurring in these locations.

Correlation coefficients among major groundwater parameters also helped give insight into major geochemical processes in the study area. Table 5 shows some of these correlation coefficients. The value of $R > 0.7$ indicates strong correlation while R values between 0.5 and 0.7 show moderate correlation between parameters. Strong correlation between Na^+ and Cl^- indicates that these ions had similar source in the study area. In deeper groundwater (DGW) in the valley section, there is poor correlation between Ca^{2+} and SO_4^{2-} suggesting that there has been geochemical evolution of groundwater along the flow path from recharge areas to these wells (e.g. Liu et al., 2015). The positive correlation of Na^+ and SO_4^{2-} suggests mixing of groundwater recharged around areas underlain by quartzofeldspathic granulites and biotite-nepheline-gneiss which are a source of Na^+ ions and groundwater contaminated from chemical fertilizers around these areas as the sources of SO_4^{2-} ions (Fig. 2d). Photo 1 shows agricultural activities around springs in the study area (Fig. 5). The strong positive correlation between Mg^{2+} and SO_4^{2-} also demonstrates possibility of cation exchange.

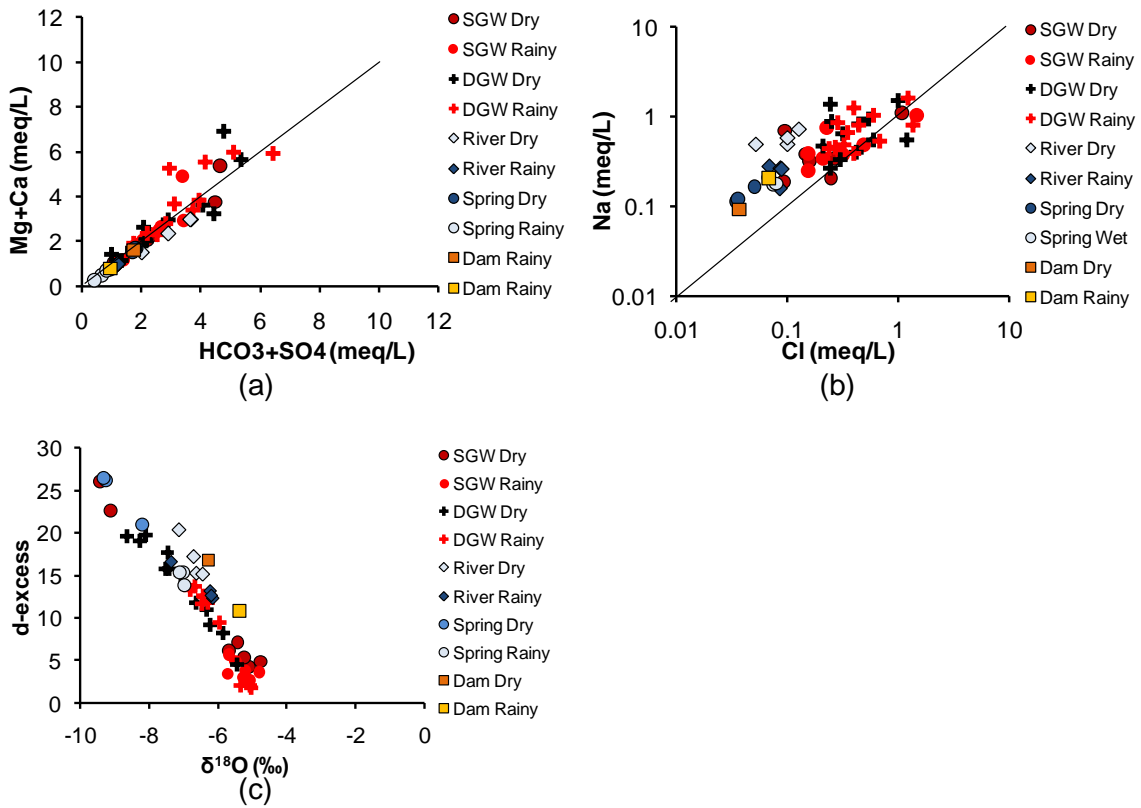


Fig. 18: (a) $\text{Ca}^{2+} + \text{Mg}^{2+}$ vs $\text{HCO}_3^- + \text{SO}_4^{2-}$ (b) Na^+ vs Cl^- (c) d-excess vs $\delta^{18}\text{O}$.

Table 5: Correlation coefficient of major parameters in groundwater (average values).

	$\delta^{18}\text{O}$	TDS	Na^+	Mg^{2+}	K^+	Ca^{2+}	Cl^-	HCO_3^-	SO_4^{2-}	NO_3^-	pH	Temp	SiO_2	Screen depth
$\delta^{18}\text{O}$	1.00													
TDS	0.26	1.00												
Na^+	0.18	0.81	1.00											
Mg^{2+}	0.14	0.90	0.65	1.00										
K^+	-0.01	0.57	0.39	0.45	1.00									
Ca^{2+}	0.11	0.84	0.53	0.78	0.61	1.00								
Cl^-	0.20	0.78	0.67	0.80	0.43	0.67	1.00							
HCO_3^-	0.14	0.84	0.58	0.80	0.54	0.89	0.46	1.00						
SO_4^{2-}	0.18	0.74	0.79	0.73	0.21	0.46	0.83	0.40	1.00					
NO_3^-	0.01	0.77	0.69	0.77	0.48	0.62	0.93	0.41	0.79	1.00				
pH	-0.28	-0.31	-0.45	-0.17	-0.08	-0.14	-0.49	0.01	-0.55	-0.42	1.00			
Temp	0.44	0.62	0.45	0.44	0.33	0.48	0.38	0.47	0.43	0.37	-0.24	1.00		
SiO_2	0.12	-0.31	-0.22	-0.36	-0.12	-0.24	-0.20	-0.30	-0.22	-0.24	-0.31	-0.04	1.00	
Screen depth	0.31	0.61	0.48	0.48	0.26	0.45	0.48	0.42	0.49	0.45	-0.64	0.67	0.32	1.00

Chloro-alkaline indices (CAI) developed by Schoeller (1965) were used to understand cation exchange between the groundwater and host environment during its residence in these geological environments. Equations 21 and 22 (CAI-1 and CAI-2) show how Schoeller indices are calculated. When the Schoeller indices are negative, an exchange of Ca^{2+} or Mg^{2+} in groundwater with Na^+ or K^+ in aquifer formations takes place. In this process, Ca^{2+} or Mg^{2+} is removed from groundwater and Na^+ or K^+ is released into the water.

$$\text{CAI1} = \frac{\{\text{Cl}^- - (\text{Na}^+ + \text{K}^+)\}}{\text{Cl}^-} \quad (21)$$

$$\text{CAI2} = \frac{\{\text{Cl}^- - (\text{Na}^+ + \text{K}^+)\}}{(\text{SO}_4^{2-} + \text{HCO}_3^- + \text{NO}_3^- + \text{CO}_3^{2-})} \quad (22)$$

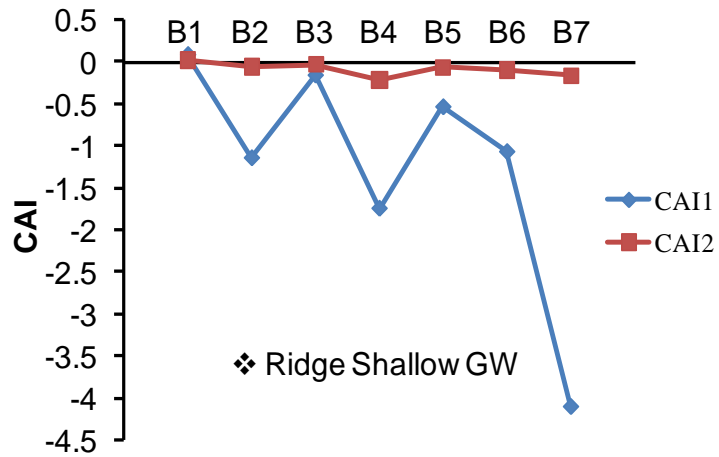


Fig. 19a: Chloro-Alkaline Indices (CAI) Values for Ridge Shallow Groundwater.

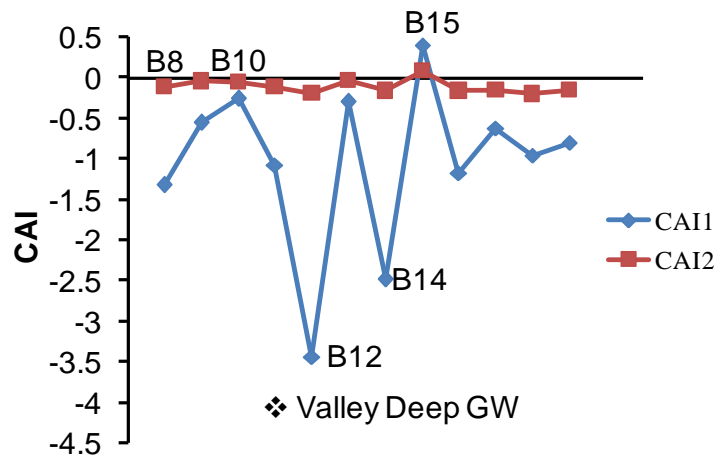


Fig. 19b: Chloro-Alkaline Indices (CAI) values for Deeper Groundwater at Valley Section.

The negative Schoeller indices usually indicate that chloro-alkaline is in disequilibrium and the reaction is known as cation-anion exchange reaction. In this process, host geological formation is the primary source of dissolved solids in water. Alternatively, if the Schoeller indices are positive, reverse ion exchange occurs. The CO_3^{2-} term in equation (22) varies in similar proportions as bicarbonate and thus does not negatively affect the outcome of CAI2. In this scenario, an exchange occurs between Na^+ in groundwater and Ca^{2+} or Mg^{2+} in aquifer material. In Upper Rivirivi Catchment, only groundwater at B1 and B15 show reverse ion exchange, with CAI values of up to 0.1 for B1 and 0.4 for B15. For most of the groundwater samples, however, negative Schoeller index values, which indicate cation-anion exchange, were registered (Fig. 19; Table A5). CAI results for most groundwater show that Na^+ and K^+ are released by Ca^{2+} and Mg^{2+} exchange. These results further justify the earlier notion that ion exchange is one of the major geochemical processes and also one of the major sources of higher concentration of Na^+ in groundwater in the study area (Fig. 18a).

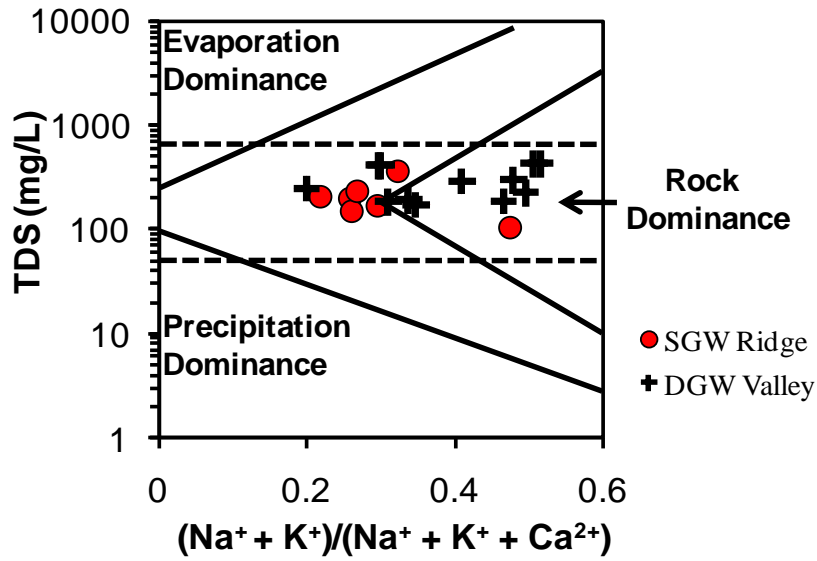


Fig. 20a: Gibbs Plot of Groundwater samples showing Total Dissolved Solids (TDS) versus $(\text{Na}^+ + \text{K}^+)/(\text{Na}^+ + \text{K}^+ + \text{Ca}^{2+})$.

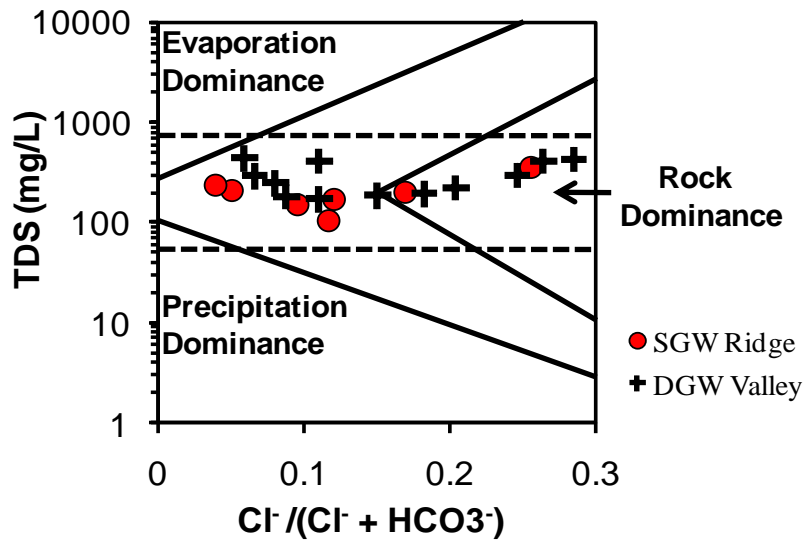


Fig. 20b: Gibbs Plot of Groundwater samples showing Total Dissolved Solids (TDS) versus $\text{Cl} / (\text{Cl} + \text{HCO}_3^-)$.

In order to make further analysis of formation mechanisms of hydrogeochemistry in Upper Rivirivi Catchment, Gibbs plots were used. Gibbs (1970) recommended two diagrams, as shown in Fig. 20, to assess the dominant effects of evaporation, precipitation and rock weathering on geochemical evolution of groundwater in semi-arid and arid regions. The diagrams show the weight ratios of $(\text{Na}^+ + \text{K}^+) / (\text{Na}^+ + \text{K}^+ + \text{Ca}^{2+})$ and $\text{Cl}^- / (\text{Cl}^- + \text{HCO}_3^-)$ against TDS. Controlling mechanisms like precipitation dominance, rock dominance and evaporation dominance are included in these diagrams.

Fig. 20 shows that in all groundwater samples, rock weathering is the dominant mechanism in this purported early geochemical evolution. For most of the shallow groundwater (SGW) and deeper groundwater (DGW), the ratio of $(\text{Na}^+ + \text{K}^+) / (\text{Na}^+ + \text{K}^+ + \text{Ca}^{2+})$ was less than 0.5 strongly indicating that rock weathering was the main mechanism controlling geochemistry. Some groundwater samples, however, show $(\text{Na}^+ + \text{K}^+) / (\text{Na}^+ + \text{K}^+ + \text{Ca}^{2+})$ ratio of slightly more than 0.5 indicating that evaporation somehow controls geochemistry to some extent. All the samples in the study area had TDS values of less than 500 mg/L and the $(\text{Na}^+ + \text{K}^+) / (\text{Na}^+ + \text{K}^+ + \text{Ca}^{2+})$ ratio spreads from low to high without a great variation of TDS, which indicated that cation exchange also played an important role by increasing Na^+ and decreasing Ca^{2+} under rock dominance conditions.

5.2 Groundwater recharge sources and its mechanisms

All water samples in the study area registered total dissolved solids (TDS) of not more than 500 mg/L, implying that they had a short residence time with little time for intense geochemical processes. The seasonal decrease in TDS concentrations in shallow waters in rainy season was therefore assumed to be as a result of mixing or contact with rainwater (dilution effect) suggesting that groundwater could be directly recharged from rainfall.

In addition to the foregoing, groundwater samples also showed a significant concentration of NO_3^- ions which is usually indicative of unconfined nature of aquifers (Ako et al., 2012). NO_3^- ions concentrations that range from 10 to 100 mg/L also strongly suggested that groundwater in this catchment is very young in age as the water samples managed to retain such significant concentrations of NO_3^- ions. Old waters are usually associated with anaerobic denitrification process that reduces NO_3^- ions in groundwater. Geochemical data further revealed that groundwater samples in this area have significant presence of Na^+ which may indicate cation exchange process that replaces divalent ions such as Ca^{2+} with monovalent ions such as Na^+ from this Mg-Ca- HCO_3 dominated water type. The presence of a 0.5 m thick clay aquitard that separates the shallow and deeper aquifers in the study area seems to support this supposition (Fig. 2e). According to geochemical evolution, such type of water types represent groundwater at the early stages of geochemical evolution (recent recharge) or rapidly circulating groundwater which has not undergone significant water-rock interactions (Kebede et al., 2005; Edmunds and Smedley, 2000). Geochemical data therefore suggest that rainfall is the main source of groundwater recharge in Upper Rivirivi Catchment. It also suggests rapid recharge phenomenon that allows addition of NO_3^- ions into groundwater.

To verify the notion that rainfall is the main source of recharge as revealed by geochemical data, stable isotopic data was considered. Clark and Fritz (1997) established that $\delta^{18}\text{O}$ and δD fingerprints can provide insights into recharge and flow processes in a

groundwater system since they are part of the water molecule itself and that any phase changes or fractionation along the flow path could also trigger change in its fingerprints.

$\delta^{18}\text{O}$ and δD showed that groundwater and surface water plot close to both Local Meteoric Water Line (LMWL) and Global Meteoric Water Line (GMWL) indicating a relatively constant isotopic composition and a well mixed system (Fig. 15). It also mirrors the average isotope composition of rainwater (-6.1‰) in Upper Rivirivi Catchment. This suggests that water in this study area is of meteoric origin and that modern rainfall is the dominant component of these waters. In addition, this suggested a rapid infiltration process that seemed to preserve precipitation isotopic signatures in these fractured hornblende-biotite-gneiss rock formations.

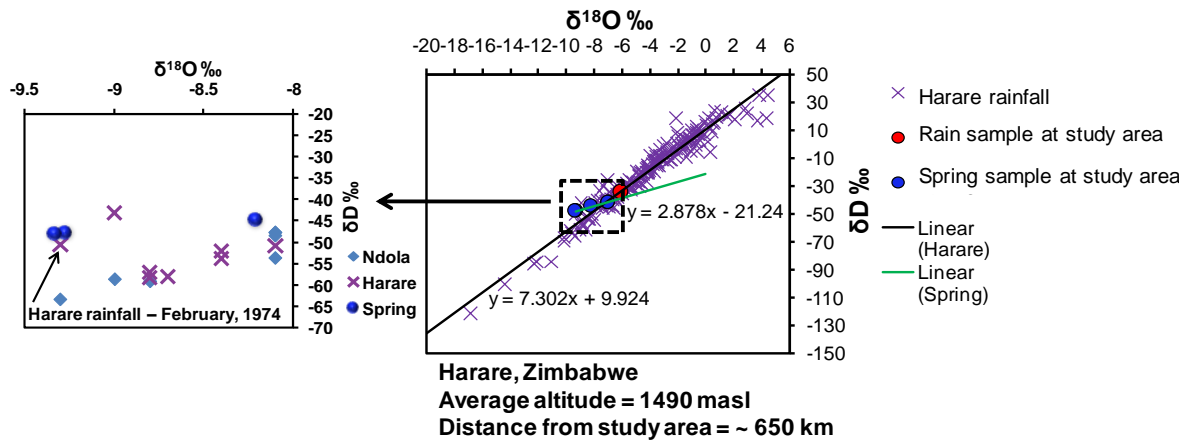


Fig. 21: Similarity between stable isotopes of spring water from study area and Precipitation sampled in February, 1974 at Harare GNIP station.

In as much as most water samples plot very close to LMWL and GMWL, two shallow groundwater samples (B6 and B7) and spring water plot away from these meteoric water lines in dry season (Fig. 15). Spatial distribution of $\delta^{18}\text{O}$ for these samples also shows more depleted values than the rest in dry season (Fig. 22). To identify possible recharge source for these samples, precipitation $\delta^{18}\text{O}$ and δD data from Harare GNIP in Zimbabwe were compared with spring water from the study area particularly because they have similar climate and sit at similar average altitudes of about 1500 masl. Fig. 21 shows that spring water is similar to Harare GNIP precipitation data from February 1974. It is suggestive that spring water might have been recharge from rainfall under this period.

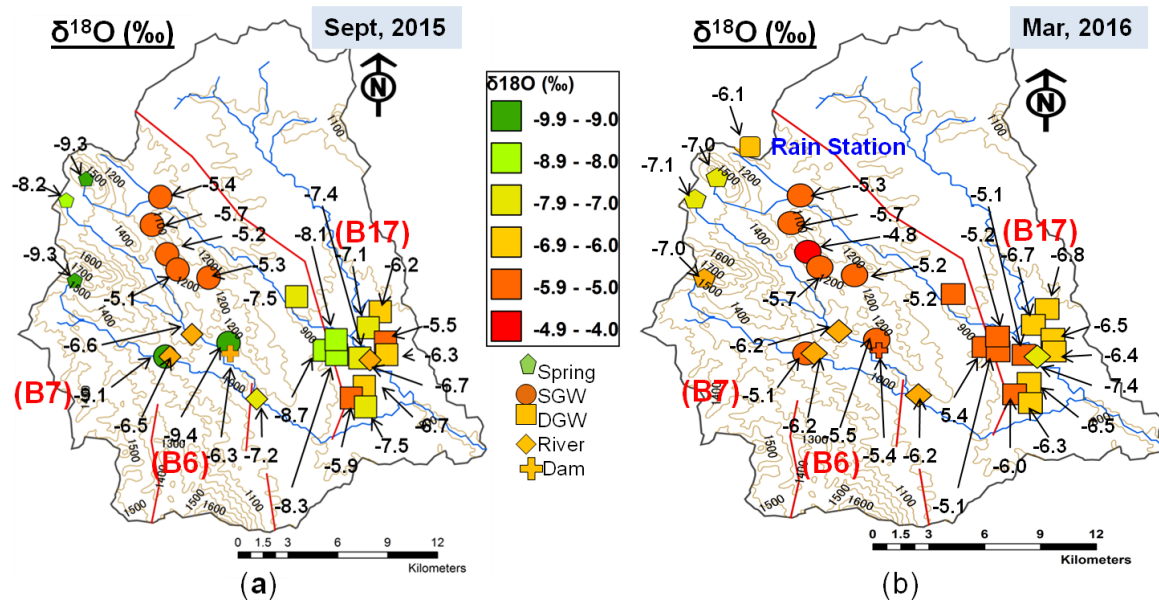


Fig. 22: Spatial Distribution of $\delta^{18}\text{O}$ in springs, shallow groundwater (circles), deeper groundwater (squares), river water (diamonds) and dam water (cross) in (a) Dry Season (b) Rainy Season. The colors of the circles, squares, diamonds and cross represent the values of $\delta^{18}\text{O}$ at each site.

Because of its conservative nature, chloride was used to further understand groundwater recharge sources and mechanisms in Upper Rivirivi Catchment. Fig. 23 shows relationship between $\delta^{18}\text{O}$ and Cl^- concentrations in the study area. It is shown from this relationship that most samples have a relatively low concentration of chloride, similar to precipitation, suggesting that precipitation is the main source of water resource in this area. Group (a) which comprises of shallow groundwater at ridge section, river water, spring water and deep groundwater at valley section, shows very similar stable isotopic and chloride concentrations with rain water. In as much as group (b) shows similar stable isotopic values with rain water, it also shows a unique chloride concentration. These three sites (B1, B15, and B17) also show highest NO_3^- (70-116 mg/L) and SO_4^{2-} (13-17 mg/L) concentrations (Table 3). Since there are a lot of agricultural activities around these wells, it is suggestive that the elevated concentrations of chloride, NO_3^- and SO_4^{2-} are from anthropogenic contamination, particularly from chemical fertilizers.

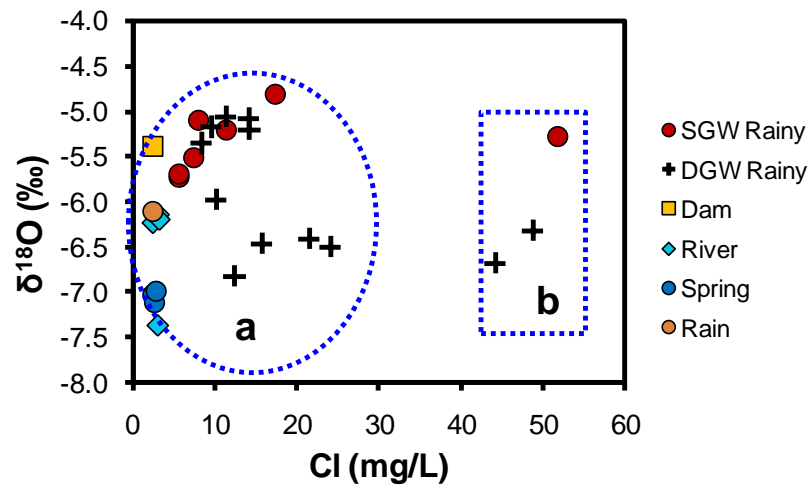


Fig. 23: Relationship between $\delta^{18}\text{O}$ and Cl^- concentrations in Rain, Shallow groundwater (SGW), Deeper groundwater (DGW), Dam, River and Spring water in Rainy season.

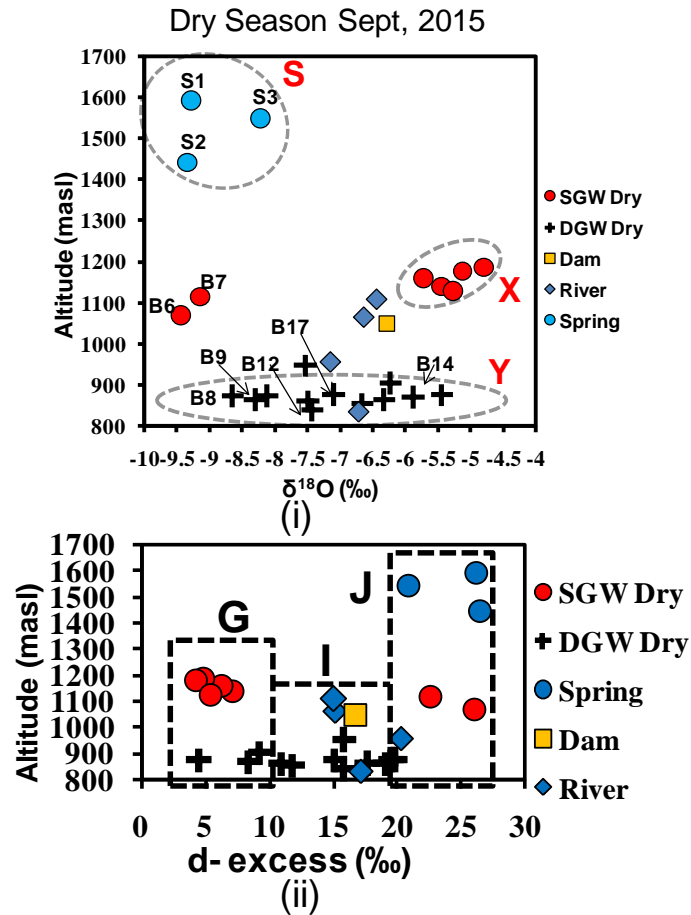
The d-excess value is an index showing the evaporation effect on the physicochemical characteristics of water. If the water evaporates, d-excess decreases (Tsujimura et al., 2007). Fig. 24 shows the variation of d-excess values with altitude in the study area. It can be seen that in dry season, shallow groundwater (SGW) at the ridge section and some deeper groundwater (DGW) displayed high $\delta^{18}\text{O}$ values and lower d-excess values than the rest of the samples, suggesting that groundwater in these sites could have been recharged from precipitation with enriched stable isotopic values as a result of evaporation process. The ridge section has thin overburden soils and fractures. It is probable therefore that enriched precipitation easily recharged groundwater through this geological setting.

Spring water, some shallow groundwater at B6 and B7 and some river water located at different altitudes showed higher d-excess values than the rest of the samples, suggesting that they could have been recharged under similar relative humidity conditions by precipitation with depleted stable isotopic values (e.g. Sakakibara et al., 2017). Dam water, river water in the middle reach and deeper groundwater at valley section (which has thicker overburden soils of up to 3 m), showed mixing trend between G and J recharge conditions. This phenomenon suggests deeper groundwater at valley section could be receiving water from springs that are located in the upstream. It thus suggests hydraulic connectivity between these two locations. Altitude versus $\delta^{18}\text{O}$ plot seems to agree with this supposition (Fig. 24a).

In rainy season, however, only two d-excess zones occurred. Shallow groundwater (SGW) and some deeper groundwater (DGW) around Ntcheu Fault, showed d-excess values under zone G, still indicating evaporation influence on recharge source and slightly different from sampled precipitation. The rest of the water samples showed similarity with sampled precipitation and thus suggesting that this precipitation could be the source of groundwater recharge in this area (Fig. 24b).

Negrel et al., (2011) stated that post-precipitation evaporation becomes an active process for isotopic enrichment when the transfer velocity from rainfall towards groundwater storage through soil and the unsaturated zone is sufficiently slow. However,

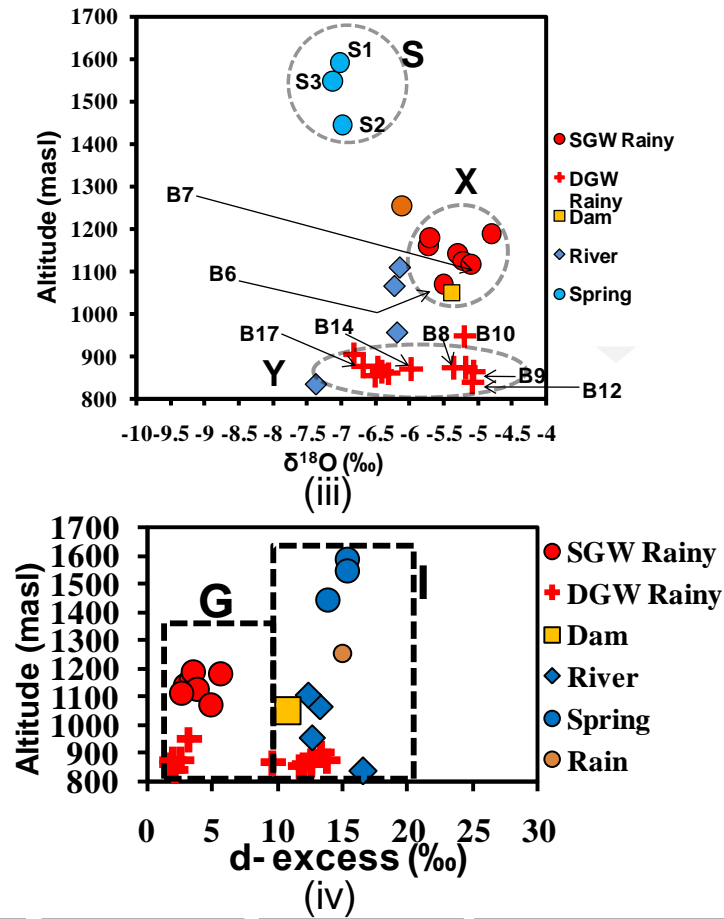
the situation seems to be different when the geological formation has fractures. In this study, the interface between thicker overburden soil (up to 3 m) and fractured rock formation seemed to ensure that only large rain events could recharge groundwater, maintaining its isotopic signal and letting small events evaporate without leaving any evaporation signal. At the ridge section, however, enriched precipitation, even if in small events, seem to preferentially recharge groundwater through an interface of thin overburden soils and fractured geological setting.



S - Springs **X** - Ridge SGW **Y** - Valley DGW **G, I, J** - Recharge Conditions

Fig. 24a: Variation of $\delta^{18}\text{O}$ in local waters with altitude in dry season (i) and variation of their d-excess values with altitude as shown in (ii).

Rainy Season Mar, 2016



S - Springs X - Ridge SGW Y - Valley DGW G, I, J - Recharge Conditions

Fig. 24b: Variation of $\delta^{18}O$ of local waters with altitude in rainy season (iii) and variation of their d-excess values as shown in (iv).

Recharge altitudes

To deduce recharge elevations, $\delta^{18}\text{O}$ and δD values in precipitation must be consistent with the notion that they decrease with increasing elevation. This notion is called altitude effect. This study area had only one rain station at the time of this research and thus it was difficult to use precipitation to deduce recharge altitudes of groundwater and river water. Instead, proxies for precipitation to estimate isotopic gradient were used. These proxies were selected along the same micro-watershed to represent changes in gradient and possible groundwater flow direction.

In addition to their location, selected samples had relatively low Total Dissolved Solids (TDS) of less than 110 mg/L suggesting limited subsurface residence time. They also had low Magnesium (Mg) values of less than 15 mg/L suggesting shorter groundwater flow path. Their pH values were relatively higher than most samples but similar to rain (around 7). This suggests that the water samples at these sites had not circulated deep enough to initiate other geochemical processes. They also had a maximum cation or anion sum of less than 1.6 meq/L (Table A6). These samples include shallow groundwater at B4, dam water, spring water and weighted rain water at the only station available. According to Jefferson et al., (2006) and Mulligan et al., (2011), in the absence of precipitation data, samples that show relatively low cation or anion compositions may be used as proxies for precipitation as they indicate groundwater which has not undergone significant geochemical evolution.

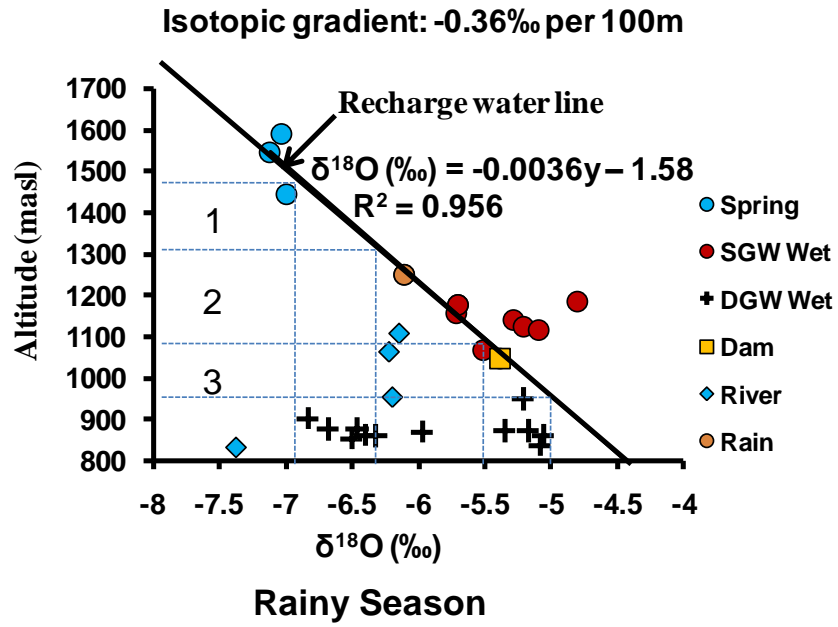


Fig. 25: Vertical distribution of $\delta^{18}\text{O}$ and recharge water line as developed in this study for Upper Rivirivi Catchment

Fig. 25 shows recharge water line (regression line of proxies of precipitation) on elevation versus $\delta^{18}\text{O}$ plot and isotopic gradient of -0.36‰ per 100 m increase in elevation in the study area as deduced from proxies for precipitation. The linear correlation between elevation and $\delta^{18}\text{O}$, as revealed from proxies for precipitation, is strong, that is, $r > 0.97$ suggesting that the relationship is reliable. The established isotopic gradient for Upper Rivirivi Catchment is within the typical values as stated by Clark and Fritz, (1997), that is, -0.17 to -0.5‰ per 100 m increase in elevation.

The established isotopic gradient helped identification of three (3) recharge zones and their estimated recharge elevations. The three water groups were identified according to their average Total Dissolved Solids (TDS) concentrations. Some wells representing deep groundwater (DGW) in the valley section, for example, B13 and B15, seem to be recharged from a regional recharge zone (zone 1 on Fig. 25) that lies between 1317 and 1513 masl. River water and B14 seem to be recharged from intermediate recharge zone (zone 2 on Fig. 25) lying between 1094 and 1317 masl. Some wells representing deep groundwater (DGW) along Ntcheu geological fault, for example, B8, B10 and B12 seem to be recharged from local recharge zone (zone 3 on Fig. 25) lying between 954 and 1094 masl. All these recharge zones are characterized by fractured Hornblende-biotite-gneiss formations with very thin (about 30 mm) overburden soils. Shallow groundwater (SGW) at ridge section seems not to be consistent with altitude effect as they demonstrated more enriched isotopic compositions than even those at lower reaches. However, d-excess values showed that it may have been recharged by similar precipitation that went through the effect of evaporation as deeper groundwater (DGW) along Ntcheu geological fault (Fig. 24b).

5.3 Recharge and flow boundaries as revealed by hydraulic tests

This section reveals dominant recharge processes and apparent flow boundaries in a fractured rock aquifer using interpretation of hydraulic tests. This is because hydraulic tests have been shown to provide simultaneous information on the hydraulic behavior of the wells, the reservoirs and the respective flow boundaries in these systems (Dewandel et al., 2014; Kruseman and Ridder, 1994).

Traditionally, the drawdown-time curves may deviate from the double porosity theoretical s-shaped curves due to human factors during pumping test operation, specific boundary conditions including partial penetration of the wells, well-bore storage, recharge boundaries or sometimes no-flow boundaries (Karay, 2013; van Tonder et al., 2002). Since the pumped wells had a small diameter (110 mm diameter), it was established that well-bore storage effect was minimal (Fig. 7). Well-bore skin effects were regarded unlikely since prior to testing, the boreholes were thoroughly developed. In addition, the main water strike zones were fully targeted to allow water flow into the well. Lithological data showed that all the pumped wells were fully penetrating (verified by screen locations) and this then ruled out partial penetration effect on the drawdown-time curves. However, log-log plots of drawdown data from study area data (Fig. 26) show recharge and apparent no flow boundary conditions enabling slight deviations from the theoretical curves.

BP1 and BP2 are juxtaposed across Ntcheu Fault (Fig. 16) and their aquifer's responses to pumping were analyzed. Table 4a shows that screens covered almost the entire sections of these wells, allowing free flow of groundwater into these boreholes. BP1 which was constantly pump tested for 12 hrs at 1 L/s discharge rate showed an increased drawdown in its log-log plot (Fig. 26a) until 3 minutes since pumping started and corresponding to a depth of 18.1 mbgl (meters below ground level) as read with Fig. 17a. However, the drawdown stabilized after 3 minutes at 18.1 mbgl until 100 minutes and 19.6 mbgl, representing presence of a recharge zone that contributed water to the well which in turn maintained water levels in the borehole. Lithological data (Fig. 16) shows vertical

fractures in the fractured amphibole gneiss and fractured hornblende-biotite-gneiss that could easily enable preferential recharge process into the delineated recharge zones. After 100 minutes, drawdown sharply increased in BP1, representing presence of a no-flow boundary.

Across the fault, log-log plot for BP2 which was constantly pumped for 12 hours at 2L/s discharge rate showed an increased drawdown until 1 minute since pumping started corresponding to a depth of 31.7 mbgl. After 1 minute, BP2 demonstrated a strong recharge zone that maintained a stable water level until 720th minute. Recharge zone depths for BP1 and BP2 show that there is an apparent flow potential towards BP2, that is, from 18.1 mbgl towards 31.7 mbgl respectively. Log-log plots also showed bilinear type of flow (line fit with slope of 0.25) as the active type of groundwater flow in BP1 and BP2. This suggests water flow influence from both fractures and rock matrix.

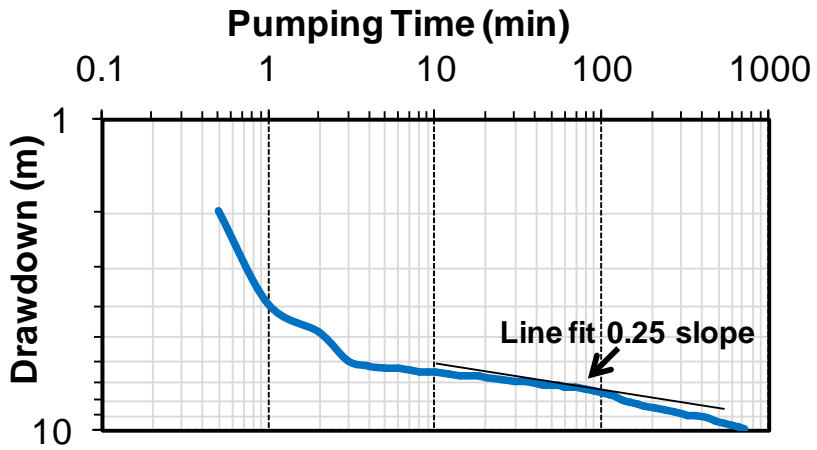


Fig. 26a: Relationship between drawdown data and pumping time at BP1.
See Figure 5 for location.

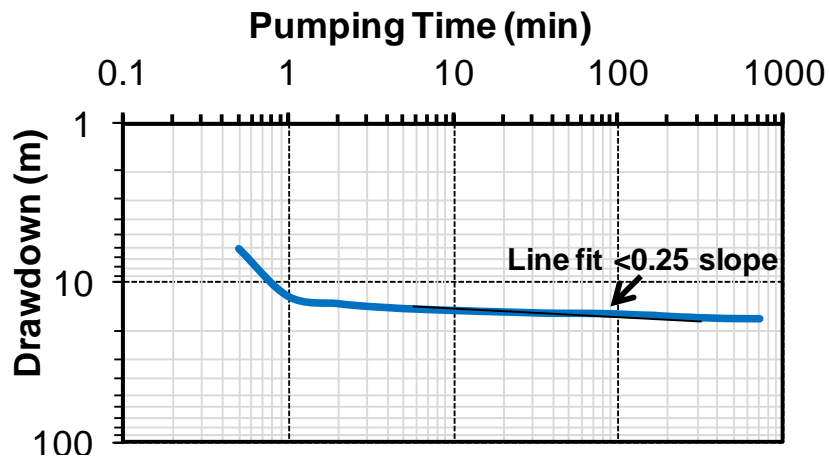


Fig. 26b: Relationship between drawdown data and pumping time at BP2.
See Figure 5 for location.

BP3 and BP4 are also located side by side across Ntcheu Fault in the lower reaches of the catchment (Fig. 16). After constantly pumping at 0.5L/s discharge rate for 12 hrs, log-log plot of drawdown data for BP3 showed an increased drawdown until 2 minutes since pumping started, corresponding to a depth of 12 mbgl when read with Fig. 17a. Stabilized drawdown was observed after 2 minutes until 4 minutes corresponding to 12.1 mbgl and signaling presence of recharge zone in the early time zone of pumping test. After 4 minutes until 15 minutes, a steep increase in drawdown was observed signifying a no-flow zone from 12.1 mbgl to 15 mbgl. Drawdown stabilized at 16 mbgl which corresponded to 16 minutes since pumping started. This stabilization in drawdown indicated an apparent presence of recharge phenomenon at this depth. A similar recharge boundary was also observed from 17 mbgl to 18.1 mbgl which corresponded to between 50 minutes to 100 minutes since pumping started respectively. After 100th minute since pumping started, drawdown data showed a no-flow boundary in the borehole peripheral. At the same time, BP4 showed pronounced stabilization of drawdown after 30 minutes to 50 minutes since pumping started corresponding to the recharge depth of between 17.5 mbgl and 17.8 mbgl respectively. The two boreholes show similar recharge depths of around 17 mbgl and 18 mbgl.

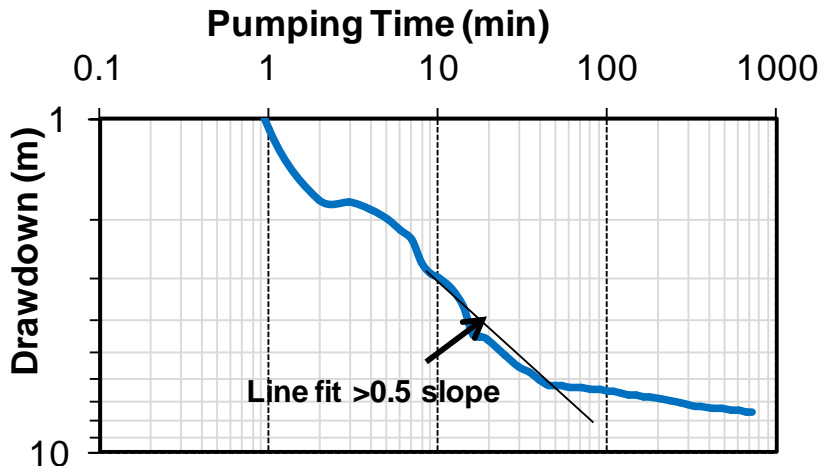


Fig. 26c: Relationship between drawdown data and pumping time at BP3.
See Figure 5 for location.

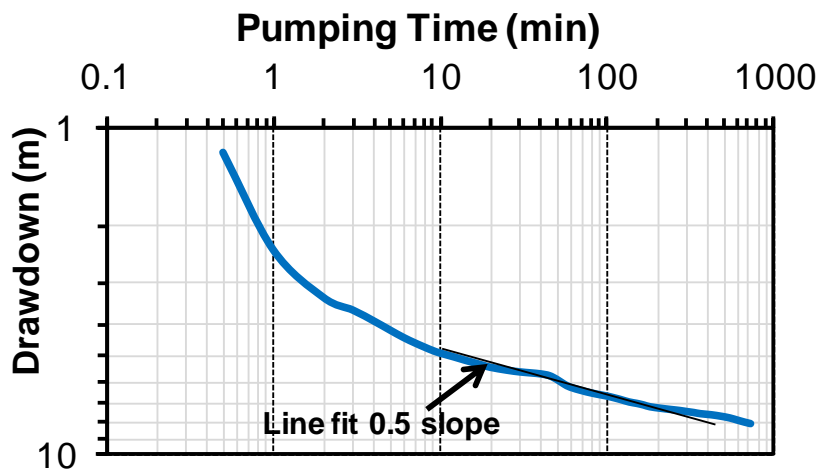


Fig. 26d: Relationship between drawdown data and pumping time at BP4.
See Figure 5 for location.

In addition, lithological data also shows presence of vertical fractures that could be feeding these recharge depths. Log-log plots of drawdown data showed (line fit with slope of 0.5 or more) that the dominant flow type in BP3 and BP4 is linear type of flow where water from fractures play a critical role in the general groundwater flow in this fractured rock system.

5.4 Fracture locations and flow types

Sarma et al., (2014), Xiao and Xu, (2014) and Bourdet et al., (1989) established that drawdown derivatives are highly sensitive to changes in drawdown behaviors that are difficult to notice on simple drawdown curves. For this reason, derivatives of drawdown are powerful tools to understand detailed behaviors of the fractured rock aquifers from drawdown data. Derivatives of drawdown data can therefore be used to estimate recharge depths and fracture locations in the fractured rock media.

However, before using derivatives of drawdown data, it was necessary to carry out additional verification of reliability of drawdown data. Recovery data is one tool that can help verify reliability of drawdown data (van Tonder et al., 2002).

Fig. 27 show water level changes with pumping time and residual recovery test results for each pumped well. The rest water levels at the beginning of pumping for BP1, BP2, BP3 and BP4 were 12.08, 19.59, 10.24 and 11.88 meters below ground level (mbgl) respectively. Residual recovery test in almost all wells showed that over 95% recovery of original static water level was reached in less than sixty (60) minutes. Specifically, BP1, BP2 and BP3 reached 90% recovery in less than six (6) minutes while BP4 reached 90% recovery just under 10 minutes after pumping stopped. By 60th minute, BP1 and BP2 had reached 98% of recovery, BP3 94% and BP4 96% of the original static water level.

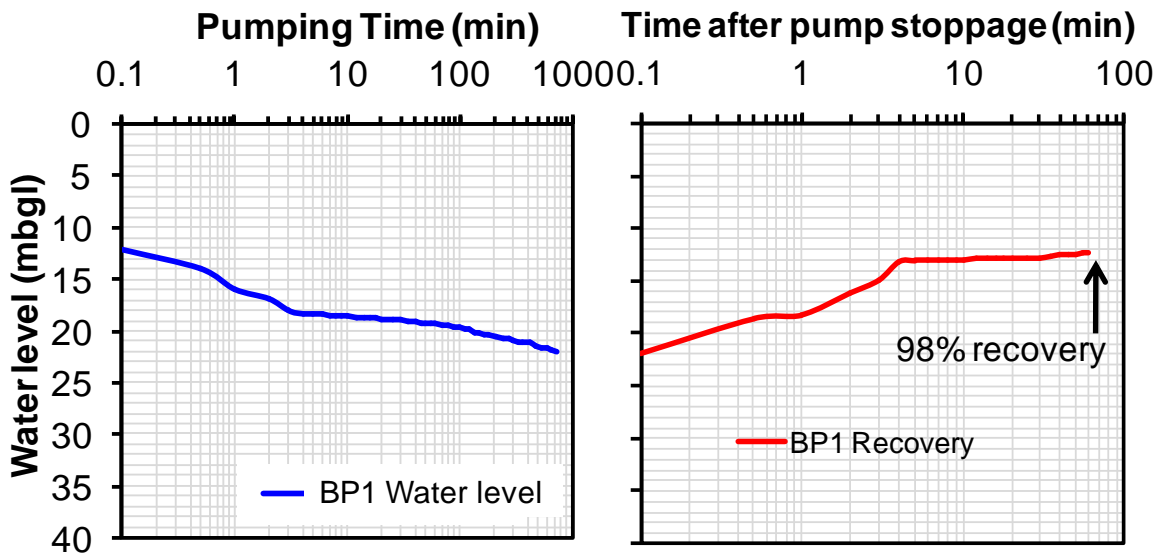


Fig. 27a: Comparing water level changes during pumping and recovery after pump stoppage at BP1.

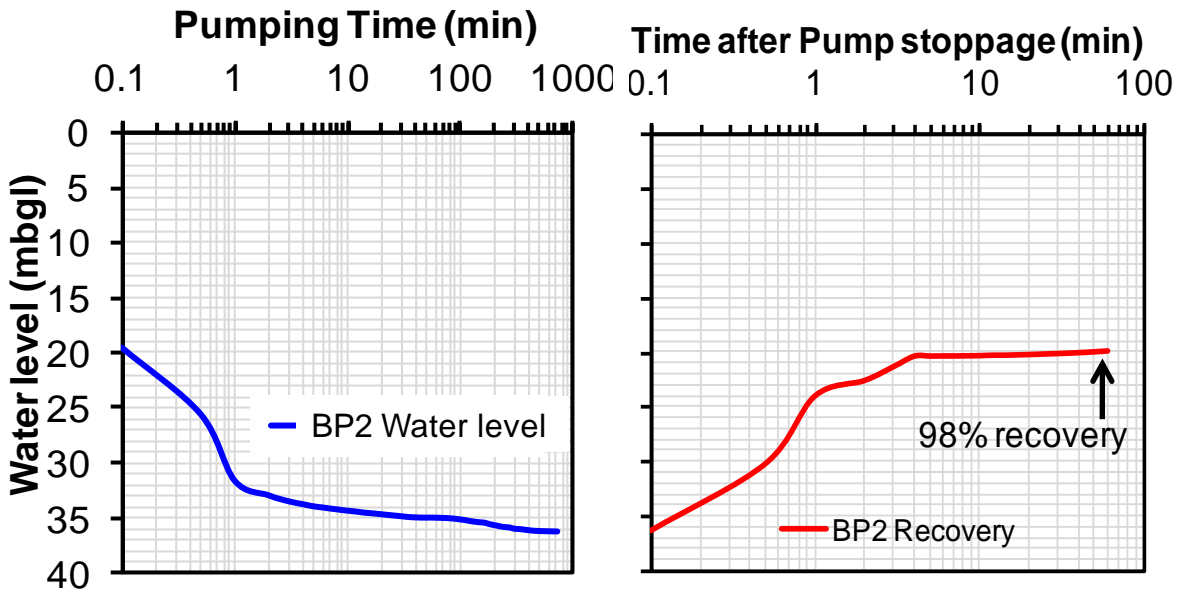


Fig. 27b: Comparing water level changes during pumping and recovery after pump stoppage at BP2.

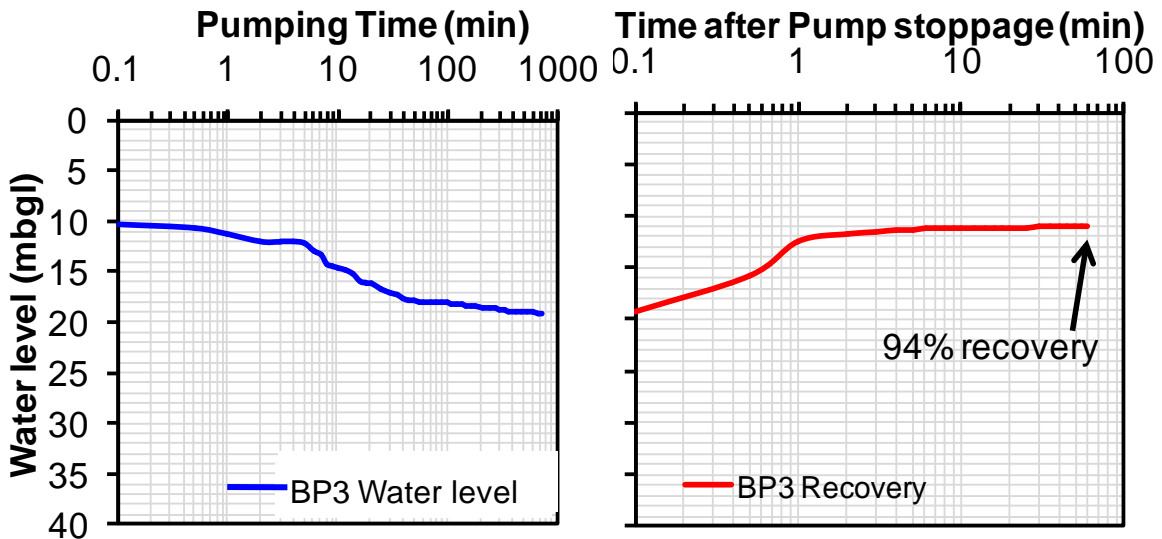


Fig. 27c: Comparing water level changes during pumping and recovery after pump stoppage at BP3.

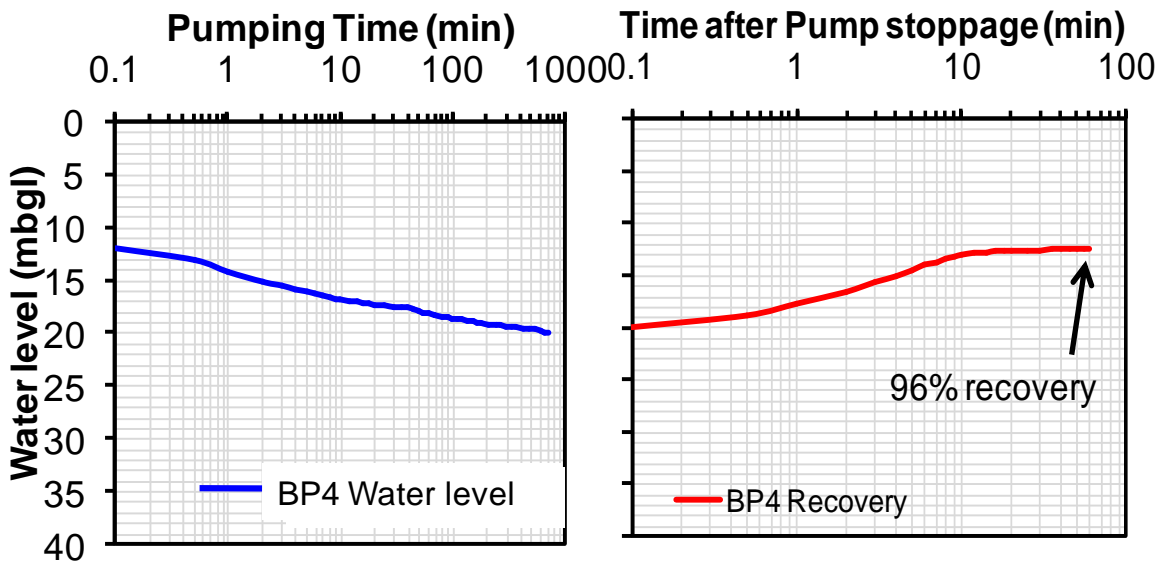


Fig. 27d: Comparing water level changes during pumping and recovery after pump stoppage at BP4.

As can be seen from Fig. 27, recovery data show a horizontal flattening way earlier (60 minutes) than total pumping time (720 minutes), suggesting that the fracture system is a continuum. The shapes of the recovery graphs are very similar to those of water level changes (Fig. 27a; 27b; 27c; 27d), implying that the quality of drawdown data is good and thus can be used for derivative diagnostic plots of drawdown to ascertain detailed hydraulic behavior of this fractured rock system. This agrees with sensitivity analysis conducted on the observed data as shown in Figure 7.

Using derivative plots of drawdown data from the pumping sites (Fig. 28a) alongside Fig. 17a, it was established that main fractures that influenced groundwater recharge at BP1 were located at around 19 mbgl which corresponded with 35 minutes since pumping started. Fifty (50) minutes after starting pumping, the derivative plots showed that these fractures got dewatered at 19.2 mbgl. The other fractures that influenced groundwater recharge process were identified at 20 mbgl which corresponded with 135 minutes since pumping started.

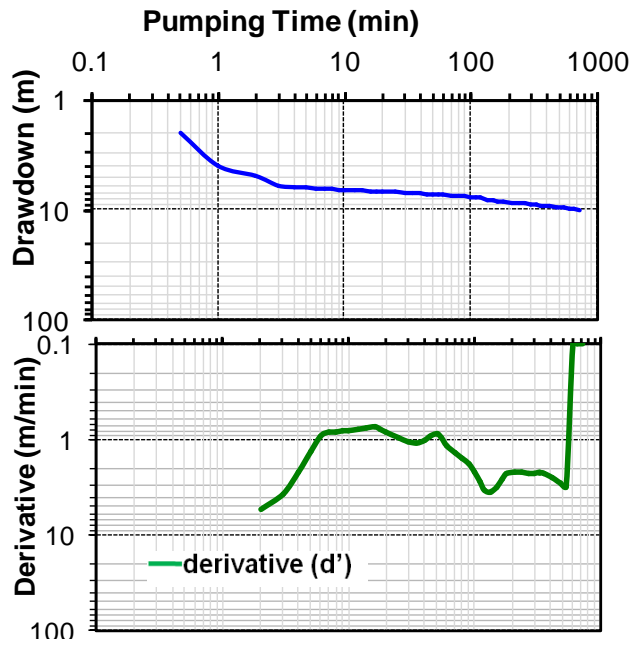


Fig. 28a: Relationship between derivatives of drawdown data and pumping time at BP1. Decreasing trend in derivative of drawdown indicates fractures.

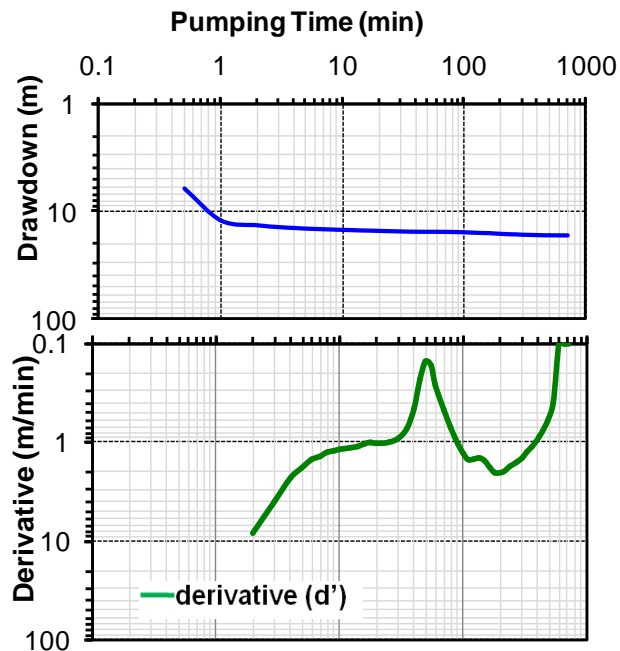


Fig. 28b: Relationship between derivatives of drawdown data and pumping time at BP2. Decreasing trend in derivative of drawdown indicates fractures.

In addition, the derivative plot for BP1 also indicates horizontal (plateau) plots in some instances. According to van Tonder et al., (2002), this phenomenon may suggest presence of bilinear type of flow occurring in the fractured rock aquifer. Since this is a double porosity rock media, the fractures are acting as the main conduits supported by less permeable rock matrix. The bilinear flow type assertion as construed from the derivative plot was also verified by line fit with slope of about 0.25 in log-log plot of drawdown data (Fig. 26a).

Derivative plot for BP2 also showed that main fractures that contributed water into this well were located at 34.9 mbgl which corresponded to 30 minutes after pumping started. The fractures got dewatered at 35.1 mbgl which is 50 minutes after pumping started. At this time, derivative of drawdown data increased dramatically. However, before the main fractures, derivative plots show horizontal line fit indicating presence of bilinear type of flow, a phenomenon involving flow from both the fractures and the rock matrix. This assertion was verified by line fit with slope of less than 0.25 in Fig. 26b. Meanwhile, location of the fractures and water levels at both BP1 and BP2 showed hydraulic gradient towards BP2, indicating possibility of groundwater flow across the fault.

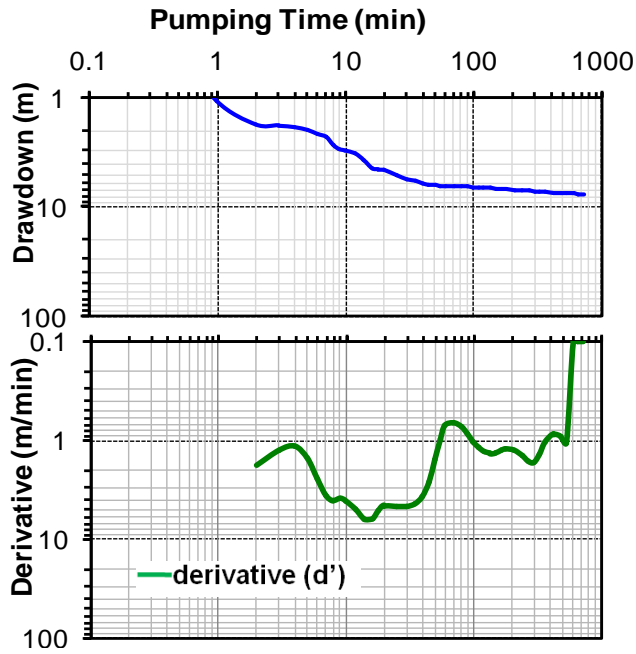


Fig. 28c: Relationship between derivatives of drawdown data and pumping time at BP3. Decreasing trend in derivative of drawdown indicates fractures.

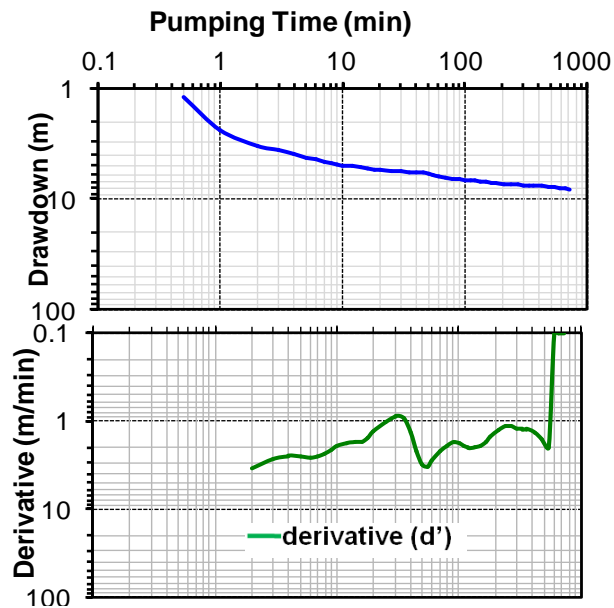


Fig. 28d: Relationship between derivatives of drawdown data and pumping time at BP4. Decreasing trend in derivative of drawdown indicates fractures.

While BP1 and BP2 showed specific singular locations of main fractures, derivative plot for BP3 showed multiple locations of fractures within the fractured hornblende-biotite-gneiss rock media. The main fractures were located at 12 mbgl which corresponding to 2 minutes since pumping started, at 16 mbgl, which corresponded to 16 minutes, and 18.8 mbgl which corresponded to 300 minutes since pumping started. For BP4, derivative plots showed that the main fractures were located at 15.2 mbgl which corresponded to 2 minutes after pumping started and 18 mbgl which corresponded to 55 minutes since pumping started. Both these derivative plots did not show pronounced horizontal line fit as was the case with BP1 and BP2, suggesting that bilinear flow could not be the most active type of flow. However, line fits with slope of around 0.5 in the log-log plots of drawdown data (Fig. 26c; 26d) suggested that linear flow was the dominant type of flow around these wells. Additionally, localized vertical fractures as deduced from outcrops and lithological data around these wells suggested rapid preferential recharge system that eventually feeds the identified main fractures.

At aquifer level, however, since BP1, BP2, BP3 and BP4 are all fully penetrating wells, the horizontal portions in the derivative plots of drawdown data shows existence of radial acting flow.

5.5 Linking hydraulic tests and stable isotopes

Variations of stable isotopic data during hydraulic tests can help in the understanding of origins of water and associated hydraulic regimes (Roques et al., 2014). Fig. 29, Fig. 30 and Fig. 32 show $\delta^{18}\text{O}$ and deuterium and subsequent groundwater level changes with increase in pumping time for BP1, BP2, BP3 and BP4. For BP1, the decrease in water level coincided with the depletion of $\delta^{18}\text{O}$ and δD while the apparent stabilization in water level showed a sharp increase in δD values, suggesting that at this stage, the well could be tapping groundwater that was recharged from the source that was affected by evaporation process (Fig. 32a). Before 4 hrs (240 minutes) of pumping time, δD values showed continued decrease, deviating from similarity with rainwater samples' average deuterium value of -34.0 ‰. However, this value still plots along LMWL (Fig. 29). Drawdown derivatives (Fig. 28a) show presence of fractures at this section. Drawdown derivatives and deuterium data therefore suggest hydrological connection between rainwater and sampled groundwater probably through the fractures.

At 4 hrs (240 minutes) of pumping time, the least δD value for BP1 is observed. At this section, drawdown derivatives (Fig. 28a) show influence of flow from both the fractures and rock matrix and a slight deviation from rainwater deuterium values, that is, -42.0 ‰ against -34.0 ‰ respectively. However, d-excess value of groundwater at this depth (15.0 ‰) is similar to rainwater (15.1‰) suggesting that the sampled rainwater could still be the source of recharge at this depth (Table 3c).

As pumping time increased, deuterium values for BP1 became more enriched. Since slopes and intercepts of groundwater regression line (6.3 and -5.22 respectively) suggest evaporation of rainwater to be the process responsible for stable isotopic enrichment in this study area, the enriched deuterium values in groundwater suggest increased contact with evaporated rainwater through the fractures. Drawdown derivatives also show presence of the fractures at a location coinciding with 5 hrs (300 minutes) after pumping started, thus

corroborating the possibility of hydrological connection between groundwater and evaporated rainwater through the fractures.

$\delta^{18}\text{O}$ and δD values for BP2 generally decreased with an increase in groundwater water level depth and stabilized together with water levels afterwards (Fig. 29; Fig. 30). Drawdown derivatives (Fig. 28b) and Transmissivity values (Fig. 17b) show that BP2 had the most permeable fractures, with averaged Transmissivity value of $136.5 \text{ m}^2/\text{day}$ but the least storative rock matrix (1.36×10^{-6}) in the study area. However, their variations were the most stable, suggesting the reason why deuterium varied less than BP1 and dampening effect of groundwater mixing. Increased permeability values and less but stable storativity and less varied deuterium values suggest that the double porosity nature of the fractured rock aquifer is more dominated by the fractures. However, the more depleted deuterium values imply detachment from the direct preferential rainwater recharge processes as is suspected in the other wells. In this case, the decrease in stable isotopic ratio suggests that water flowing into this BP2 could have been recharged under colder conditions, particularly higher altitude areas. It means therefore that BP2 could be receiving groundwater from regional recharge zone.

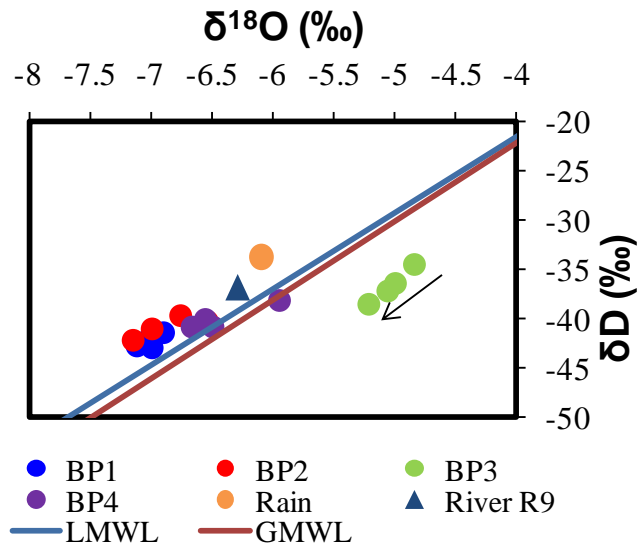


Fig. 29: $\delta^{18}\text{O}$ and δD for pumped wells at 0hr, 4hr, 8hr and 12hr of pumping test time.

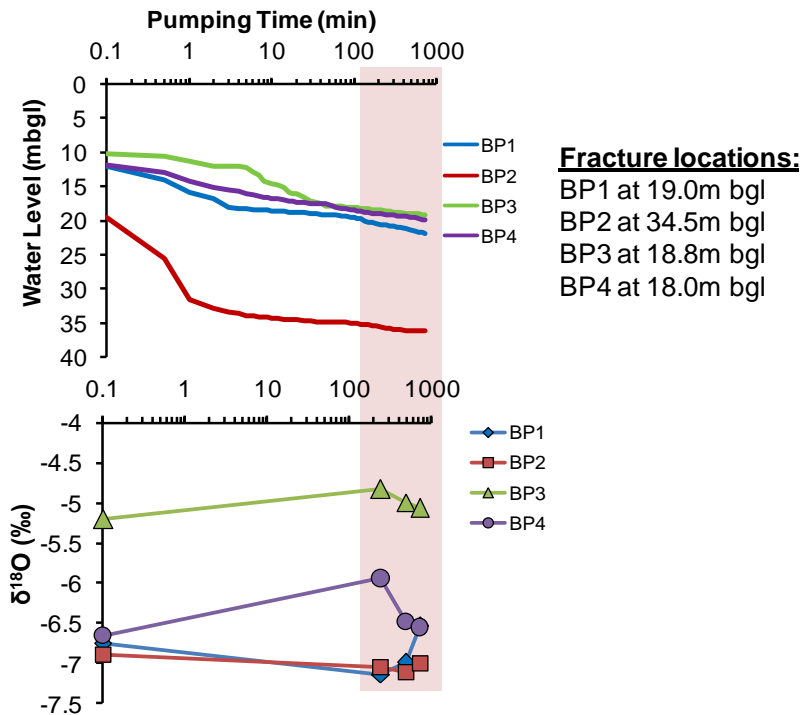
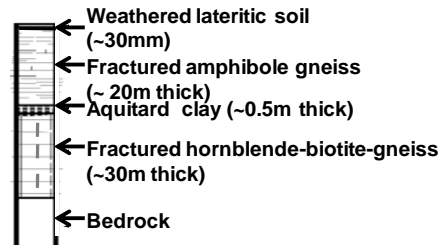
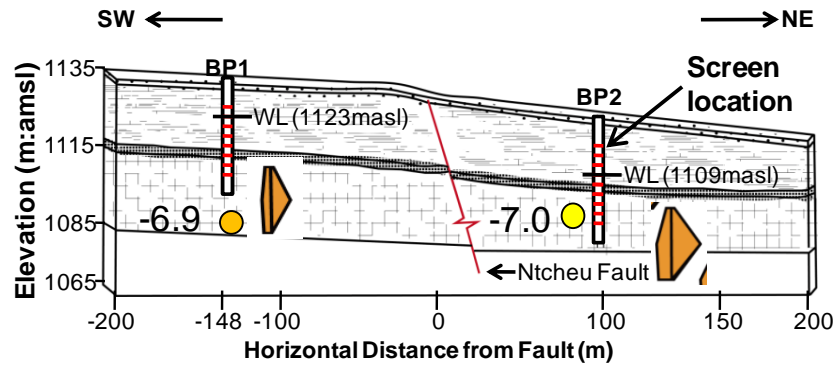


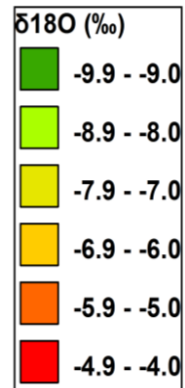
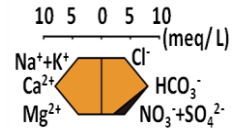
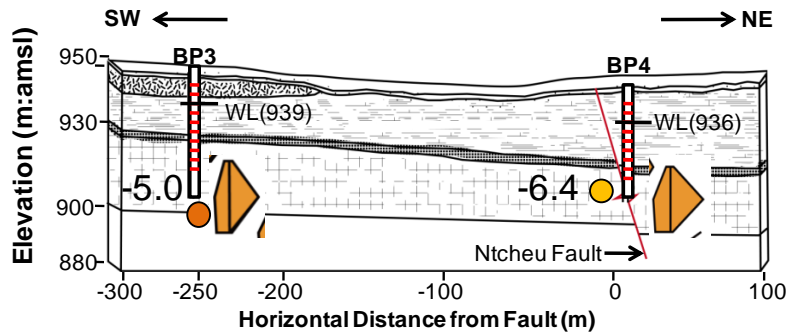
Fig. 30: Variations in water level and $\delta^{18}\text{O}$ values with pumping time at pumped wells.

In India, Sukhija et al., (2006) demonstrated that preferential rainwater recharge process through fractures easily maintains similar stable isotopic signatures in groundwater than lateral or through thick overburden soil. Due to pronounced deviation from rainwater deuterium value, it is postulated here that BP2 may have horizontal running fractures. Silica (SiO_2) values for BP2 also show deviation from rainfall, that is, 128.6 mg/L against 0.05 mg/L, suggesting longer flow paths as these waters are thought to be under early stages of geochemical evolution (Fig. 33). Depleted stable isotopic values in lateral groundwater recharge processes were similarly reported in China by Zhang et al., (2014) and Yuan et al., (2011).



Legend - Lithology

(31a)



Legend - Lithology

(31b)

Fig. 31: Stable isotopic and geochemical variations at pumped wells with thin overburden soils, geological fault and fractured hornblende-biotite-gneiss rock formation.

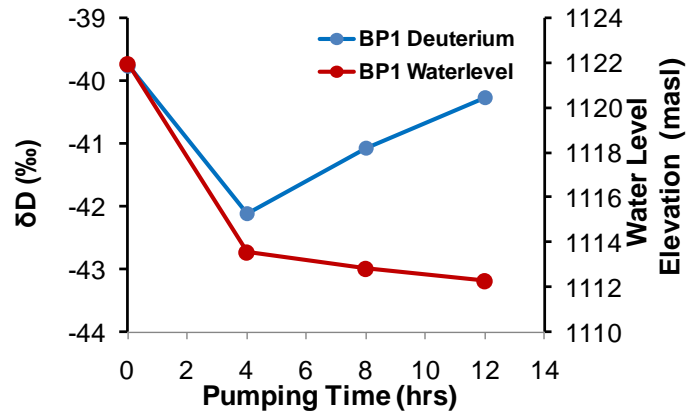


Fig. 32a: Relationship between Water level, Deuterium and Pumping Time at BP1

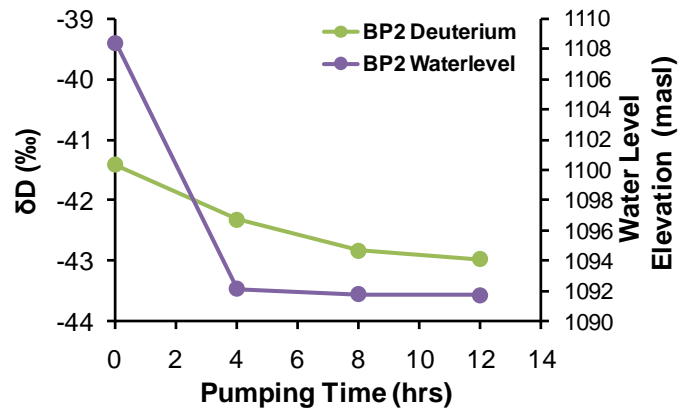


Fig. 32b: Relationship between Water level, Deuterium and Pumping Time at BP2

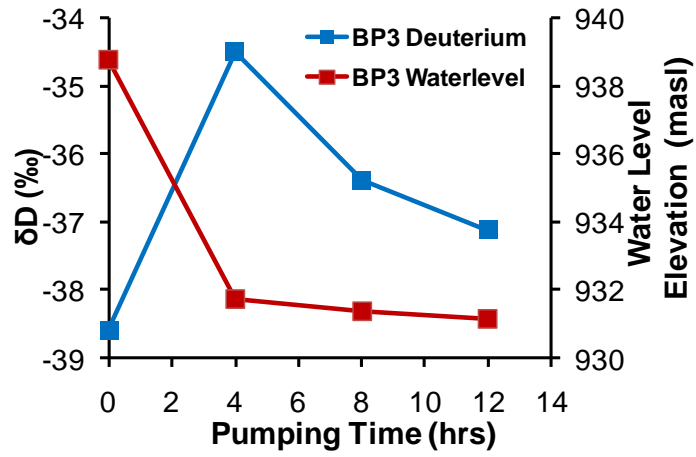


Fig. 32c: Relationship between Water level, Deuterium and Pumping Test at BP3

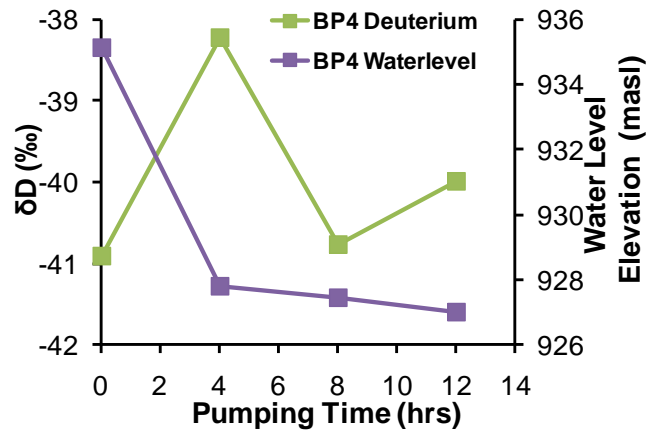


Fig. 32d: Relationship between Water level, Deuterium and Pumping Test at BP4

Fig. 32c shows that as groundwater level decreases deuterium values increase and decrease as water level stabilizes. Fig. 28c shows that until 5 hrs (300 minutes) since pumping started, drawdown derivative shows existence of fractures that seem to enable interaction with rainwater as seen from similarity in deuterium values, that is, δD_{BP3} equals 34.5 ‰ and δD_{Rain} equals 34.0 ‰. After 5 hrs (300 minutes), flow from both the fractures and rock matrix seem to dominate, with slightly enriched deuterium values. The $\delta^{18}O$ and δD values for pumped wells show that stable isotopic values for BP3 are more enriched than any other well under study (Fig. 29). Average d-excess value for BP3 (3.6 ‰ against 15.1 ‰ for rain) suggests that it was recharged by evaporated rainwater under different relative humidity conditions than the sampled rainfall.

BP4 shows varied deuterium values with decrease in groundwater level. As water level stabilizes, deuterium values continue to vary, decreasing at 8 hours and then increasing again at 12 hours. Influence of the fractures at 4 hrs (240 minute) and 12 hrs (720 minutes) and of the rock matrix and fractures at 8 hrs (480 minutes) is also evident. Drawdown derivatives (Fig. 28d) and Transmissivity data (Fig. 18) also show agreement with this interpretation.

At zero pumping, however, $\delta^{18}O$ value decreases from -6.9 ‰ at BP1 to -7.0 ‰ at BP2 while geochemical concentration increases from BP1 towards BP2. Hydraulic gradient also increases towards BP2 (Fig. 31a). At the same time, $\delta^{18}O$ decreases from -5.0 ‰ at BP3 to -6.4 ‰ at BP4 while geochemical concentration and hydraulic gradient also increase towards BP4 (Fig.31b)

Regional groundwater flow processes

Fig. 13 and Table 3 show geochemical concentration increasing with decrease in elevation (NW - SE direction) except around ridge area in the study area. According to Mulligan et al., (2011), increased geochemical concentration is usually associated with longer groundwater flow paths as a result of rock-water interaction along the flow paths. Poor correlation between Ca^{2+} and SO_4^{2-} ions in the deeper groundwater (DGW) gives another clue as to the possibility of geochemical evolution of groundwater along flow path from upstream recharge area to the valley section (e.g. Ako et al., 2012).

The $\delta^{18}\text{O}$ compositions also show similarities between springs in the high altitudes (-9.3 ‰ to -8.2 ‰ in dry season) and deep groundwater (-8.7 ‰ to -7.5 ‰) along the valleys (Fig. 22). In addition, d-excess values for spring water and some deeper groundwater (DGW) at the valley section also show possibility of recharge under similar relative humidity conditions (Fig. 24a), contrary to most of shallow groundwater (SGW) that is located in between springs and deeper groundwater.

Recharge water line also shows that some wells representing deep groundwater (DGW) in the valley section, for example, B13 and B15, seem to be recharged from a regional recharge zone that lies between 1317 and 1513 masl, similar to spring water recharge areas (Fig. 25). These phenomena suggest existence of regional groundwater recharge and flow system and thus possibility of lateral fracture connectivity linking the two water reaches in this fractured rock aquifer. Similar regional flow systems were observed by Liu et al., (2012) in mountain-plain transitional area in China and by Yamanaka et al., (2011) in lower central plains of Thailand.

5.6 Local flow process and effect of Ntcheu Fault

Elevated geochemical and stable isotopic compositions and hydraulic heads of shallow groundwater along the ridge show distinct water type suggesting local flow system. Hydraulic head and geochemical concentrations increase from B3 towards B1 and B4 towards B5 (Fig. 34). Specifically, $\delta^{18}\text{O}$ values vary from -5.2 ‰ at B3 to -5.4 ‰ at B1 and -5.1 ‰ at B4 to -5.3 ‰ at B5. Hydraulic head at B3 is 1165 masl while at B1 is 1120 masl and 1148 masl at B4 and 1120 masl at B5 in dry season. Similar trend is observed in rainy season where hexa-diagrams show increased concentrations from B3 towards B1 and B4 towards B5. Decreasing $\delta^{18}\text{O}$ values are observed from B3 towards B1 (-4.8 to -5.3 ‰) while slightly increasing from B4 towards B5 (-5.7 to -5.2 ‰). In this regard, geochemical and isotopic compositions of B4 and B5 that are neighbour features along the ridge but drilled in two different aquifers indicate possibility of inter-aquifer connectivity (aquifer leakage) with groundwater flowing from B4 through the clay aquitard and towards B5 (Fig. 34). B6 however, seems to show a slightly different water regime as it displayed a more depleted isotopic values than the other wells at the ridge section. The stable isotopic values are similar to spring water in the upstream areas (Fig.22).

Boreholes juxtaposed across Ntcheu Fault show similar $\delta^{18}\text{O}$ compositions that is -8.7 ‰ and -8.3 ‰ in dry season and -5.4 ‰ and -5.1 ‰ in rainy season for B8 and B9, -6.9 ‰ and -7.0 ‰ for BP1 and BP2 and -5.0 ‰ and -6.4 ‰ for BP3 and BP4 in rainy season (Fig. 31; Fig. 34). Geochemical concentrations increase in the SW-NE direction, that is, from BP1 towards BP2 and BP3 towards BP4 and in the W-E direction from B8 towards B9. Hydraulic gradient also follows similar pattern as geochemical concentration. Silica (SiO_2) values which normally indicate groundwater flow path as demonstrated by Mandal, et al., (2011), show increase from BP1 towards BP2, that is 112.3 mg/L to 128.6 mg/L respectively (Table 3; Fig. 33). This also suggests possible flow path and thus hydraulic connectivity between these two neighbour boreholes. Stable isotopic, geochemical compositions and hydraulic data of the wells juxtaposed across Ntcheu Fault

therefore strongly suggest permeability across the geological fault. To further verify this notion, lithological data from a borehole drilled in the fault itself at Wanyemba Village (BP4) (Fig. 4; Fig. 5; Fig. 31) was analyzed. In its lithological profile, it showed a 20 m thick section of a permeable mixture of decomposed clayey sand and fractured Hornblende-biotite-gneiss. This analysis shows that Ntcheu Fault acts as lateral conduit to groundwater flow in the NW-SE direction.

Additionally, $\delta^{18}\text{O}$ and δD values for the pump tested wells juxtaposed across Ntcheu Fault (BP1, BP2, BP3, BP4) also revealed similarities with rain sample ($\delta^{18}\text{O} = -6.1\text{‰}$ and $\delta\text{D} = -33.8\text{‰}$) suggesting that recent rainfall could be the source of recharge in these wells. $\delta^{18}\text{O}$ and δD values for all the sites do not vary much with depth and pumping time (Fig. 29; Fig. 30). $\delta^{18}\text{O}$ and δD values for BP1 and BP2 range from -6.8‰ to -6.5‰ and -39.8‰ to -40.3‰ and -6.9‰ to -7.0‰ and -41.4‰ to -43.0‰ respectively. BP3 and BP4 slightly plot away from rain sample and both LMWL and GMWL. $\delta^{18}\text{O}$ (‰) and δD (‰) values for BP3 range from -5.2‰ to -5.1‰ and -38.6‰ to -37.1‰ and -6.7‰ to -6.6‰ and -40.9‰ to -39.9‰ for BP4. BP3 in particular shows relatively enriched $\delta^{18}\text{O}$ (‰) values. The slope of the regression line of the stable isotopic data for these wells is lower than that of LMWL, that is, $\delta\text{D} (\text{‰}) = 2.7(\delta^{18}\text{O} (\text{‰})) - 22.7$ against $\delta\text{D} (\text{‰}) = 7.62(\delta^{18}\text{O} (\text{‰})) + 8.99$, also suggesting that isotopic fractionation during rainwater evaporation could be the cause of the enrichment as is the case with the other sampled wells. This could be the reason why its values plot slightly under from both LMWL and GMWL.

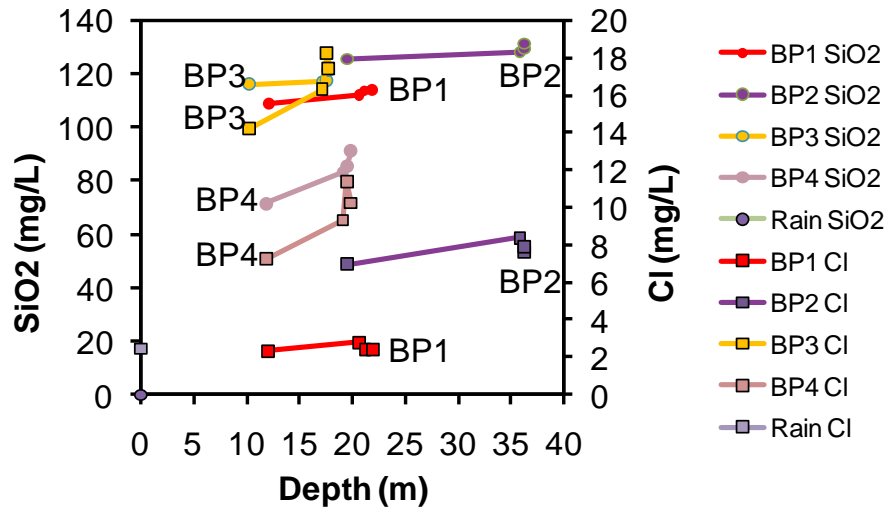


Fig. 33: Silica and Chloride values in pumped wells across Ntcheu Fault

Table 6: Correlation coefficient of major parameters in pumped wells (BP1, BP2, BP3, and BP4).

	$\delta^{18}\text{O}$	TDS	Na^+	Mg^{2+}	K^+	Ca^{2+}	Cl^-	HCO_3^-	SO_4^{2-}	NO_3^-	pH	Temp	SiO_2	Screen depth
$\delta^{18}\text{O}$	1.00													
TDS	0.52	1.00												
Na^+	0.08	0.85	1.00											
Mg^{2+}	0.56	0.78	0.42	1.00										
K^+	0.38	0.49	0.39	0.37	1.00									
Ca^{2+}	0.15	0.91	0.91	0.71	0.39	1.00								
Cl^-	0.85	0.74	0.27	0.86	0.44	0.49	1.00							
HCO_3^-	-0.02	0.80	0.83	0.69	0.37	0.96	0.36	1.00						
SO_4^{2-}	0.16	0.82	0.98	0.32	0.37	0.81	0.26	0.70	1.00					
NO_3^-	0.75	0.94	0.67	0.79	0.48	0.73	0.86	0.59	0.69	1.00				
pH	0.62	0.42	0.27	0.24	0.24	0.16	0.44	0.02	0.37	0.60	1.00			
Temp	0.54	0.66	0.42	0.48	0.52	0.49	0.69	0.32	0.45	0.68	0.21	1.00		
SiO_2	-0.02	-0.53	-0.81	0.06	-0.17	-0.52	0.05	-0.41	-0.90	-0.44	-0.44	-0.18	1.00	
Screen depth	-0.50	-0.22	-0.19	0.06	-0.06	0.07	-0.18	0.23	-0.35	-0.42	-0.77	-0.13	0.53	1.00

One further observation was made on BP4. This well showed a relatively lower SiO₂ concentration than BP3 which is located on the upstream side of the fault (Fig. 33). Since BP4 is drilled right into the geological fault with permeable decomposed material, it was suspected that the geological fault could be acting as a preferential recharge zone from local precipitation. The notion that the geological fault acts as a preferential recharge zone around BP4 was not further analyzed in detail under this study. It therefore provides a good thematic area for further research. Generally, however, Table 6 shows that Mg²⁺ and SO₄²⁻ had poor correlation (R = 0.32) indicating that there might have been very weak cation exchange process in the solution (e.g. Liu et al., 2015). This is corroborated by a strong correlation between Ca²⁺ and SO₄²⁻ (R = 0.81) which suggests that no significant geochemical evolution might have taken place. Chloride concentrations in these groundwaters were very similar to rainwater (Table 3c). This tries to strongly hint that groundwater in the pumped wells could have been recently recharged from precipitation.

Further analysis of δ¹⁸O values and total dissolved solids (TDS) data revealed that in dry season, deeper groundwater (DGW) at B12 (-7.4 ‰ and 426 mg/L) was similar with its neighbour feature River sample site, R8 (-6.7 ‰ and 252 mg/L). Hydraulic gradient also increased from R8 towards B12. This suggested a probable surface water and groundwater interaction. Similar interpretation was made in Lake Nyos catchment in Cameroon by Kamtchueng et al., (2015).

It is evident from the foregoing therefore that overburden soil thickness, fractures and boreholes proximity to faults affect recharge processes in Rivirivi Catchment.

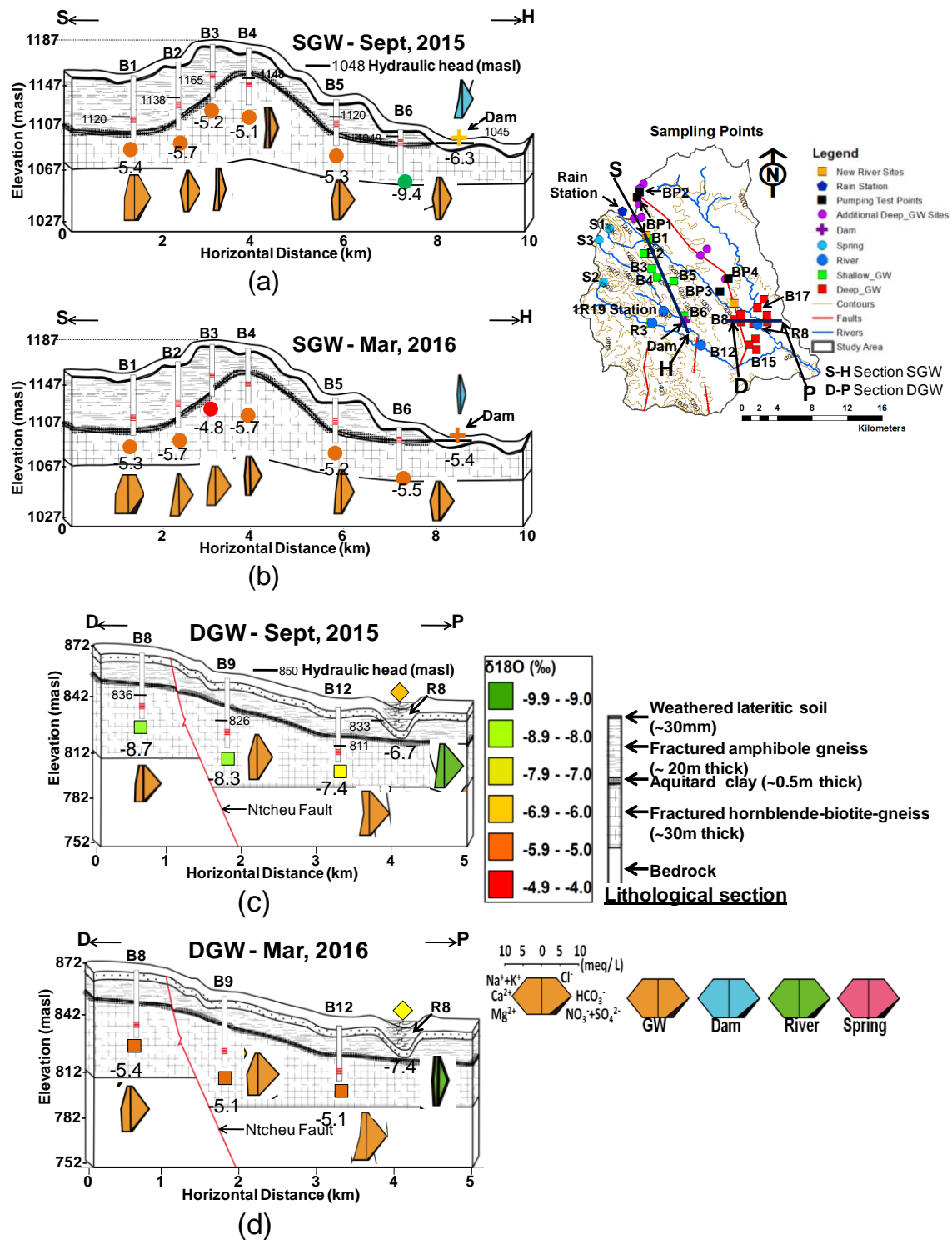


Fig. 34: Geochemical, hydraulic head and isotopic variations with season, well depth, neighbour features and overburden soil thickness (thin at *a* and *b* and thick at *c* and *d*) at unpumped wells

Chapter 6: Conclusions

In this study, stable isotopes, geochemistry and pumping tests have shown that apart from topography, overburden soil conditions, nature of the underlying geology (in this case fractured hornblende-biotite-gneiss of the basement complex) and geological fault zone are the main hydrogeological factors that control groundwater resource in Upper Rivirivi Catchment. These factors may not have same magnitude of effect in other geological formations and climatic environments as evidenced by results from Negrel et al., (2011) in India.

Geochemical data has clearly shown that the catchment is dominated by Mg-Ca-HCO₃ water facies and that this kind of water regime is at an early stage of geochemical evolution. Stable isotopic data showed less variation with seasonality and location at Ridge shallow groundwater (SGW) unlike Valley deeper groundwater (DGW). However, Ridge SGW maintained similar d-excess and $\delta^{18}\text{O}$ values with rainwater, suggesting that rainfall could be the main source of recharge in this area.

In line with the foregoing, an isotopic gradient of -0.36‰ per 100 m increase in elevation was established. The recharge water line showed that there are three (3) delineated recharge zones in the study area. These include regional recharge zone at an elevation of between 1317 and 1513 masl, intermediate recharge zone lying between 1094 and 1317 masl and local recharge zone which lies between 954 and 1094 masl. Most river water samples showed to have been recharged from intermediate recharge zone (1094 to 1317 masl). However, SGW at ridge section shows unique phenomenon as it is not consistent with the established altitude effect.

Geochemical, stable isotopic and pumping test data also revealed that the interface between fractured Hornblende-biotite-gneiss and thin overburden soils of up to 30 mm, mainly at Ridge section, create pathways that enable rapid preferential recharge processes

into SGW aquifers. Meanwhile, the interface between thicker overburden soils of up to 3 m along the valley section and fractured rock formation seems to enable only large rain events to recharge the aquifers, allowing water from small rain events evaporate completely without leaving any evaporation signal in the medium.

It was further revealed in this study that Ntcheu Fault that cuts through the fractured Hornblende-biotite-gneiss acts as a lateral conduit for groundwater flow in the NW-SE direction and as a probable preferential recharge pathway. This information is important because it informs us that whatever groundwater resource management practices happening upstream of the fault may directly affect those in the downstream unlike when the fault acts as a barrier to groundwater flow.

In addition, pumping test data coupled with stable isotopes and geochemistry indicated that the geological formation in Upper Rivirivi Catchment is fractured enough to allow linear groundwater flow between aquifers, allow localized flow at Ridge section and aid regional flow from spring area in the upstream to the valley section. The presence of elevated concentrations of NO_3^- signified that the resource was rapidly replenished by contaminated groundwater.

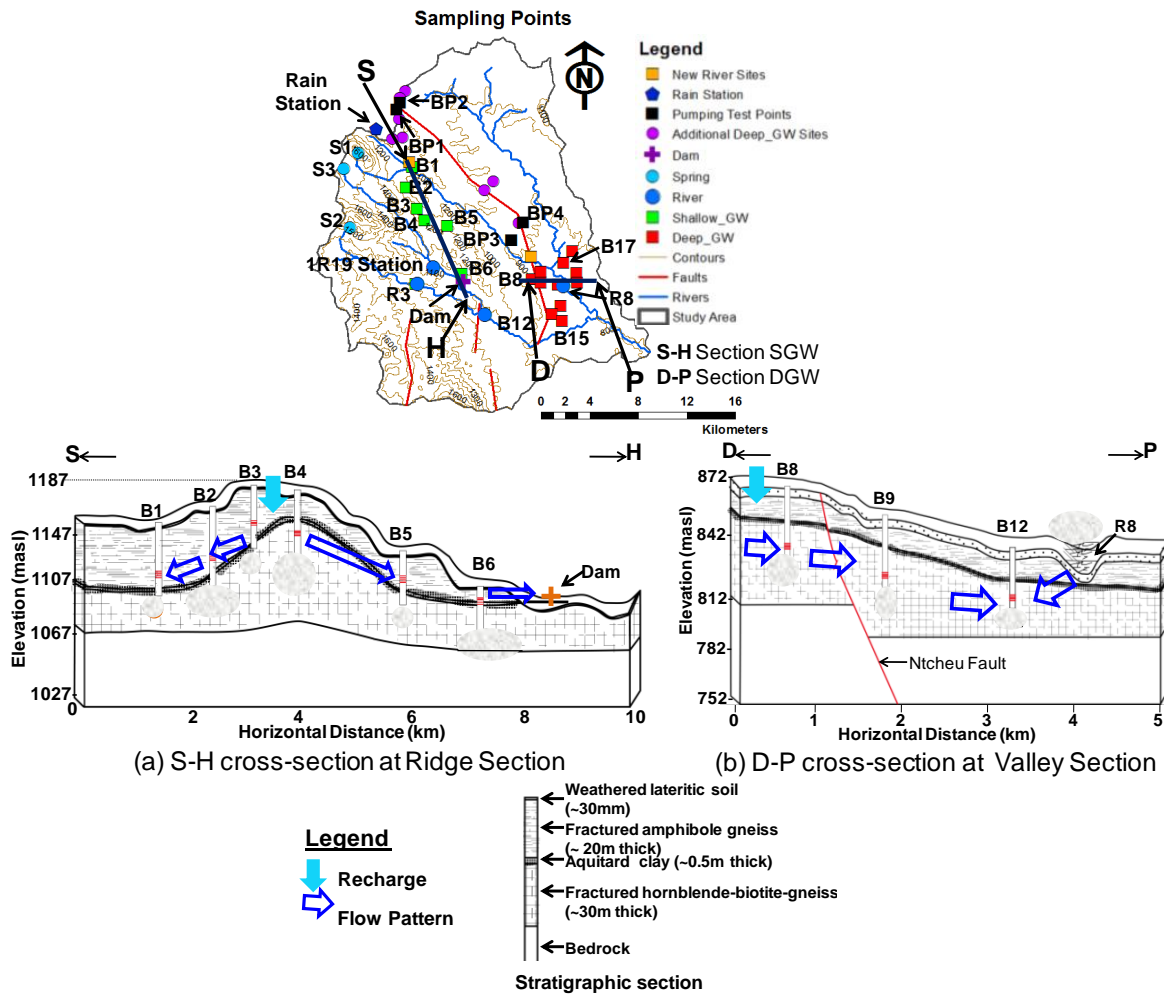


Fig. 35: Conceptual model of localized recharge and flow processes as deduced from geochemistry, stable isotopes and hydraulic head data at S-H Ridge section and D-P Valley section in Rivirivi Catchment. See map for location of S-H and D-P.

Fig. 35 shows the conceptual model of the recharge and flow processes as established in this study. The nature and type of the geological formation in the study area enables rapid groundwater recharge and flow processes that leave the aquifers susceptible to inter-annual climatic variabilities and anthropogenic contamination. Understanding the nature and manner of these processes is therefore critical if we are to sustainably manage water resources particularly in these vulnerable fractured rock formations with unknown aquifer parameters.

In conclusion, the approach and interpretation of these findings may be replicated in other data scarce catchments with similar geological settings. At a local scale, it is expected that these findings will provide first cues towards sustainable development and management of groundwater resource in Upper Rivirivi Catchment. As a data scarce catchment, these findings are expected to provide a springboard for further detailed research. It is highly recommended therefore that a comprehensive study to quantify groundwater resource at catchment level should be considered.

Acknowledgement

The author would like to express his sincere gratitude to his academic supervisor, Professor Dr Maki TSUJIMURA for his untiring moral support and insightful contributions throughout the course of this study. His thoughtful guidance and unconditional assistance have made this work possible.

The author is indebted to his PhD committee members comprising Professor Dr Kuniaki MIYAMOTO, Professor Dr Jun ASANUMA, and Professor Dr Zhenya ZHANG for their professional review and insightful comments on this work.

His sincere appreciation also goes to Professors guiding the Watershed research group, to which he was a member. These included Professor Dr Michiaki SUGITA, Professor Dr. Jun ASANUMA, and Professor Dr. Tsutomu YAMANAKA. The interactions during the joint seminars enriched the author's understanding of hydrological processes.

This work would not have been possible without funding from Japan Ministry of Education, Culture, Sports, Science and Technology under MEXT Scholarship terms. The author will remain forever indebted.

The moral and technical support the author received from Malawi's Ministry of Agriculture, Irrigation and Water Development during field surveys cannot go unmentioned. To this end, the author would like to acknowledge Ms Modesta Kanjaye (Director of Water Resources), Mr. Prince Mleta (Deputy Director - Groundwater Resources) and Mr. Macpherson Nkhata (Chief Hydrogeological Research Officer) for their unflinching support, even at a time when they were not obliged to.

The author's fellow Tsujimura Lab members made his stay in Japan a memorable feat. Thank you all for your support. Special mention should go to his Japanese lab mates who helped him settle in during his early days.

To his wife, Dorica and dear daughters Derora and Daphne; this is for you!

References

- Ako Ako, A., Shimada, J., Hosono, T., Ichiyanagi, K., Elambo, Nkeng, G., Eneke, T.E.G., Njila, R. N., (2012) Hydrogeochemical and isotopic characteristics of groundwater in Mbanga, Njombe and Penja (Banana Plain) - Cameroon. *J. Afr. Earth Sci.* 75, 25-36
- Alazard, M., Boisson, A., Marechal, J., Perrin, J., Dewandel, B., et al. (2016) Investigation of recharge dynamics and flow paths in a fractured crystalline aquifer in semi-arid India using borehole logs: implications for managed aquifer recharge. *Hydrogeol. J.* 24(1): 35-57
- Altinörs, A., Önder, H., (2008) A double-porosity model for a fractured aquifer with non-Darcian flow in fractures. *Hydrol. Sci. J.* 53: 868–882. doi:10.1623/hysj.53.4.868
- Apaydin, A., (2010) Relation of tectonic structure to groundwater flow in the Beypazari region, NW Anatolia, Turkey. *Hydrogeol. J.* 18: 1343–1356. doi:10.1007/s10040-010-0605-1
- Ayenew, T., Kebede, S., Alemyahu, T., (2008). Environmental isotopes and hydrochemical study applied to surface water and groundwater interaction in the Awash River basin. *Hydrol. Process.* 22:1548-1563. doi:10.1002/hyp.6716
- Bai M., Elsworth D., Roegiers J., (1993) Multi-porosity/multi-permeability approach to the simulation of naturally fractured reservoirs. *Water Resour. Res.* 29(6): 1621-1633.
- Balsamo, F., Bezerra, F.H.R., Vieirra, M.M., Storti, F., (2013). Structural control on the formation of iron-oxide concentrations and Liesegang bands in faulted, poorly lithified Cenozoic sandstones of the Paraiba Basin, Basin. *GSA Bulletin* 125 (5/6): 913-931. DOI: 10.1130/B30686.1
- Barenblatt GI, Zheltov YP, Kochina IN (1960) Basic Concepts in the Theory of Seepage of Homogeneous Liquids in Fissured Rocks. In *Well Testing in Heterogeneous Formations*. An Exxon Monograph. TD Streltsova.

John Wiley & Sons, New York, 413 p.

- Beekman, H.E., Selaolo, E.T., De Vries, J.J., (1999) Groundwater Recharge and Resources Assessment in the Botswana Kalahari. Executive Summary GRES-II, Geological Survey of Botswana and Faculty of Earth Sciences, Vrije Universiteit, Amsterda, 48p
- Bense, V.F., Person, M.A., (2006). Faults as conduit-barrier systems to fluid flow in siliciclastic sedimentary aquifers. *Water Resour. Res.* 42, W05421.
doi: 10.1029/2005WR004480.
- Bense, V.F., van Balen, R.T., de Vries, J.J., (2003). The impact of faults on the hydrogeological conditions in the Roer Valley Rift System: an overview. *Netherlands Journal of Geosciences* 82(1): 41-54
- Berkowitz, B., (2002) Characterizing flow and transport in fractured geological media: A review. *Adv. Water Resour.* doi:10.1016/S0309-1708(02)00042-8
- Bloomfield, K., & Garson, M. S. (1965) The geology of the Kirk Range, Lisungwe Valley area, (17). Retrieved from
<http://trove.nla.gov.au/work/12100223?versionId=14269459>
- Bourdet D, Gringarten AC., (1980) Determination of fissure volume and block size in fractured reservoirs by type-curve analysis. Paper SPE 9293, 1980 SPE Annual Fall Techn. Conf and Exhib., Dallas.
- Chavula GSM., (2012) Groundwater availability and use in Malawi. In Groundwater Availability and Use in Sub-Saharan Africa: A review of 15 countries, Pavelic P, Giordano M, Keraita B, Ramesh V, Rao T. (Eds.). International Water Management Institute (IWMI). Colombo, Sri Lanka; 78-90. doi: 10.5337/2012.213.
- Chilton, P.J., Foster, S.S.D., (1995). Hydrogeological characteristics and water-supply potential of Basement Aquifers in Tropical Africa. *Hydrogeol. J.* 3(1):36-49
- Chorowicz, J., (2005) The East African rift system. *J. Afr. Earth Sci.* 43: 379-410

- Clark, I., Fritz, P., (1997) *Environmental Isotopes in Hydrology*, CRC Press, Boca Raton, USA. 342
- Cook P.G., (2003) *A Guide to Regional Groundwater Flow in fractured rock aquifers*. CSIRO Land and Water. 115 p.
- Craig, H., (1961) Isotopic Variations in Meteoric Waters. *Science* (80-). 133, 1702–1703. doi:10.1126/science.133.3465.1702
- Dassi, L., (2010) Use of chloride mass balance and tritium data for estimation of groundwater recharge and renewal rate in an unconfined aquifer from North Africa: a case study from Tunisia. *Environ Earth Sci* 60: 861-871
- Delinom RM (2009) Structural geology controls on groundwater flow: Lembang Fault case study, West Java, Indonesia. *Hydrogeol. J.* doi: 10.1007/s10040-009-0453-z.
- Department of Climate Change and Meteorological Services (2016) Climate Data for Malawi. http://www.metmalawi.com/requests/data_requests.php. Last accessed October, 18, 2016
- de Vries, J. J., & Simmers, I., (2002) Groundwater recharge: An overview of process and challenges. *Hydrogeol. J.* 10(1), 5–17. <https://doi.org/10.1007/s10040-001-0171-7>
- Dewandel, B., Aunay, B., Marechal, J., Roques, C., et al., (2014) Analytical solutions for analysing pumping tests in a sub-vertical and anisotropic fault zone draining shallow aquifers. *J. Hydrol.* 509: 115-131
- Doveri, M., & Mussi, M., (2014) Water isotopes as environmental tracers for conceptual understanding of groundwater flow: An application for fractured aquifer systems in the “Scansano-Magliano in Toscana” area (Southern Tuscany, Italy). *Water* (Switzerland), 6(8), 2255–2277. <https://doi.org/10.3390/w6082255>
- Edoulati, N., Boutaleb, S., Bettar, I., Ouchbani, A., (2013) Contributions of chemical and isotopic tools for understanding the groundwater modes of recharge and flow in the lower Cretaceous aquifer in the Moroccan Sahara.

J. Water Resour. Protec. 5: 183-199.

- Edmunds, W. M., Smedley, P., (2000) Residence time indicators in groundwater: the East Midlands Triassic sandstone aquifer. *Appl. Geochemistry* 15: 737-752
- Folch, A., Mencio, A., Puig, R., Soler, A., Mas-Pla, J., (2011) Groundwater development effects on different scale hydrogeological systems using head, hydrochemical and isotopic data and implications for water resources management: The Selva basin (NE Spain). *J. Hydrol.* 403, 83–102. doi:10.1016/j.jhydrol.2011.03.041
- Folch, A., Mas-Pla, J., (2008). Hydrogeological interactions between fault zones and alluvial aquifers in regional flow systems. *Hydrol. Process.* 22:3476-3487. doi: 10.1002/hyp.6956
- Fontes, J.-Ch., (1980) Environmental Isotopes in groundwater hydrology. Handbook of Environmental Isotope Geochemistry, (P. Fritz, J-Ch. Fontes, Eds) Elsevier, Amsterdam, 75-140
- Gastmans, D., Hutcheon, I., Menegario, A.A., Chang, H.K., (2016) Geochemical evolution of groundwater in a basaltic aquifer based on chemical and stable isotopic data: Case study from the Northeastern portion of Serra Geral Aquifer, Sao Paulo state (Brazil). *J. Hydrol.* 535, 598–611. doi:10.1016/j.jhydrol.2016.02.016
- Gleeson, T., Novakowski, K., Kurt Kyser, T., (2009) Extremely rapid and localized recharge to a fractured rock aquifer. *J. Hydrol.* 376, 496–509. doi:10.1016/j.jhydrol.2009.07.056
- Guihéneuf, N., Boisson, A., Bour, O., Dewandel, B., Perrin, J., Dausse, A., Viossanges, M., Chandra, S., Ahmed, S., Maréchal, J.C., (2014) Groundwater flows in weathered crystalline rocks: Impact of piezometric variations and depth-dependent fracture connectivity. *J. Hydrol.* 511, 320–324. doi:10.1016/j.jhydrol.2014.01.061
- Hamza, S.M., Ahsan, A., Daura, H.A., Imteaz, M.A., Ghazali, A.H., Mohammed, T.A., (2016) Fractured rock aquifer delineation and assessment using spatial

analysis in Kano, Nigeria. *Arab. J. Geosci.* 9. doi:10.1007/s12517-016-2355-4

Hill, J. L., and Kidd, C. H. R., (1980) Rainfall-runoff relationships for 47 Malawi catchments. Water Resources Branch. Department of Lands, Valuation and Water, Report No. WRB-TP7

Holland, M., Witthuser, K.T., (2011) Evaluation of geologic and geomorphologic influences on borehole productivity in crystalline bedrock aquifers of Limpopo Province, South Africa. *Hydrogeol. J.* 19, 1065–1083. doi:10.1007/s10040-011-0730-5

Horne R.N., (1997) Modern well test analysis: A computer-aided approach. Petroway Inc. Palo Alto. USA.

IAEA/WMO., (2006) Global Network of Isotopes in Precipitation. The GNIP Database. <http://www.iaea.org/water>. Last access October 20, 2015.

Jefferson, A., Grant, G., Rose, T., (2006) Influence of volcanic history on groundwater patterns on the west slope of the Oregon High Cascades, *Water Resour. Res.* 42, W12411, doi: 10.1029/2005WR004812

Kambuku, D., Tsujimura, M., Kagawa, S., (2018) Groundwater recharge and flow processes as revealed by stable isotopes and geochemistry in fractured Hornblende-biotite-gneiss, Rivirivi Catchment, Malawi. *Afr. J. Environ. Sci. Technol.* 12(1): 1-14. doi: 10.5897/AJEST2017.2406

Kambuku, D.D., (2009) Assessment of conjunctive use of small earth dams and boreholes for sustainable rural livelihoods in a semi-arid area: Case of Lilongwe West Rural Groundwater Project area, Malawi. MSc Thesis. University of Zimbabwe. <http://hdl.handle.net/10646/911>.

Kamtchueng, B.T., Fantong, W.Y., Wirmvem, M.J., Tiodjio, R.E., Fouépé Takounjou, A., Asai, K., Bopda Djomou, S.L., Kusakabe, M., Ohba, T., Tanyileke, G., Hell, J.V., Ueda, A., (2015). A multi-tracer approach for assessing the origin, apparent age and recharge mechanism of shallow groundwater in the Lake Nyos catchment, Northwest, Cameroon. *J. Hydrol.* 523, 790–803. doi:10.1016/j.jhydrol.2015.02.008

- Karay G (2013) Evaluating methods of pumping tests to analysing flow properties in fractured rocks, second Conference of Junior Researchers in Civil Engineering. Budapest. pp 235-242.
- Kazemi H, Seth MS, Thomas GW (1969) The interpretation of interference tests in naturally fractured reservoirs with uniform fracture distribution. *Soc of Petrol. Engrs. J.*, pp 463-472.
- Kebede, S., Travi, Y., Asrat, A., Alemayehu, T., Ayenew, T., (2005) Groundwater recharge, circulation and geochemical evolution in the source region of Blue Nile River, Ethiopia. *Appl. Geochemistry*. 20 (9): 1658-1676.
- Knoema., (2015) Malawi Statistics. <https://knoema.com/MWMS2011/malawi-statistics-2015?region=1002090-ntcheu>. Last access December 26, 2016.
- Kruseman and De Ridder, N.A., G.P., (1994) Analysis and evaluation of pumping test data. Int. Inst. L. Reclam. Improv. Wageningen, Netherlands. Publ. 47.
- Lachaal, F., Chekirbane, A., Chargui, S., Sellami, H., Tsujimura, M., Hezzi, H., Faycel, J., Mlayah, A., (2016) Water resources management strategies and its implications on hydrodynamic and hydrochemical changes of costal groundwater: Case of Grombalia shallow aquifer, NE Tunisia. *J. African Earth Sci.* 124, 171–188. doi:10.1016/j.jafrearsci.2016.09.024
- Lapworth DJ, MacDonald AM, Tijani MN, Darling WG, Goody DC, Bonsor HC, Araguas-Araguas LJ., (2013) Residence times of shallow groundwater in West Africa: implications for hydrogeology and resilience to future changes in climate. *Hydrogeol. J.* 21: 673–686.
- Lerner, D.N., Issar A.S., Simmers I (1990) Groundwater Recharge: A guide to understanding and estimating natural recharge. IAH Int Contrib Hydrogeol 8. Heinz Heise, Hannover, 345 pp
- Li, Z., Chen, X., Liu, W., Si, B., (2017). Determintion of groundwater recharge mechanisms in the deep loessial unsaturated zone by environmental tracers. *Sci. Tot. Env.* 586: 827-835. doi: 10.1016/j.scitotenv.2017.02.061

- Liu, J., Chen, Z., Zhang, Y., Li, Z., Zhang, L., Liu, F., (2016). Stable isotope evidences on sources and mechanisms of groundwater recharge in Hohhot basin, China. *Environ. Earth Sci.* 75, 410. doi:10.1007/s12665-015-4886-5
- Liu, F., Song, X., Yang, L., et al., (2015) Identifying the origin and geochemical evolution of groundwater using geochemistry and stable isotopes in the Subei Lake Basin, Ordos energy base, Northwestern China. *Hydrol. Earth Syst. Sci.*, 19: 551-565.
- Liu, Y., Yamanaka, T., (2012) Tracing groundwater recharge sources in a mountain-plain transitional area using stable isotopes and hydrochemistry. *J of Hydrol.* 464-465: 116-126
- Macdonald, A.M., Calow, R.C., (2009). Developing groundwater for secure rural water supplies in Africa. *Desalination* 248: 546-556.
- Mandal, A.K., Zhang, J., Asai, K., (2011) Stable isotopic and geochemical data for inferring sources of recharge and groundwater flow on the volcanic island of Rishiri, Japan. *Appl. Geochemistry* 26, 1741–1751. doi:10.1016/j.apgeochem.2011.05.001
- Mapoma, H.W.T., Xie, X., (2014) Basement and alluvial aquifers of Malawi: An overview of groundwater quality and policies. *Afr. J. Environ. Sci. Technol.* 8(3): 190-202. doi: 10.5897/AJEST2013.1639
- Marechal , J., Varma, M., Riotte, J., Vouillamoz, J., Kumar, M., et al., (2009) Indirect and direct recharges in a forested watershed: Mule Hole, India. *J. Hydrol.* 364: 272-284
- Ministry of Agriculture, Irrigation and Water Development (MoAIWD) (2015) National Water Resources Master Plan. CTI Engineering International Co., Ltd. Lilongwe, Malawi
- Moench, A.F., (1984) Double Porosity Models for a Fissured Groundwater Reservoir with Fracture Skin. *Water Resour. Res.* 20, 831–846. doi:10.1029/WR020i007p00831
- Monjerezi, M., Vogt, R.D., Aagaard, P., Gebru, A.G., Saka, J.D.K., (2011) Using

$^{87}\text{Sr}/^{86}\text{Sr}$, $\delta^{18}\text{O}$ and $\delta^2\text{H}$ isotopes along with major chemical composition to assess groundwater salinization in lower Shire valley, Malawi. *Appl. Geochemistry* 26, 2201–2214. doi:10.1016/j.apgeochem.2011.08.003

Monjerezi, M., Vogt, R.D., Aagaard, P., Saka, J.D.K., (2012) The hydro-geochemistry of groundwater resources in an area with prevailing saline groundwater, lower Shire Valley, Malawi. *J. Afr. Earth Sci.* 68, 67–81. doi:10.1016/j.jafrearsci.2012.03.012

Mulligan, B.M., Ryan, M.C., Cámbara, T.P., (2011) Delineating volcanic aquifer recharge areas using geochemical and isotopic tools. *Hydrogeol. J.* 19, 1335–1347. doi:10.1007/s10040-011-0766-6

Negrel, P., Pauwels, H., Dewandel, B., Gandolfi, J.M., Mascré, C., Ahmed, S., (2011) Understanding groundwater systems and their functioning through the study of stable water isotopes in a hard-rock aquifer (Maheshwaram watershed, India). *J. Hydrol.* 397, 55–70. doi:10.1016/j.jhydrol.2010.11.033

Neuman SP (2005) Trends, prospects and challenges in quantifying flow and transport through fractured rocks. *Hydrogeol. J.* 13: 124-147 doi:10.1007/s/0040-004-0397-2.

Nimmo, J.R., Healey, R.W., and Stonestrom, D.A., (2005) Aquifer Recharge in Anderson, M.G., and Bear, J., eds., *Encyclopedia of Hydrological Science: Part 13. Groundwater*: Chichester, UK, Wiley, v.4,p.2229-2246. doi:10.1002/0470848944.hsa161a. <http://www.mrw.interscience.wiley.com/ehs/articles/hsa161a/frame.html>.

Oxtobee, J.P., Novakowski, K.S., (2003) Groundwater/Surface water interaction in a Fractured Rock Aquifer. *Ground Water* 41, 667–681.

Pavelic P, Giordano M, Keraita B, Ramesh V, Rao T. (Eds.) (2012) Groundwater availability and use in Sub-Saharan Africa: A review of 15 countries. International Water Management Institute (IWMI). Colombo, Sri Lanka; 274.

Praamsma, T., Novakowski, K., Kyser, K., Hall, K., (2009) Using stable isotopes and hydraulic head data to investigate groundwater recharge and discharge

in a fractured rock aquifer. *J. Hydrol.* 366, 35–45.
doi:10.1016/j.jhydrol.2008.12.011

Roques, C., Bour, O., Aquilina, L., Dewandel, B., Leray, S., Schroetter, J.M., Longuevergne, L., Le Borgne, T., Hochreutener, R., Labasque, T., Lavenant, N., Vergnaud-Ayraud, V., Mougin, B., (2014) Hydrological behavior of a deep sub-vertical fault in crystalline basement and relationships with surrounding reservoirs. *J. Hydrol.* 509, 42–54.

doi:10.1016/j.jhydrol.2013.11.023

Sakakibara, K., Tsujimura, M., Song, X., Zhang, J., (2017) Spatiotemporal variation of the surface water effect on the groundwater recharge in a low-precipitation region: Application of the multi-tracer approach to the Taihang Mountains, North China. *J. Hydrol.* 545: 132-144

Sarma, D., Xu, Y., (2014). An approach to sustainable rural water supply in semi-arid Africa with a case study from Namibia. *Hydrogeol. J.* 22, 1681–1692.
doi:10.1007/s10040-014-1178-1

Scanlon B.R., Healy R.W., and Coo P.G., (2002) Choosing appropriate techniques for quantifying groundwater recharge. *Hydrogeol J.* 10:18– 3

Senthilkumar, M., Arumugam, R., Gnanasundar, D., Thambi, D.S.C., Sampath Kumar, E., (2015) Effects of geological structures on groundwater flow and quality in hardrock regions of northern Tirunelveli district, Southern India. *J. Earth Syst. Sci.* 124, 405–418.

Shapiro, A.M., (2002) Fractured-rock aquifers; understanding an increasingly important source of water. *Fact Sheet* - U.S.Geological Surv.

Singh CK, Kumar A, Shashtri S, Kumar P, Mallick P (2017) Multivariate statistical analysis and geochemical modeling for geochemical assessment of groundwater of Delhi, India. *J. Geochem. Explo.* 175: 59-71.
doi.org/10.1016/j.gexplo.2017.01.001

Sophocleous, M., (2004) Groundwater Recharge, in Groundwater, [Eds. Luis Silveira, Stefan Wohnlich and Eduardo J. Usunoff], in Encyclopedia of Life

Support Systems (EOLSS), Development under the Auspices of the UNESCO, Eolss Publisher, Oxford, UK, <http://www.eolss.net>.

Stadler, S., Osenbruck, K., Suckow, A.O., Himmelsbach, T., Hotzl, H., (2010) Groundwater flow regime, recharge and regional-scale solute transport in the semi-arid Kalahari of Botswana derived from isotope hydrology and hydrochemistry. *J. Hydrol.* 388: 291–303.
doi: 10.1016/j.jhydrol.2010.05.008

Stehfest H (1970) Algorithm 368 - Numerical Inversion of Laplace Transform. *Communication of the ASM*, 13(1): 47-49.

Steinbruch, F., Weise, S.M., (2014) Analysis of water stable isotopes fingerprinting to inform conservation management: Lake Urema Wetland System, Mozambique. *Phys. Chem. Earth* 72, 13–23. doi:10.1016/j.pce.2014.09.007

Sukhija, B.S., Reddy, D. V., Nagabhushanam, P., Bhattacharya, S.K., Jani, R.A., Kumar, D., (2006) Characterisation of recharge processes and groundwater flow mechanisms in weathered-fractured granites of Hyderabad (India) using isotopes. *Hydrogeol. J.* 14, 663–674. doi:10.1007/s10040-005-0461-6

Tsujimura, M., Abe, Y., Tanaka, T., Shimada, J., Higuchi, S., Yamanaka, T., Davaa, G., Oyunbaatar, D., (2007) Stable isotopic and geochemical characteristics of groundwater in Kherlen River basin, a semi-arid region in eastern Mongolia. *J. Hydrol.* 333, 47–57. doi:10.1016/j.jhydrol.2006.07.026

UNDP (2006) Beyond Scarcity: Power, Poverty and the Global Water Crisis: UN Human Development Report 2006, United Nations Development Program, Human Development Report Office, New York, NY.

UNEP (1997) World atlas of desertification, 2nd edn. In: Middleton N, Thomas, D (coordinating eds) Edward Arnold, London.

UN Water (2015) Water and Sustainable Development: From Vision to Action: Means and tools for Implementation and the role of different actors. Report of 2015 UN-Water Zaragoza Conference.
www.un.org/waterforlifedecade/waterand-sustainabledevelopment2015/index.shtml. last access 20 August 2017.

- Van Tonder, G.J., Bardenhagen, I., Riemann, K., van Bosch, J., Dzanga, P., Xu, Y., (2002) Manual on Pumping Test Analysis in Fractured Rock Aquifer. WRC Report No. 1116/1/02. ISBN No. 186845 861X
- Van Tonder G. J., Botha J. F., Chiang W. H., Kunstmann H, Xu Y., (2001) Estimation of the Sustainable Yields of boreholes in fractured rock formations. *J. Hydrol.* 241: 70-90.
- Verbovsek, T., Kanduc, T., (2016) Isotope Geochemistry of Groundwater from Fractured Dolomite Aquifers in Central Slovenia. *Aquat. Geochemistry* 22, 131–151. doi:10.1007/s10498-015-9281-z
- Verweji, H.J.M., Barker, J.A., (1999) Well Hydraulics and Yield Analysis. In Water Resources of hard rock aquifers in arid and semi-arid zones. UNESCO Publication 58. Edited by JW Lloyd, Paris
- Villeneuve, S., Cook, P.G., Shanafield, M., Wood, C., White, N., (2015) Groundwater recharge via infiltration through an ephemeral riverbed, central Australia. *J. Arid Environ.* 117, 47–58. doi:10.1016/j.jaridenv.2015.02.009
- Wang, L., Li, G., Dong, Y., Han, D., Zhang, J., (2015) Using hydrochemical and isotopic data to determine sources of recharge and groundwater evolution in an arid region: a case study in the upper–middle reaches of the Shule River basin, northwestern China. *Environ. Earth Sci.* 73, 1901–1915. doi:10.1007/s12665-014-3719-2
- Warren, J.E., Root, P.J., (1963) The behavior of naturally fractured reservoirs. *Soc of Petrol. Engrs. J.* 3: 245-255
- Warshaw, R.D., (1965) The Geology of Ntcheu-Balaka area. Bulletin No. 19. Geological Survey Department, Zomba. Malawi.
- Williams, A.J., Crossey, L.J., Karlstrom, K.E., Newell, D., Person, M., Woolsey, E., (2013) Hydrogeochemistry of the Middle Rio Grande aquifer system - Fluid mixing and salinization of the Rio Grande due to fault inputs. *Chem. Geol.* 351, 281–298. doi:10.1016/j.chemgeo.2013.05.029

- Worldwatch (2017). Groundwater Shock: The pollution of the World's Major Freshwater Stores. www.worldwatch.org/node/481. Last access 19 September, 2017.
- Xiao, L., Xu, Y., (2014) Diagnostic analysis of pumping tests using derivative of $dlgs/dlgt$ with case study. *Ground Water* 52, 208–217. doi:10.1111/gwat.12175
- Yamanaka, T., Shimada, J., Tsujimura, M., Lorphensri, O., Mikita, M., Hagihara, A., Onodera, S., (2011) Tracing a confined groundwater flow system under the pressure of excessive groundwater use in the lower central plain, Thailand. *Hydrol. Process.* 25, 2654–2664. doi:10.1002/hyp.8007
- Yuan, R., Song, X., Zhang, Y., Han, D., Wang, S., Tang, C., (2011) Using major ions and stable isotopes to characterize recharge regime of a fault-influenced aquifer in Beiyishui River Watershed, North China Plain. *J. Hydrol.* 405, 512–521. doi:10.1016/j.jhydrol.2011.05.048
- Zhang Y, Li F, Zhao G, Li J, Zhu O (2014) An attempt to evaluate the recharge source and extent using hydrogeochemistry and stable isotopes in North Henan Plain, China. *Environ. Monit. Assess.* 186:5185–5197. DOI: 10.1007/s10661-014-3768-8.

APPENDIX

Table A1: BP1 Pumping Test Data. Rest Water Level (RWL) = 12.08mbgl drawdown (d_p) is difference in subsequent water levels i.e. (h_1-h)

BP1	Time (min)	d_p (m)	T (m^2/day)	S	BP1	Time (min)	d_p (m)	T (m^2/day)	S
	0.5	1.97	-	-		110	7.67	5.6	0.0018
	1	3.93	-	-		120	7.76	4.3	0.0022
	2	4.85	-	-		135	8.05	4.2	0.0022
	3	5.98	4.2	0.000571		150	8.17	5.0	0.0022
	4	6.21	6.2	0.000571		165	8.28	6.3	0.0022
	5	6.28	14.9	0.000571		180	8.37	7.2	0.0022
	6	6.36	18.6	0.000571		210	8.52	7.4	0.0022
	7	6.41	18.8	0.000571		240	8.62	7.3	0.0022
	8	6.46	19.4	0.000571		270	8.75	6.9	0.0022
	9	6.5	19.3	0.000571		300	8.85	6.6	0.0022
	10	6.54	19.4	0.000571		330	8.96	7.4	0.0022
	12	6.6	20.2	0.000571		360	9.04	7.5	0.0022
	14	6.66	21.6	0.000571		420	9.12	6.5	0.0022
	16	6.69	21.7	0.000571		480	9.34	5.2	0.0022
	18	6.73	21.3	0.000571		540	9.51	4.8	0.0022
	20	6.77	18.6	0.000571		600	9.65	5.1	0.0022
	25	6.84	17.0	0.000571		660	9.77	-	0.0022
	30	6.93	14.6	0.000571		720	9.89	-	0.0022
	35	7.01	13.7	0.000571					
	40	7.08	15.0	0.000571					
	45	7.13	17.9	0.000571					
	50	7.16	19.8	0.000571					
	55	7.19	17.1	0.000571					
	60	7.23	13.0	0.000571					
	70	7.32	11.5	0.000571					
	80	7.4	10.0	0.000571					
	90	7.49	8.7	0.000571					
	100	7.58	7.7	0.000571					

Q = 1L/s

Table A2: BP2 Pumping Test Data. RWL= 19.59mbgl drawdown (d_p) is difference in subsequent water levels i.e. (h_1-h)

BP2	Time (min)	d_p (m)	T (m^2/day)	S	BP2	Time (min)	d_p (m)	T (m^2/day)	S
	0.5	6.05	-	-		110	15.66	20.2	1.35E-06
	1	12.09	-	-		120	15.73	20.5	1.35E-06
	2	13.41	-	-		135	15.81	23.1	1.35E-06
	3	13.95	10.3	1.14E-06		150	15.86	21.8	1.35E-06
	4	14.21	14.3	1.12E-06		165	15.90	17.3	1.35E-06
	5	14.41	18.1	1.13E-06		180	16.02	14.3	1.35E-06
	6	14.51	21.2	1.14E-06		210	16.16	15.5	1.35E-06
	7	14.61	23.6	1.14E-06		240	16.28	18.2	1.35E-06
	8	14.68	24.4	1.14E-06		270	16.32	19.6	1.35E-06
	9	14.75	26.0	1.15E-06		300	16.44	22.1	1.35E-06
	10	14.80	26.5	1.14E-06		330	16.47	24.5	1.35E-06
	12	14.89	27.3	1.14E-06		360	16.51	29.6	1.35E-06
	14	14.98	28.8	1.13E-06		420	16.60	32.8	1.35E-06
	16	15.03	30.8	1.25E-06		480	16.64	48.4	1.35E-06
	18	15.08	31.7	1.30E-06		540	16.66	85.4	1.35E-06
	20	15.13	30.6	1.30E-06		600	16.67	119.2	1.35E-06
	25	15.23	30.6	1.30E-06		660	16.68	-	1.35E-06
	30	15.31	33.0	1.35E-06		720	16.69	-	1.35E-06
	35	15.38	40.6	1.35E-06					
	40	15.41	62.6	1.35E-06					
	45	15.43	136.5	1.35E-06					
	50	15.43	280.9	1.30E-06					
	55	15.43	239.2	1.30E-06					
	60	15.44	104.2	1.31E-06					
	70	15.46	68.8	1.35E-06					
	80	15.49	42.9	1.35E-06					
	90	15.54	29.7	1.35E-06					
	100	15.60	23.0	1.35E-06					

$Q = 2L/s$

Table A3: BP3 Pumping Test Data. RWL= 10.24mbgl drawdown (d_p) is difference in subsequent water levels i.e. (h_1-h)

BP3	Time (min)	d_p (m)	T (m^2/day)	S	BP3	Time (min)	d_p (m)	T (m^2/day)	S
	0.5	0.36	-	-		110	6.59	6.5	0.0022
	1	1.08	-	-		120	6.64	6.0	0.0022
	2	1.75	-	-		135	6.71	5.8	0.0022
	3	1.78	7.4	0.0007		150	6.77	5.8	0.0022
	4	1.86	8.7	0.0007		165	6.83	6.2	0.0022
	5	1.99	5.2	0.0018		180	6.88	6.8	0.0022
	6	2.15	3.1	0.0022		210	6.94	6.8	0.0022
	7	2.3	2.0	0.0022		240	7.02	5.7	0.0022
	8	2.71	1.8	0.0022		270	7.09	4.6	0.0022
	9	2.91	2.1	0.0022		300	7.19	4.4	0.0022
	10	2.99	2.3	0.0022		330	7.27	5.2	0.0022
	12	3.22	1.6	0.0022		360	7.31	8.4	0.0022
	14	3.66	1.1	0.0022		420	7.36	9.9	0.0022
	16	4.41	1.2	0.0022		480	7.40	9.3	0.0022
	18	4.50	1.7	0.0022		540	7.45	7.4	0.0022
	20	4.59	1.9	0.0022		600	7.50	6.1	0.0022
	25	5.1	1.7	0.0022		660	7.57	-	0.0022
	30	5.55	1.6	0.0022		720	7.62	-	0.0022
	35	5.77	1.8	0.0022					
	40	6.05	2.1	0.0022	Q = 0.5L/s				
	45	6.28	2.7	0.0022					
	50	6.31	5.0	0.0022					
	55	6.36	9.4	0.0022					
	60	6.39	11.9	0.0022					
	70	6.42	12.8	0.0022					
	80	6.46	11.3	0.0022					
	90	6.50	9.2	0.0022					
	100	6.54	7.7	0.0022					

Table A4: BP4 Pumping Test Data RWL = 11.88mbgl drawdown (d_p) is difference in subsequent water levels i.e. (h_1-h)

BP4	Time (min)	d_p (m)	T (m^2/day)	S	BP4	Time (min)	d_p (m)	T (m^2/day)	S
	0.5	1.19	-	-		110	6.75	4.0	0.0022
	1	2.37	-	-		120	6.83	3.8	0.0022
	2	3.32	-	-		135	6.95	4.0	0.0022
	3	3.63	3.2	0.0007		150	7.02	4.1	0.0022
	4	3.92	3.3	0.0007		165	7.10	4.3	0.0022
	5	4.18	3.0	0.0008		180	7.19	5.2	0.0022
	6	4.4	3.0	0.0009		210	7.27	6.2	0.0022
	7	4.57	3.1	0.0009		240	7.33	7.3	0.0022
	8	4.71	3.3	0.0009		270	7.38	7.0	0.0022
	9	4.83	3.7	0.0009		300	7.44	6.3	0.0022
	10	4.92	4.3	0.0009		330	7.49	6.2	0.0022
	12	5.05	4.5	0.0009		360	7.55	6.6	0.0022
	14	5.17	4.5	0.0009		420	7.61	6.3	0.0022
	16	5.27	4.5	0.0009		480	7.69	5.0	0.0022
	18	5.36	4.9	0.0009		540	7.78	3.8	0.0022
	20	5.44	6.2	0.0009		600	7.90	3.2	0.0022
	25	5.55	7.5	0.0009		660	8.01	-	0.0022
	30	5.62	9.6	0.0009		720	8.10	-	0.0022
	35	5.66	10.0	0.0009					
	40	5.70	6.1	0.0009	Q = 0.5L/s				
	45	5.77	3.3	0.0022					
	50	5.93	2.3	0.0022					
	55	6.12	2.1	0.0022					
	60	6.26	2.8	0.0022					
	70	6.41	3.5	0.0022					
	80	6.52	4.4	0.0022					
	90	6.60	4.7	0.0022					

Table A5: Chloro-alkaline (CAI) indices for water samples in study area

Id	TDS	Na	K	Ca	X-axis (A)	Cl	HCO3	X-axis (B)	SO4	NO3	CAI1	CAI2
B1	355.0	1.075272	0.087199	2.420659	0.324429	1.270240	3.700477	0.255545	0.309750	1.014091	0.08484	0.02145
B2	205.0	0.218356	0.047315	0.945709	0.219312	0.123878	2.329911	0.050485	0.046242	0.034332	-1.14460	-0.05882
B3	201.0	0.347194	0.080691	1.221557	0.259412	0.368831	1.807075	0.169507	0.043402	0.030888	-0.16011	-0.03139
B4	105.0	0.387799	0.025256	0.454666	0.476023	0.150402	1.138338	0.116705	0.006153	0.047570	-1.74633	-0.22033
B5	171.0	0.360592	0.089514	1.070684	0.295968	0.292844	2.147784	0.119987	0.043758	0.108020	-0.53702	-0.06839
B6	149.0	0.331731	0.050422	1.087824	0.259972	0.184491	1.753761	0.095184	0.075423	0.109449	-1.07139	-0.10196
B7	235.0	0.731361	0.088210	2.220559	0.269584	0.160439	3.907680	0.039438	0.037767	0.029925	-4.10830	-0.16580
B8	184.5	0.458982	0.061944	1.155389	0.310757	0.224067	2.336704	0.087500	0.020638	0.205808	-1.32487	-0.11582
B9	251.0	0.371814	0.069770	1.775449	0.199178	0.283831	3.276839	0.079713	0.142260	0.121261	-0.55580	-0.04456
B10	194.5	0.396477	0.118849	1.009331	0.337995	0.408728	1.835974	0.182085	0.101874	0.201199	-0.26081	-0.04983
B11	173.5	0.393475	0.198159	1.112375	0.347201	0.285430	2.313391	0.109831	0.075404	0.241936	-1.07278	-0.11640
B12	435.0	1.318030	0.123721	1.404291	0.506581	0.324122	5.201631	0.058657	0.205177	0.304452	-3.44817	-0.19569
B13	417.0	0.537103	0.295665	1.968663	0.297265	0.642145	5.180641	0.110281	0.033288	0.792829	-0.29685	-0.03173
B14	293.5	0.869161	0.065985	1.352146	0.408844	0.267927	3.817494	0.065581	0.063412	0.287408	-2.49030	-0.16007
B15	415.5	0.677642	0.097251	1.811477	0.299606	1.287173	3.594505	0.263674	0.250293	1.727723	0.39799	0.09193
B16	188.0	0.650805	0.076240	0.835180	0.465391	0.334375	1.889765	0.150339	0.115937	0.495653	-1.17434	-0.15698
B17	434.0	1.565246	0.265780	1.719411	0.515718	1.129088	2.837429	0.284655	0.253896	1.708121	-0.62169	-0.14625
B18	225.5	0.818878	0.049540	0.885329	0.495178	0.443619	1.734679	0.203654	0.168596	0.251443	-0.95758	-0.19715
B19	297.5	0.984776	0.054322	1.130589	0.478916	0.578358	1.776373	0.245615	0.278426	0.946475	-0.79663	-0.15351
D1	82.5	0.150348	0.060754	0.657784	0.242957	0.052335	1.312831	0.038336	0.021415	0.018323	-3.03368	-0.11738
R2	114.5	0.384841	0.044463	0.693463	0.382363	0.060034	1.559758	0.037063	0.005856	0.013565	-6.15098	-0.23384
R3	153.5	0.378295	0.175269	0.733882	0.429970	0.092451	2.380827	0.037380	0.040064	0.020151	-4.98765	-0.18890
R4	160.0	0.422140	0.058354	0.730357	0.396824	0.093472	1.981182	0.045054	0.051393	0.020100	-4.14051	-0.18855
S1	30.5	0.188365	0.030972	0.502071	0.304040	0.058796	1.148339	0.048707	0.001502	0.019716	-2.73048	-0.13727
S3	55.0	0.145455	0.047941	0.572255	0.252590	0.054026	1.180773	0.043753	0.020990	0.016612	-2.57967	-0.11439
S2	34.0	0.150761	0.069028	0.490120	0.309602	0.057240	1.024942	0.052893	0.004450	0.020223	-2.83980	-0.15487
R8	154.0	0.445716	0.073005	0.599950	0.463694	0.104957	2.171709	0.046101	0.040385	0.028887	-3.94223	-0.18464

Table A6: Ionic balance for water samples in study area. B4, D1 and Spring used as proxies of precipitation

Id	Na(meq/L)	Mg(meq/L)	K(meq/L)	Ca(meq/L)	sum	Cl (meq/L)	HCO3 (meq/L)	SO4 (meq/L)	NO3 (meq/L)	sum	Ion Balance %
	23	12.2	39.1	20		35.5		48	62		
B1	1.03	2.48	0.037	2.42	5.97	1.46	3.10	0.34	1.14	6.04	0.6
B2	0.25	1.54	0.020	0.95	2.75	0.16	2.62	0.04	0.03	2.85	1.8
B3	0.49	1.43	0.037	1.22	3.18	0.49	2.72	0.04	0.03	3.28	2.2
B4	0.39	0.49	0.028	0.64	1.56	0.16	1.39	0.01	0.04	1.60	1.3
B5	0.38	1.14	0.013	0.90	2.43	0.32	2.08	0.04	0.09	2.53	2.0
B6	0.34	0.75	0.037	1.15	2.28	0.21	1.98	0.07	0.12	2.38	2.2
B7	0.76	0.57	0.011	2.33	3.66	0.23	3.47	0.04	0.03	3.76	1.4
B8	0.45	1.17	0.040	1.34	3.00	0.24	2.67	0.02	0.18	3.10	1.6
B9	0.48	1.79	0.050	2.03	4.35	0.32	3.88	0.15	0.10	4.45	1.1
B10	0.39	1.14	0.050	1.21	2.79	0.40	2.20	0.10	0.20	2.89	1.8
B11	0.45	1.40	0.028	1.42	3.29	0.27	2.83	0.07	0.22	3.39	1.5
B12	1.24	3.93	0.071	2.00	7.25	0.40	6.25	0.25	0.44	7.35	0.7
B13	0.53	2.87	0.040	3.13	6.56	0.68	5.17	0.02	0.79	6.66	0.8
B14	0.85	1.50	0.020	1.90	4.26	0.28	3.77	0.06	0.26	4.36	1.2
B15	0.80	2.44	0.030	2.82	6.08	1.38	2.79	0.26	1.75	6.18	0.8
B16	0.66	1.06	0.030	0.86	2.61	0.35	1.74	0.11	0.52	2.71	1.9
B17	1.61	2.95	0.050	2.63	7.25	1.25	3.95	0.27	1.88	7.35	0.7
B18	0.80	1.36	0.057	0.96	3.17	0.44	2.45	0.15	0.22	3.27	1.6
B19	1.02	2.24	0.060	1.45	4.77	0.61	2.94	0.27	1.05	4.87	1.0
D1	0.21	0.27	0.040	0.51	1.02	0.07	1.03	0.00	0.02	1.12	4.7
R2	0.28	0.33	0.020	0.58	1.21	0.07	1.23	0.01	0.01	1.31	3.9
R3	0.27	0.34	0.040	0.66	1.30	0.09	1.22	0.03	0.02	1.35	1.9
R4	0.26	0.34	0.031	0.65	1.29	0.09	1.16	0.03	0.02	1.30	0.4
S1	0.21	0.14	0.030	0.20	0.58	0.07	0.59	0.00	0.03	0.68	7.9
S3	0.18	0.15	0.078	0.34	0.74	0.07	0.75	0.00	0.02	0.84	6.3
S2	0.18	0.11	0.030	0.17	0.49	0.08	0.48	0.00	0.03	0.59	9.3
R8	0.16	0.30	0.075	0.39	0.93	0.08	0.81	0.02	0.03	0.95	1.1
Rain	0.06	0.05	0.049	0.08	0.24	0.07	0.14	0.05	0.03	0.29	9.4